CONTENT

CONTENT

NEW GEOLOGICAL DATA ON VĂIDOAIA MINING FIELD, ROŞIA MONTANĂ Au-Ag EPITHERMAL DEPOSIT, APUSENI MOUNTAINS, ROMANIA

Sergiu DRĂGUŞANU[1], Călin Gabriel TĂMAŞ[1]*

[1]Department of Geology, Babeş-Bolyai University, 1, Kogălniceanu Street, 400084 Cluj-Napoca, Romania.
**calin.tamas@ubbcluj.ro*

Abstract: Văidoaia mining field is located in the north-eastern part of Roșia Montană low to intermediate sulfidation Au-Ag ore deposit, Apuseni Mountains, Romania. Significant traces of old mining works are visible within this perimeter at the surface and are partially still accessible in the underground. They are testifying an intense mining activity once. However, very limited geological and ore deposit data are available for this perimeter from previous studies. The country rocks from Văidoaia massif consist of Cretaceous sedimentary rocks (sandstones), vent breccia, and a dacite lava flow remnant. Adularia-sericite and silicification are the characteristic hydrothermal alterations. The K-alteration is represented by two types of adularia, *i*) adularia I formed by K-metasomatosis of the magmatic feldspar phenocrysts from dacite (lava flow and clasts within vent breccia), and *ii*) adularia II deposited from the hydrothermal fluids as euhedral to subhedral crystals together with hydrothermal quartz. White mica is occurring as small flakes on the adularised feldspar phenocrysts or in dacite groundmass. Silicification occurs within the groundmass of the dacite rocks and within the matrix of vent breccia. Hydrothermal quartz veinlets and vugs infillings are also quite frequent in dacite and vent breccia. Different styles of primary mineralizations occur, *i.e.* disseminated, stockworks, veins and breccia dykes. The disseminations were controlled by the porosity of the rocks (vent breccia), the stockworks are occurring along the contacts between vent breccia and Cretaceous flysch, while the veins are represented by small sized quartz structures hosted mainly by the vent breccia. The most important ore bodies are represented by several breccia dyke structures, five of them creating a parallel system striking WWN-EES with a steep S dip, and another one up to 50 cm width, which is heading NNE and has a dip of 70° towards WWN. These breccia dykes were the main exploitation targets in Văidoaia mining field. The mineralogy of the ore is very simple, with pyrite, gold and traces of chalcopyrite. The largest gold grain identified so far is measuring 80 micrometers. The gangue minerals are represented by quartz, calcite, and adularia II. At least two hydrothermal brecciation events were noticed. These brecciation events triggered the deposition of a black hydrothermal cement rich in organic matter known by the local miners as *chinga*, and of gold. The mineralizations from Văidoaia massif are typical low-sulfidation.

Keywords: Roșia Montană, Văidoaia, epithermal mineralization, hydrothermal alterations, breccia structures, gold

1. INTRODUCTION

The Roşia Montană ore deposit is the largest gold deposit in Europe (Manske et al., 2006). The ore deposit is located in the Apuseni Mountains, west-central Romania (Fig. 1), in the north-western part of the Golden Quadrilateral - the most important historical gold mining region of Romania.

Roşia Montană is a typical epithermal deposit. It was interpreted as a low to intermediate sulfidation Au-Ag deposit (Leary et al., 2004; Manske et al., 2006; Tămaş, 2010) related to a Neogene maar-diatreme complex (Tămaş, 2010).

At the ore deposit scale several mining fields were separated, the most important being Cetate, Cârnic, Orlea, and Ţarina. Two smaller and less known mining fields exist in the eastern and north-eastern part of the deposit, *i.e.* Coş and Văidoaia (Fig. 1).

The present work offers new data on the lithology, the hydrothermal alterations, the ore bodies, and the ore mineralogy from Văidoaia mining field.

2. GEOLOGICAL SETTING

The Apuseni Mountains are located in the eastern central part of the Alpine – Balkan – Carpathian – Dinaride geodynamic province. They are situated between the Transylvanian Basin in the east and the Pannonian Basin in the west. The basement of the region is formed by two lithospheric blocks, Tisia-Dacia in the South, where Apuseni Mountains are located, and ALCAPA in the North (Balla, 1987; Csontos et al., 1992; Royden, 1993; Csontos, 1995; Fodor et al., 1999). These tectonic blocks experienced during Eocene to Early Miocene opposite-sense rotations, *i.e.* Tisia-Dacia block developed a clockwise rotation while ALCAPA block was affected by a counterclockwise rotation.
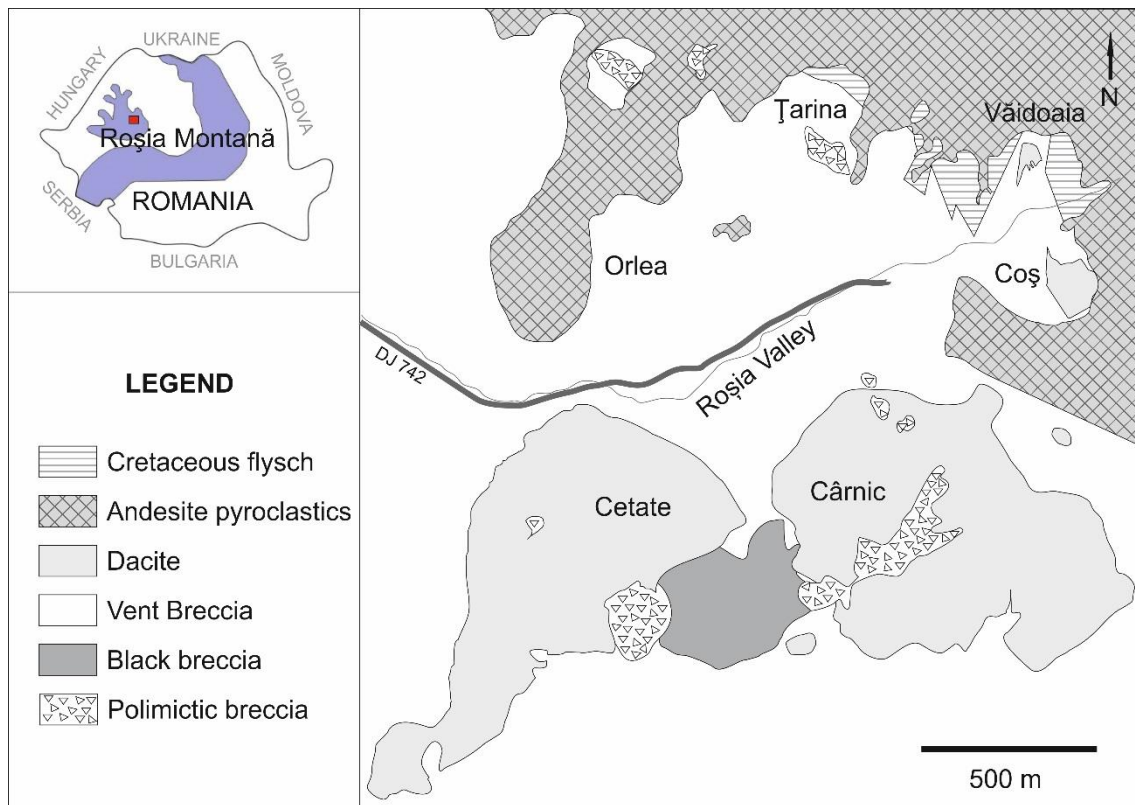
Fig. 1. Geological map of Roşia Montană ore deposit with the main mining fields (Roşia Montană Gold Corporation SRL courtesy). The upper left inset shows the geographic location of Roşia Montană in west-central Romania.

These opposite blocks rotations coupled with the nearby Mecsek-Villany area which was stopping the rotation (Seghedi et al., 2007) triggered the set-up of an extensional tectonic regime on the western border of the Apuseni Mountains (Royden, 1988; Săndulescu, 1988; Balintoni and Vlad, 1998). As a result, three graben-like basins appeared within the Apuseni Mountains and focused the Neogene sedimentation and the magmatic activity (Seghedi et al., 2004). The timing of the Neogene volcanism from Apuseni Mountains was established at 15-7 Ma (Roşu et al., 1997 and 2004a) with a final pulse at about 1.6 Ma (Pécskay et al., 1995; Roşu et al., 2004a).

According to Seghedi et al. (2007) the decompression melting of the lower crust and/or lithospheric mantle (Balintoni et al., 1997) triggered the generation of the magmas. Subordinate, asthenospheric upwelling process was involved for generation of small amount of magma (Seghedi et al. 2007).

Porphyry Cu-Au and epithermal Au-Ag±Te ore deposits formed during Neogene volcanic activity. Three main metallogenetic periods have been delineated by Roşu et al. (2004b), *i*) 13.6 Ma (Roşia Montană); *ii*) 12.5-10 Ma (regional development); and *iii*) 9.5-8.5 Ma (Baia de Arieş). At the Apuseni Mountains scale the ore deposits are concentrated within Brad-Săcărâmb, Stănija-Zlatna, Roșia Montană-Bucium-Baia de Arieş metallogenetic districts. An isolated porphyry copper deposit occurs at Deva, south of Mureș valley but it is connected to the Neogene volcanism as well.

3. LOCAL GEOLOGY

Roșia Montană ore deposit is genetically controlled by 13.5 Ma dacite volcanic activity (Roşu et al., 1997 and 2004a). The basement of the perimeter consists of Cretaceous sedimentary rocks represented mainly by sandstones, shales, marls and conglomerates (flysch). These rocks are outcropping in the surrounding area of the deposit (Bordea et al., 1979).

The Cretaceous basement was pierced by phreatomagmatic eruptions which created the Roşia Montană maar-diatreme structure (Tămaş, 2010). The infilling of this large scale structure was previously interpreted by Borcoş and Mantea (1968) as a succession formed from "volcano-sedimentary formation", "grey marls horizon", and "marly-clayly schists horizon". Leary et al. (2004) considered the same rocks as "Vent breccia", Wallier et al. (2006) interpreted this lithological unit as volcaniclastic breccias, while Tămaş (2007) as intracrateral breccias. All these terms aimed in fact to give an idea of the genetic

mechanism of formation, precisely phreatomagmatic eruptions, and to support the co-existence of sedimentary and volcanic sequences. According to Tămaș (2010), the vent breccia is the underground expression of Roșia Montană maar-diatreme structure being the first volcanic product of a hydrovolcanic activity which continued afterwards with the emplacement of Cetate dacite followed by other phreatomagmatic breccia pipe structures, *e.g.* Cetate including Black, Corhuri and Corna breccias. The vent breccia/Roșia Montană breccia is a polymictic matrix-supported breccia with metamorphic rocks (gneisses, garnet micaschists, and quartzites), volcanic rocks (dacite) and sedimentary rocks (sandstones, clays). The clasts are generally rounded and range in size from several millimeters up to tens of centimeters. The matrix is a typical rock flour type and it is formed from comminuted country rocks (Wallier et al. 2006).

The vent breccia/Roșia Montană breccia was intruded by Cetate dacite bodies outcropping in Cetate and Cârnic hills (Fig. 1). These dacite plugs are today separated by a maar-diatreme breccia structure, known as Glamm formation (Mârza et al., 1990; 1995) or Black Breccia (Leary et al., 2004; Manske et al., 2006). The same structure was interpreted by Tămaș (2002, 2007, and 2010) as the fluidization channel of the Cetate breccia pipe. The phreatomagmatic brecciation including Cetate breccia and its fluidization channel passed through the Roșia Montană diatreme and brecciated the dacite already emplaced. At the end of the volcanic activity the phreatomagmatic brecciation was followed by the hydrothermal activity, *i.e.* hydrothermal alterations and formation of the bulk Au-Ag mineralization (Tămaș, 2002). The precious metals ore bodies are represented by disseminations, breccias, stockworks and veins hosted by dacite, diatreme breccias and Cretaceous flysch (Tămaș 2002).

The last volcanic pulse from Roșia Montană is the so-called Rotunda andesite. The andesite products occur in the northern part of the perimeter and are represented by a rooted body (Rotunda hill), lava flows and volcaniclastics (Bordea et al., 1979).

The Roșia Montană ore deposit is delineated by a widespread alteration halo. Several authors (Cozubaș, et al., 1986; Mârza and Ghergari, 1992; Mârza et al., 1997; Tămaș, 2002) studied the hydrothermal alterations from Roșia Montană and identified the adularisation (K-metasomatosis), phyllic alteration, argillic alteration, silicification, and carbonatation. More recently, Wallier et el. (2006) separated four major types of hydrothermal alteration within Roșia Montană ore deposit, *i.e.* chlorite-calcite alteration, adularia alteration, phyllic alteration and silicification. These hydrothermal alterations have affected all rocks types within the perimeter.

4. SAMPLES AND METHODS

Field work including surveying, geological mapping, and sampling was carried out at surface (Fig. 2 and 3) and in the underground in an irregular morphology large stope and an adit. The underground stope, known in the local miners slang under the common name *Coranda Văidoaia* is the result of the historical mining activity. It is located in vent breccia, close to the contact with the sedimentary rocks and the dacite body. It is partially backfilled and several vertical pillars are still in place ensuring the stability of this opening located in the vicinity of the surface. An adit heading west starting from the northern part of the stope is passing through the vent breccia and then the Cretaceous flysch. At the surface several traces of surface mining along vein structures/breccia dykes are still well-preserved west of the entrance in the underground stope.

From the outcrops and the mining workings were collected 250 samples from which were prepared 100 polished sections and 20 thin sections studied on transmitted and reflected light polarizing microscopes. The thin sections study allowed to validate the rock types and the hydrothermal alterations identified in the field, while the polished sections made possible the identification of the ore minerals. Based on field evidences, macroscopic and microscopic observation was prepared a geological map showing apart the lithological units, the hydrothermal alterations and several mineralized structures.

5. RESULTS

The previous studies on Roșia Montană ore deposit were mainly focused on its southern part, in Cârnic and Cetate hills respectively (Cozubaș, et al., 1986; Mârza and Ghergari, 1992; Mârza et al., 1997; Ciobanu et al., 2004; Feier et al., 2004; Leary et al., 2004; Tămaș, 2002, 2007, 2010; Tămaș et al. 2006 and 2014; Wallier et al., 2006, etc.). The same, the ore samples studied by Petrulian (1934) came mostly from the deep part of the Roșia Montană mine located below the +714 m Sfânta Cruce din Orlea mining level.

Fig. 2. Văidoaia mining field viewed from the south with remnants of mining works. The main lithological units are as indicated. The width of the view is approximately 250 m.

Fig. 3. The northern slope of Văidoaia massif with historical exploitation works exposed at the surface. The central opening is continuing underground towards north in its lower part forming a stope known by the locals as *Coranda Văidoaia*.

Geological and ore deposit data for the northern part of Roșia Montană were given by Ghițulescu and Socolescu (1940) and Pitulea et al. (1974) which presented the gold placers covered by Rotunda andesite pyroclastic deposits. More recently, Minuț et al. (2004) revealed the occurrence of hydrothermal breccias along the contact between the diatreme breccia (vent breccia) and the Cretaceous basement in the northern part of the ore deposit in Țarina and Igre mining fields as well as in the eastern part of Cârnic.

The present study is focused on the north-eastern edge of the Roșia Montană diatreme where the contact with the Cretaceous sedimentary rocks is outcropping (Fig. 1, 2 and 4). This area corresponds to the Văidoaia mining field (Fig. 2). The same contact between Roșia Montană diatreme/vent breccia and the Cretaceous sedimentary rocks was followed during the old mining activity towards north-west and west in Igre, Țarina, and Orlea mining fields and towards east in Coș mining field. From a metallogenetic perspective the contact between different lithological units seems to be once again an excellent environment for hosting hydrothermal ore bodies.

Until now the geological and mineralogical data for Văidoaia mining field remained scarce with only general information available from the published geological maps of the Roșia Montană ore deposit (Bordea et al., 1979; Leary et al., 2004; Tămaș et al., 2014). Several rock types, hydrothermal alterations and mineralization styles have been encountered in the field and were detailed by optical microscopy study.
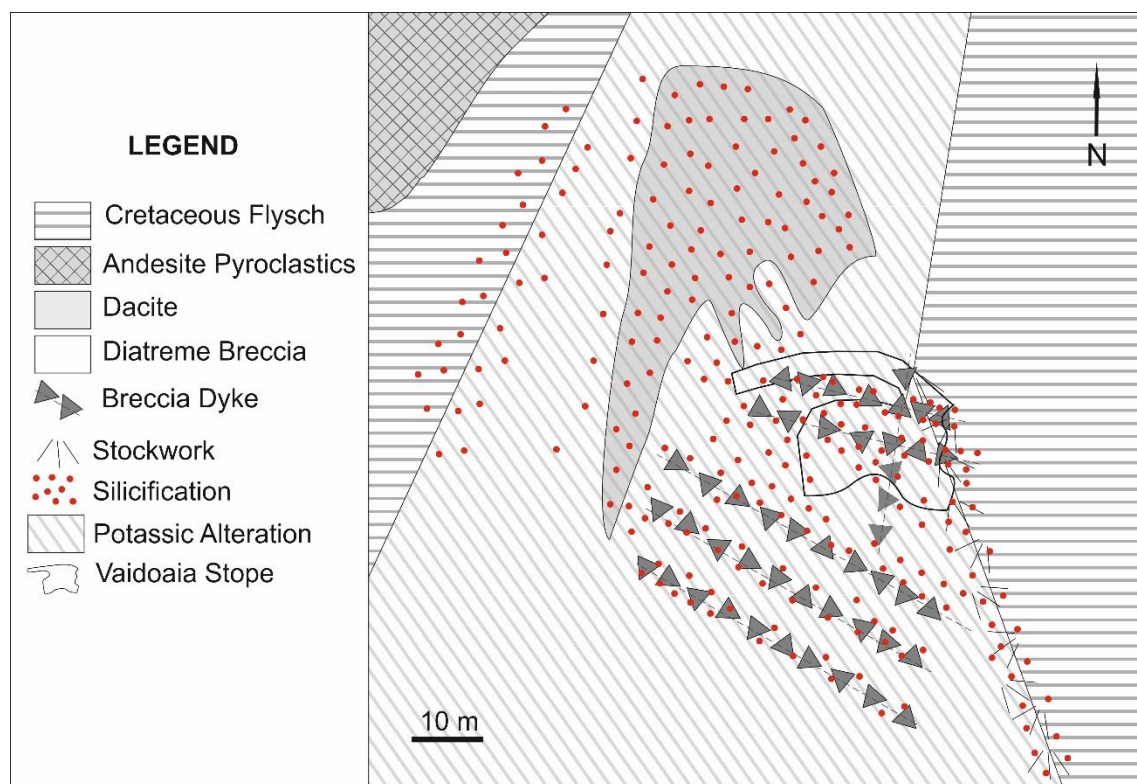
Fig. 4. Surface geology of Văidoaia mining field, provided by Roșia Montană Gold Corporation. The map also shows the distribution of the hydrothermal alterations and the main mineralized structures.

5.1. Lithology

According to the available geological maps a dacite body surrounded by Roșia Montană diatreme breccia/vent breccia occurs in the central part of Văidoaia mining field. The northern development of the diatreme breccia is covered by the Rotunda andesite type volcaniclastic deposits. Towards east and west the vent breccia has sharp contacts with the Cretaceous flysch which represents the basement. North of Văidoaia mining field the andesite volcaniclastics creates a compact layer hiding any other lithological units.

5.1.1. Cretaceous sedimentary rocks

The Cretaceous sedimentary rocks from Văidoaia mining field were firstly mentioned by Tămaș (1995) and they are represented by sandstones. These rocks are outcropping at the surface (Fig. 2 and 4) but they were observed in the underground, too.

The sandstones from Văidoaia are matrix poor (maximum 15 %) being dominated by quartz polycrystalline grains and metamorphic lithoclasts, among which the quartzite ones are the most frequent. Microcline and white micas subordinately occur as isolated grains. Shale clasts are not uncommon within the sandstones. In some samples, organic matter (incarbonized wood fragments) has been identified macroscopically. The grains of the sandstones are usually sub-angular but locally a subrounded morphology may prevail. The predominant grains contact type is floating grains and subordinately point contact and long contact. They are indicating a loose rock packing and a poor maturity.

5.1.2. Diatreme/vent breccia

This rock type is the most abundant within Văidoaia mining field and it is the most developed lithological unit at the Roşia Montană ore deposit scale as well.

The vent breccia occurring in Văidoaia mining field is a typical fine to coarse-grained rock flour matrix supported breccia (Fig. 5 and 6). Locally the vent breccia shows a clast supported appearance (Fig. 6). The matrix is varying from medium grain to coarse grain size and its composition reflects the lithology of the country rocks, *i.e.* dacite, Cretaceous shales and sandstones, and metamorphic rocks. The matrix holds together rounded to angular rock fragments ranging in size from millimeters up to several centimeters. Dacite and Cretaceous shales and sandstones are the most frequent clasts, while metamorphic clasts, *i.e.* micaschists, gneiss and quartzite occur subordinately, however they are quite common (Fig. 6). Apart the above-mentioned clast lithologies, the microscopic study revealed the occurrence of microdiorite rock fragments as well as many crystal clasts, *e.g.* magmatic and metamorphic quartz, adularised feldspars, white micas, garnets, and less frequent volcanic glass fragments. Exotic clasts of several centimeters in size represented by rounded to subangular carbonized wood fragments were also observed within the vent breccia (Fig. 5). Due to coarse grain matrix and the clast supported appearance, the open spaces are relatively frequent within the vent breccia (Fig. 6).

5.1.3. Dacite

The dacite outcropping at Văidoaia was considered by Tămaş (2007) an erosional remnant, this dacite spot representing a rest of lava flow from the dacite body forming Cârnic massif. According to the above cited author a similar erosional remnant is located west of Cetate massif and that one was connected with the dacite body outcropping in Cetate massif.

The dacite from Văidoaia has a gray color with a bluish tint. It is pervasive hydrothermally altered and it is often densely fractured. It is a typical porphyritic rock with millimeters sized feldspars and magmatic quartz phenocrysts set in a fine-grained groundmass (Fig. 7a,b). The dacite from Văidoaia has less and smaller phenocrysts as compared with the dacite from Cetate and Cârnic massifs. Locally at Văidoaia the dacite consists only of a fine-grained groundmass with no macroscopically visible phenocrysts. Microscopically was confirmed the presence of several magmatic phenocrysts. The magmatic quartz is frequently fractured and it is magmatically corroded being represented by subrounded grains (Fig. 7c,d) and angular fragments (Fig. 7e,f). The magmatic feldspars are represented by altered potassic (orthoclase) and plagioclase feldspars. The alterations hide partially the primary characteristics of the feldspars but sometimes relicts of plagioclase zonation or polysynthetic twinning allow their identification. Rare quartzite fragments were observed under polarizing microscope.

5.2. Hydrothermal alterations

The hydrothermal alteration of a rock is the evidence of the hydrothermal fluids flow through that rock by various paths, *i.e.* interconnected pores, cracks, fractures, contacts or brecciated zones. The existence of hydrothermal altered rocks suggests the potential occurrence of a mineralization. The hydrothermal alterations are the result of the interaction between the country rocks and the hydrothermal fluids and consequently specific peculiarities occur from the reaction of a given rock with a hydrothermal fluid. As shown previously by many authors (Idriceanu et al., 1965; Borcoş, 1968; Mârza et al., 1997; Tămaş et al., 2006, etc.) the hydrothermal fluids that formed Roşia Montană ore deposit are generally low-salinity with homogenization temperatures ranging generally from 200 to about 300^0C. These types of fluids were apparently responsible for the hydrothermal alterations from Văidoaia mining field as well, where dacite, vent breccia and Cretaceous sandstones represent the country rocks. The field evidences strengthened by microscopic observations confirm the occurrence of silicification, potassic alteration (adularia), and phyllic alteration (white mica) in Văidoaia mining field. These alterations possess specific peculiarities for each of the country rocks and for this reason they are presented below by rock type.
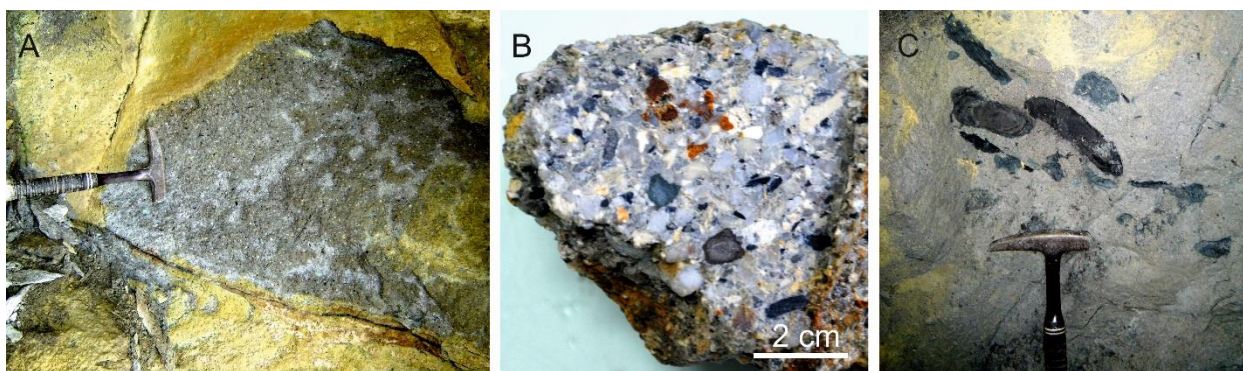
Fig. 5. Vent breccia occurring in Văidoaia mining field: a) matrix supported breccia with dominant dacite millimeters-sized clasts, exposed on the walls of old surface workings; b) detail of polymictic vent breccia with up to 1 cm Cretaceous (sandstones, shales), dacite and metamorphic rock fragments; c) carbonized wood and elliptical shales fragments within the vent breccia (underground Văidoaia stope).
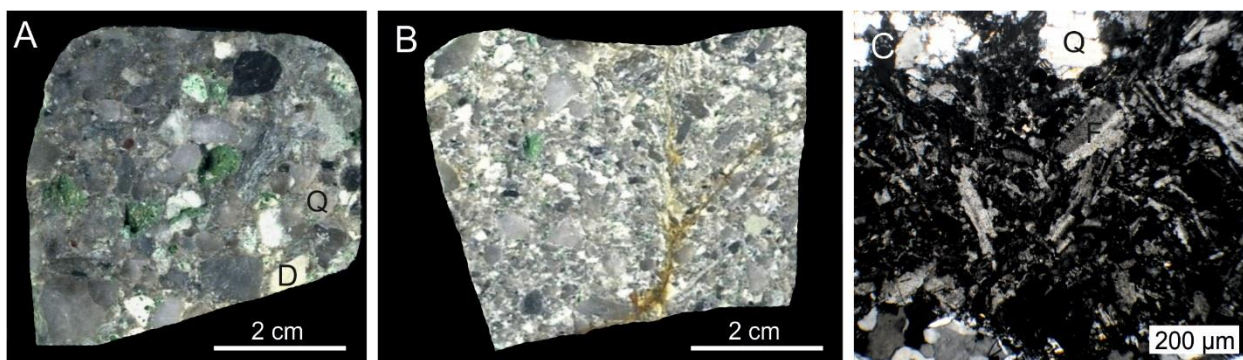
Fig. 6. Detail views of the vent breccia from Văidoaia: a) clast supported breccia with metamorphic (quartzite), Cretaceous (shales) and dacite angular to sub-angular clasts; the breccia has a coarse matrix and numerous open spaces; c) microscopic view in plane polarized light under crossed polarizers of a microdiorite/andesite clast from the vent breccia. Abbreviations: F-feldspars; Q-magmatic quartz; D – dacite.

The dacite from Văidoaia shows intense to week silicification, a moderate K-alteration, and a minor phyllic alteration. The silicification occurs within the groundmass of the rock being expressed by hydrothermal quartz veinlets and vugs infillings. The magmatic quartz phenocrysts are sometimes covered by hydrothermal quartz rims (Fig. 7c,d). The K-alteration is represented by, *i)* adularia formed by K-metasomatosis upon magmatic feldspar phenocrysts (Fig. 8a,b); and *ii)* adularia deposited from the hydrothermal fluids in available open spaces and in this case it is accompanied by hydrothermal quartz (Fig. 8b,c,d). The first type of adularia corresponds to the adularia I described by Tămaș (2002), while the second type of adularia mentioned above corresponds to the adularia II described by the same author. Adularia I is preserving the morphology of the magmatic feldspars phenocrysts, while adularia II is occurring as euhedral to subhedral crystals (Fig. 8c,d). Hydrothermal quartz is sometimes present within the pores formed during K-metasomatosis of the feldspar phenocrysts due to volume reduction. Sericite is occurring as small flakes developed within the groundmass of the rock or on the adularised feldspar phenocrysts (Fig. 8a).

The vent breccia exposed in Văidoaia mining field was also altered but in different ways for the matrix and the clasts. The silicification occurs especially in the matrix of the vent breccia (Fig. 9a) as tiny hydrothermal quartz grains cementing the matrix, as veinlets and as pockets. The hydrothermal quartz is deposited also on the rock fragments within the breccia (dacite, shales, etc.). The intensity of the silicification is varying from high to moderate. The matrix is also sericitised, from minor to intense. The potassic alteration is represented by the occurrence of adularia. Two types of adularia have been observed, *i)* adularia I formed by K-metasomatosis on the potassium and plagioclase feldspars phenocrysts; and *ii)* adularia II deposited in vugs and accompanied by hydrothermal quartz (Fig. 9b). These types of adularia correspond with the adularias observed in the dacite from Văidoaia previously described.
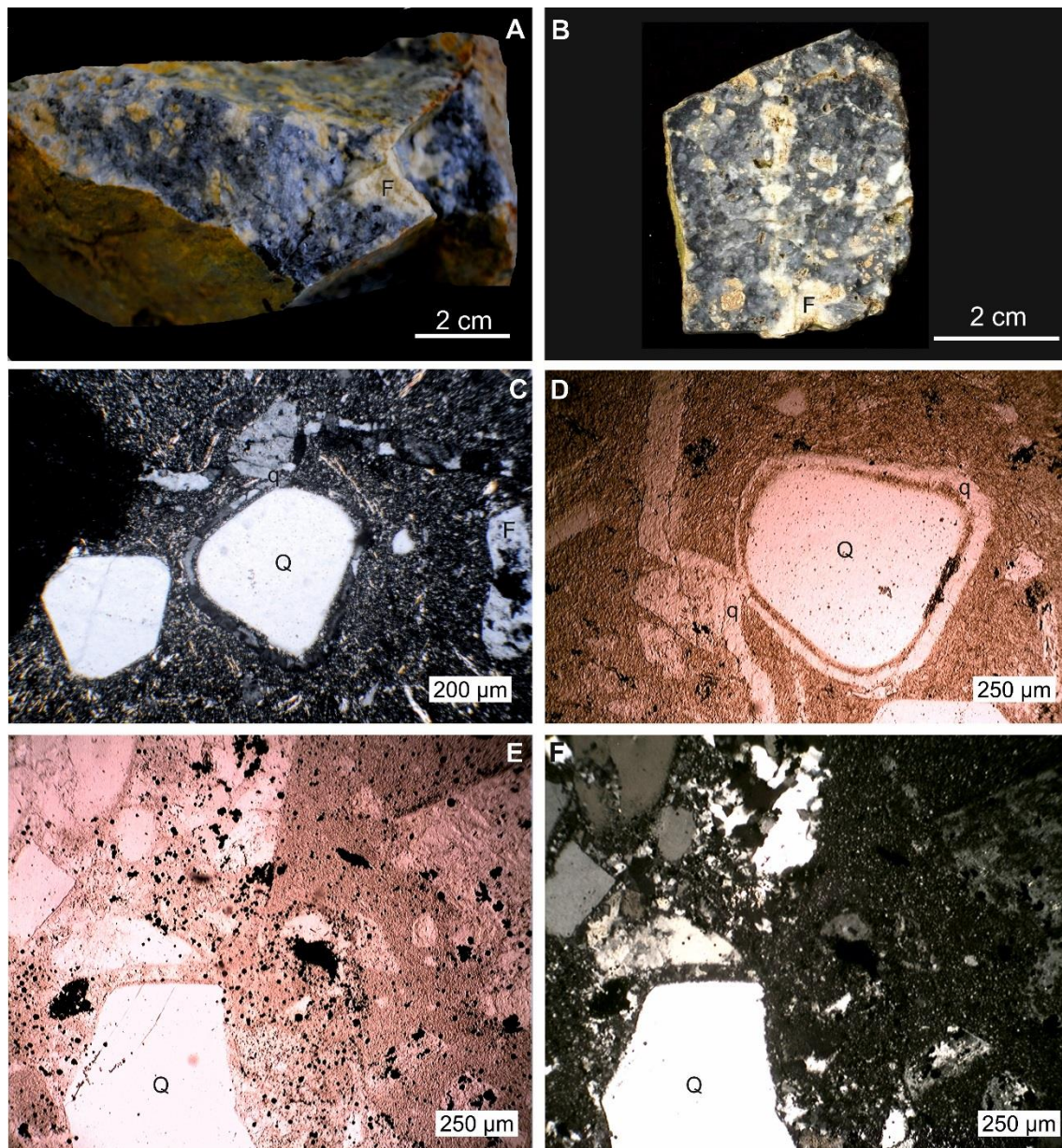
Fig. 7. The dacite from Văidoaia massif: a) hand specimen of porphyritic dacite with dominant feldspar phenocrysts; b) polished slice of dacite showing adularised feldspar phenocrysts set into a silicified groundmass; c) microscopic view in plane polarized light under crossed polarizers of the dacite with rounded to subangular magmatic quartz crystals bordered by a rim of hydrothermal quartz, adularised potassic feldspars and a hydrothermal quartz veinlet; d) microscopic view in plane polarized light of a magmatic quartz phenocryst bordered by a rim of hydrothermal quartz and a hydrothermal quartz veinlet - detail of the Fig. 7c; e) microscopic view in plane polarized light of broken magmatic quartz phenocrysts forming angular fragments; f) Microscopic view in plane polarized light under crossed polarizers of angular to subangular magmatic quartz phenocrysts accompanied by smaller adularised and slightly sericitised feldspar phenocrysts held in a fine grain groundmass. Abbreviations: Q-magmatic quartz; q-hydrothermal quartz; F-adularised feldspars.

Adularia I developed only on rock fragments from the vent breccia containing feldspars phenocrysts or clasts (dacite, breccias), while the second type of adularia (adularia II) occurs as open spaces filling or along veinlets. Adularia II is deposited directly from the hydrothermal fluids and postdates the adularia I. It occurs frequently as euhedral crystals intimately associated with hydrothermal quartz.

The Cretaceous flysch represented by sandstones in Văidoaia mining field, has been affected only by silicification which seals its pores and increases its hardness. Small quartz veins and black hydrothermal cement *chinga* crosscut the sandstones and determined locally an increase of the intensity of silicification.
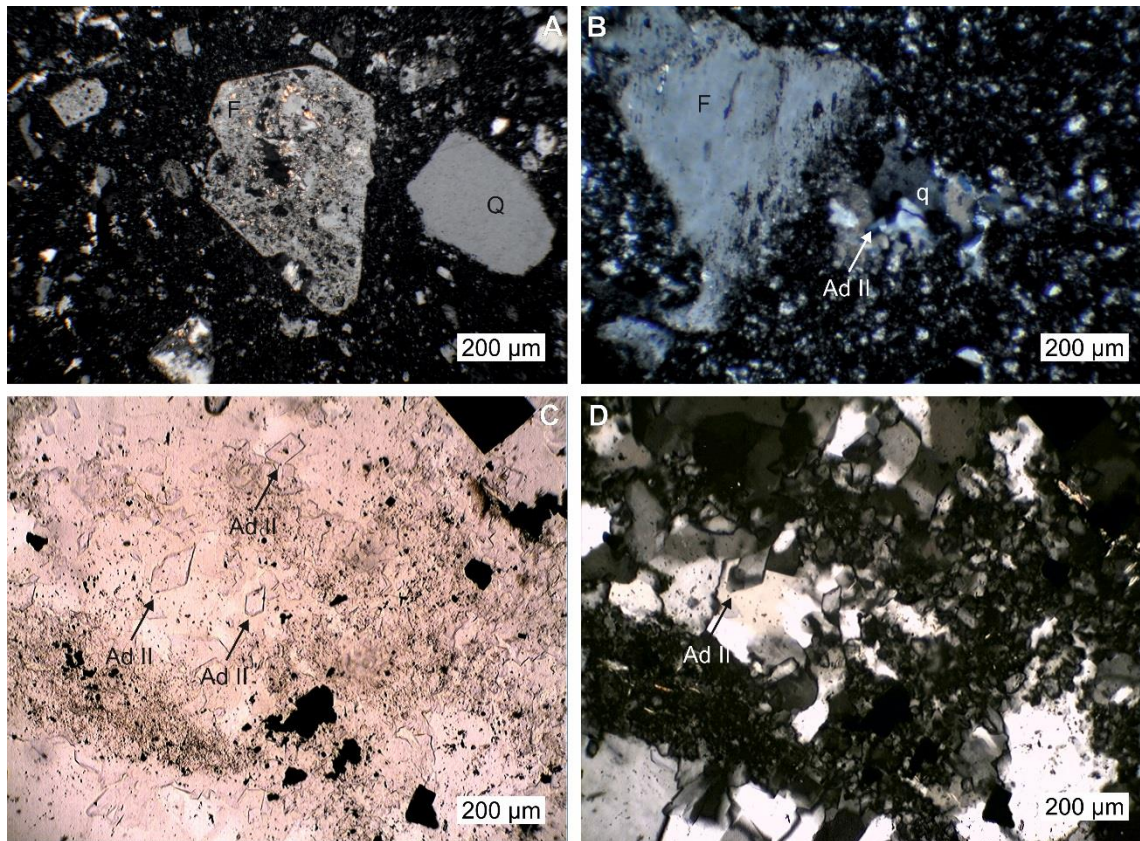
Fig. 8. Microscopic views of the alterations from the dacite occurring in Văidoaia massif: a) adularised feldspar phenocryst affected by incipient phyllic alteration (sericite); b) adularised feldspar phenocryst accompanied by adularia II and hydrothermal quartz deposited within open spaces; c and d) adularia II, hydrothermal quartz and opaque minerals (sulfides) deposited in open spaces. The image c is in plane polarized light and the images a, b, and d are under crossed polarizers. Abbreviations: Q-magmatic quartz; F-adularised feldspar (adularia I); Ad II-adularia II; q-hydrothermal quartz.
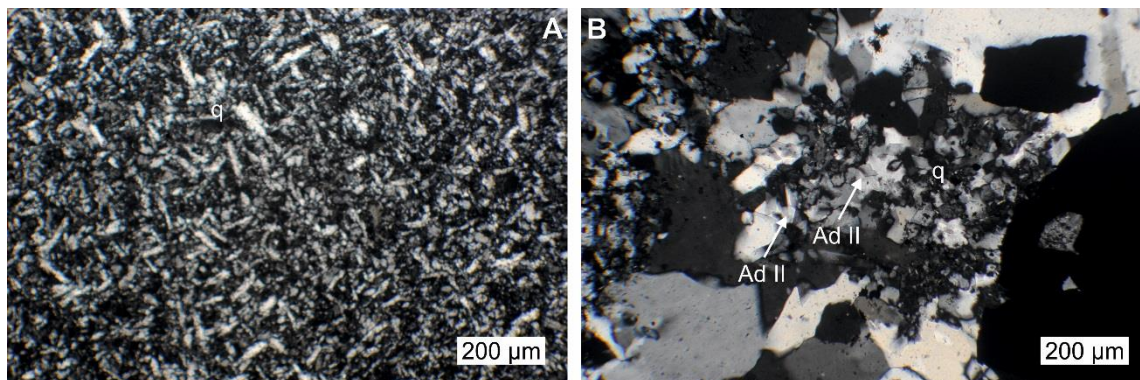
Fig. 9. Alterations peculiarities within the vent breccia: a) microscopic view of an intense silicification of the vent breccia matrix associated with a minor phyllic alteration (sericite flakes); b) microscopic view of euhedral adularia II rhombus crystals accompanied by hydrothermal quartz veins. The images are under crossed polarizers. Abbreviations: Ad II-adularia II; q-hydrothermal quartz.

5.3. Mineralizations

Primary and secondary mineralizations were identified in Văidoaia mining field. The primary mineralizations are expressed by disseminations, stockworks, veins and breccia dykes, while the secondary mineralizations consist of placer deposits along Roșia stream.

The disseminations were controlled by the porosity of the coarse matrix of the vent breccia. Pyrite is widespread within vent breccia and its exposure at surface generated an almost continuously yellowish-brown blanket on the country rock (Fig, 10a). Pyrite disseminations were noticed also in dacite and in a lesser extent in Cretaceous rocks.

9

The stockworks are occurring in Cretaceous rocks, in vent breccia and along the eastern contact of the vent breccia with the Cretaceous sandstones. The stockwork fissures could be distributed roughly parallel (Fig. 10b) or randomly in the host rocks (Fig. 10d). The individual fissures are filled with hydrothermal quartz and pyrite. The stockwork zones were mined at the surface but also in the underground (Fig. 10c). The stockwork mineralizations along the fissures are accompanied by pyrite disseminations within the matrix of the host vent breccia. The stockwork zones are systematically intense silicified.

Fig. 10. Outcrop scale mineralizations characteristics: a) typical oxidation pattern developed on vent breccia outcrops due to surface alteration of disseminated pyrite; b) parallel stockwork fissures filled with hydrothermal quartz and pyrite; c) stockwork zone opened in the adit heading west of *Coranda* Văidoaia - note the trace of the mining drill through the stockwork; d) randomly distributed stockwork fissures within an intense silicified vent breccia.

The veins are quite frequent and are represented by small sized quartz veins hosted by vent breccia, Cretaceous sandstones and dacite. The so-called *chinga* veins are better developed. The term *chinga* is used by the local miners to denominate a black, compact and hard material found frequently along veins and within breccia structures. Tămaş (2002) interpreted it as a hydrothermal cement containing organic substance. This material was frequently emplaced into country rocks by injection under pressure as indicated by textural evidences. This hydrothermal cement contains pyrite as well as precious metals minerals. Elsewhere in Roșia Montană ore deposit, *e.g*. Cetate and Cârnic massifs, Tămaş (2002, 2007, etc.) described hydrothermal breccias with *chinga* cement. The vent breccia from Văidoaia is crosscut by such *chinga* veins exceeding sometimes 1 cm width (Fig. 11a). These veins occur as individual structures or as twin or even branching ones (Fig. 11b).

This type of veins is marked by an intense adjoining silicification and often they are accompanied by a micro-brecciation of the host rock. We state here that these veins should be considered as hydrothermal breccia dyke structures taking into account the nature of their infilling. Sometimes the black hydrothermal cement is creating breccia pockets. Late hydrothermal brecciation affected locally the *chinga* cement forming pockets of hydrothermal breccias with *chinga* clasts cemented by subsequent quartz and calcite cement (Fig. 11c,d).
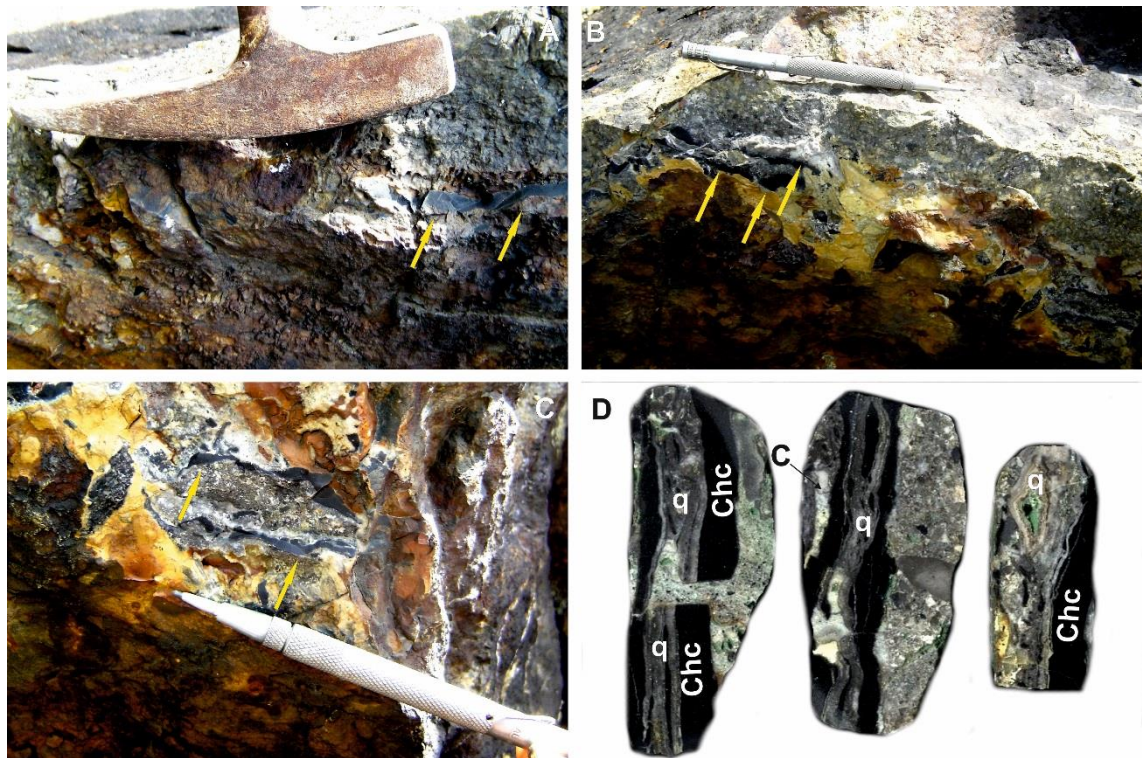
Fig. 11. Macroscopic peculiarities of the veins from Văidoaia mining field: a) individual *chinga* vein (arrows) crosscutting silicified vent breccia; b) branching *chinga* vein (arrows) with intense adjoining silicification of the host vent breccia; c) late hydrothermal breccia with *chinga* clasts and quartz - calcite hydrothermal cement; d) detail of the late hydrothermal brecciation of chinga cement, consolidated with hydrothermal quartz and calcite. Abbreviations: C-calcite; q-hydrothermal quartz; Chc-*chinga* hydrothermal cement.

The main mineralized structures from Văidoaia massif are represented by breccia dyke structures (Fig. 4). The best developed breccia structure is exposed on the main face line of the old Văidoaia open pit and it is heading NNE and has a dip of about 70° towards WWN (Fig. 12a,b). This main breccia dyke structure, we name here Văidoaia breccia dyke is hosted by vent breccia and has up to 50 cm width. It was mined at the surface and then in the underground, with safety pillar preserved in Văidoaia stope (Fig. 12c). The breccia is clast supported with up to 10 cm sub-rounded to sub-angular clasts. The rocks fragments within breccia are often covered by a hydrothermal quartz rim. Among several clasts there are sometimes open spaces.

A series of five parallel breccia dykes are also present having an overall NW strike and a dip of about 80° towards SW. The southernmost three breccia dyke structures from this parallel breccia dyke system were mined at the surface (Fig. 13a,b), while the northern two are exposed only in underground in the Văidoaia stope. These breccia dykes reach up to 1 m width. Each individual structure was tracked on over 10 m on strike within the old mining workings, however their initial length was certainly more important abutting probably towards SE and NW to the eastern and respectively the western contact vent breccia - Cretaceous rocks (Fig. 4).

The upper course of Roşia stream is passing south of Văidoaia mining field and its catchment area is superposed on Văidoaia and Coş massifs. The actual placer deposits from Văidoaia area were investigated by Pop (2008). The processing of a quantity of 8.5 kg of alluvial sediments and the microscopic study of the concentrate obtained by panning revealed the presence of white, pink and grey quartz, garnets, magnetite, pyrite and gold. A number of 49 gold flakes were counted within the concentrate with dimensions ranging from 0.01 to 1 mm. The grade from Văidoaia placer deposit evaluated by Pop (2008) using an empirical method proposed by Goossens (1991) is about 1.2 g/t Au.

Fig. 12. Field characteristics of the breccia dyke structures from Văidoaia: a) the main N-S Văidoaia breccia dyke exposed on the northern face line of the old open pit from Văidoaia massif; note that the exploitation followed the strike of this breccia body leading to the development of the underground Văidoaia stope (*coranda*); b) closer view on Văidoaia breccia dyke; the exploitation work is located in the footwall of the breccia ore body; c) Văidoaia breccia dyke developed towards north in the underground in two branches and the image shows the vertical safety pillar preserved within Văidoaia *Coranda* between the two branches; the ceiling of the left underground stope corresponds with the hanging wall of the western breccia dyke branch; the vertical pillar is connected with the wall exposed on the left by a horizontal safety pillar supporting an upper exploitation level above, as seen also in Fig. 12a; the width of the vertical pillar is approximately 1.5 m and the thickness of the horizontal one is about 50 cm; d) Văidoaia breccia dyke as exposed on the ceiling of the surface mining works - clast supported breccia with subrounded-subangular rock fragments held together by a hydrothermal cement composed mostly of quartz; the width of the breccia dyke is approximately 40 cm. Abbreviations: Vp-vertical safety pillar; Hp-horizontal safety pillar.
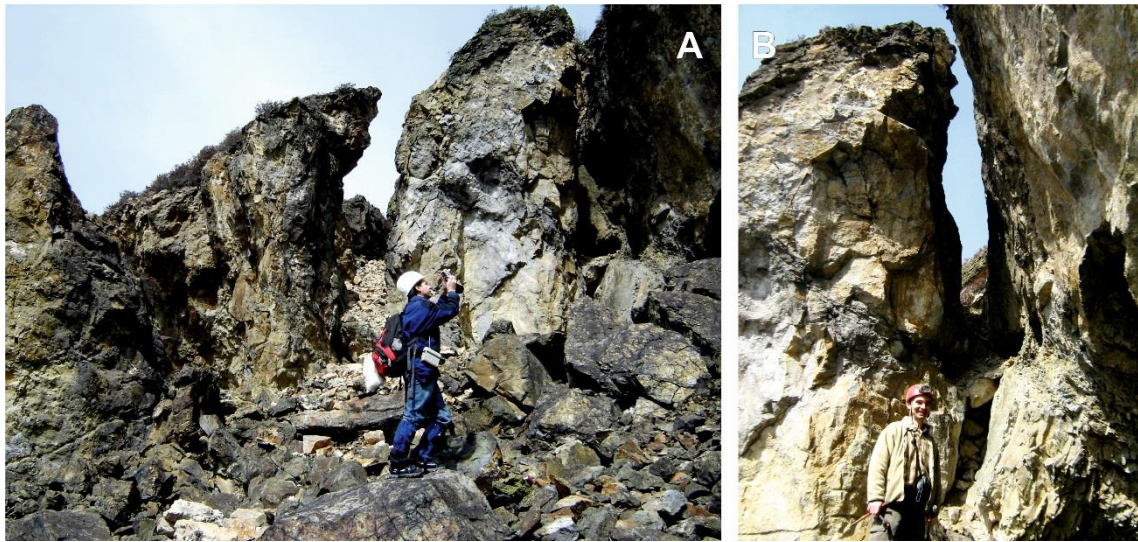
Fig. 13. Old surface extraction works from Văidoaia massif centered on breccia dyke structures: a) the traces of three surface stopes of about 6 m visible depth following three parallel breccia dykes ore bodies from the parallel breccia dyke system occurring in Văidoaia mining field; b) closer view on the south-western surface stope which followed a breccia dyke; the empty space corresponds to the extracted breccia dyke ore body; the mining of all these three breccia dykes continued downwards but the stopes are presently backfilled and no other access is available today from the underground for allowing to estimate the vertical development of the exploitation workings along these ore bodies.

5.4. Ore mineralogy

The microscopic study of the ore samples using a transmitted light polarizing microscope revealed the ore mineralogy. Pyrite is the main mineral for disseminations and stockworks, while chalcopyrite occurs subordinately. The pyrite reaches maximum 5 volumetric % in veins.

Gold was observed in veins and breccias. A quartz vein with adularia II and intense adjoining silicification of the vent breccia host rock revealed the presence of gold hosted by pyrite (Fig. 14a,b). The gold is deposited on euhedral pyrite crystals and in voids within pyrite reaching up to 60 micrometers length. A hydrothermal breccia with *chinga* cement rebrecciated and transformed in a late hydrothermal breccia with *chinga* fragments and quartz-calcite cement contains abundant pyrite and gold (Fig. 14c,d). The precious metal is enveloping tiny pyrite grains and hydrothermal quartz and calcite euhedral crystals. The largest gold grain occurs as infilling of a void among pyrite, quartz and calcite and it is measuring about 80 micrometers.

6. DISCUSSION

The dacite from Văidoaia massif has the characteristics of a lava flow. The dacite is dominated by microcrystalline groundmass with some volcanic glass. The magmatic quartz and the feldspar phenocrysts are smaller as compared with the phenocrysts found in the dacites from Cârnic and Cetate massifs. Moreover, the quartz phenocrysts are frequently broken/brecciated.

The country rocks from Văidoaia massif, i.e. Roșia Montană diatreme/vent breccia, dacite, Cretaceous sandstones show significant hydrothermal alterations. The silicification is present in all rock types and it delineates the mineralized zones. Potassic alteration affected the dacite lava and the dacite rock fragments from the vent breccia. Two types of adularia were observed, adularia I and II. The adularia I formed due to K-metasomatosis of primary feldspars while adularia II deposited together with hydrothermal quartz within the open spaces from the ore bodies. The adularia I delineates a wide K-alteration halo on dacitic substrate while the adularia II is found only within the ore bodies allowing thus the discrimination of ore zones from the "regionally" adularised dacite rocks. If potassic alteration (adularia I) increases the porosity by transforming the magmatic feldspar phenocrysts (orthoclase) into adularia the silicification increases the hardness of the rock by sealing the pores with hydrothermal quartz. The silicification is accompanied by adularia II deposition. The phyllic alteration is subordinately present.
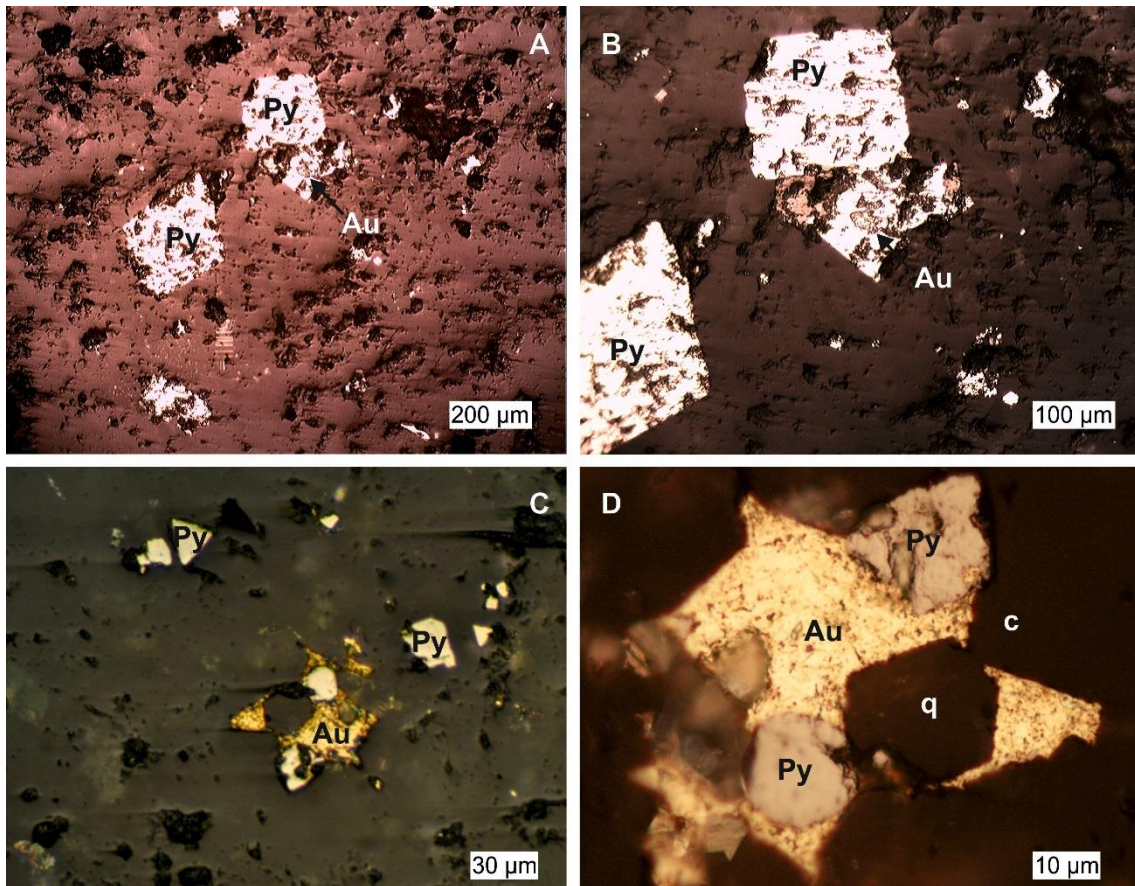
Fig. 14. The ore mineralogy from Văidoaia massif as revealed by polarizing reflected light microscopy (plane polarized light): a) general view of pyrite - gold association from a quartz-adularia II vein; b) detail of the previous image showing gold filling vugs within pyrite; c) general view of the pyrite-gold association from a hydrothermal breccia; d) detail of the previous image showing gold filling the open spaces among various other hydrothermal minerals (pyrite, quartz, calcite). Abbreviations: Au-gold; py-pyrite; q-hydrothermal quartz; c-calcite.

The relationships among the hydrothermal alterations and ore deposition indicate the following chronology: K-metasomatosis (adularia I), phyllic alteration (sericite), hydrothermal brecciation I (*chinga* cement), silicification (including hydrothermal quartz) and potassic alteration (adularia II) synchronous with a shorter time late hydrothermal brecciation with quartz and calcite cement carrying gold.

The ore bodies from Văidoaia massif were generated during the release of hydrothermal fluids along the contact vent breccia-Cretaceous sandstones. Additional pathways for the hydrothermal fluids were the breccia dyke structures, Văidoaia breccia dyke being one of them. This structure seems to extend towards SSW within the vent breccia the north-eastern contact vent breccia-Cretaceous sandstones. The stockwork zones and the breccia pockets developed close to the breccia dyke structures, which represented the main fluid circulation paths. At least two hydrothermal brecciation events took place in Văidoaia massif, the first one responsible for *chinga* emplacement, and the second one consisting in rebrecciation of *chinga* cement.

The breccia dyke structures from Văidoaia massif seem to be the result of the interaction between contrasting lithologies contact, the tectonic control and the hydrothermal activity. The parallel breccia dykes are the result of the hydrothermal fluids flow along several parallel take off planes formed by the subsidence of the vent breccia within the Roşia Montană maar-diatreme structure towards its inner part. The Văidoaia breccia dyke represents the southern extension of the contact Cretaceous basement - vent breccia. Moreover, the particular shape of the contacts between Cretaceous sandstones and the vent breccia within Văidoaia area suggests a tectonic relationship and a sinking of the vent breccia supporting the dacite remnant as compared with the Cretaceous shoulders located east and west of it. This sinking is also the reason which allowed the preservation of the dacite lava flow only in that particular area, while in the adjacent sides, due to their uplifted position both the dacite lava flows and the subjacent vent breccia were completed eroded down to the Cretaceous basement.

The mineralogical study allowed to reconstruct the paragenetic sequence of ore and gangue deposition from Văidoaia massif (Fig. 15). The precious metal deposition was apparently closely related to a late hydrothermal brecciation event. The gangue minerals are represented by quartz and calcite.
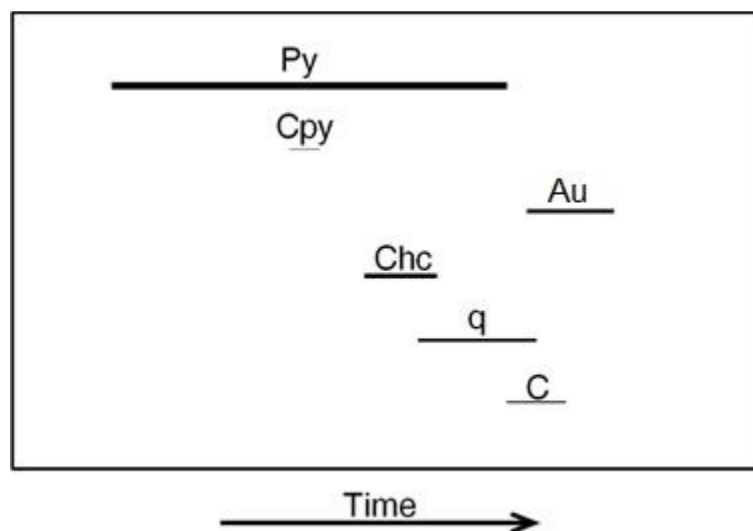
Fig. 15. Paragenetic sequence of the gold mineralization from Văidoaia massif, Roşia Montană including also the emplacement of *chinga* hydrothermal cement. Abbreviations: Au-gold; Cpy-chalcopyrite; Py-pyrite; C-calcite; q-quartz; Chc-*chinga* type hydrothermal cement.

The importance of the contact zone between the vent breccia and the Cretaceous basement was revealed by Minuţ et al. (2004) for the ore deposition control in Ţarina and Igre. Recently Tămaş (2012, unpublished) shown that the main Roman and Modern exploitation zones from Cătălina Monuleşti underground mining workings from Coş massif are located along the contact zones vent breccia-Cretaceous flysch.

On the basis of available geological information it is possible to propose a model of old mining activity. Presently, in Văidoaia massif there are evident traces of an old open pit. The surface mining developed west of the eastern contact vent breccia-Cretaceous flysch within the vent breccia. In the western part of the massif there are three elongated stopes open from the surface along three breccia dyke structures. Their intersection zone with Văidoaia breccia dyke represented the main ore zone which was exploited at the surface as indicated by the actual surface morphology. Towards ESE the open pit focused on the same breccia dykes located within the hanging wall of the contact vent breccia-Cretaceous flysch. The footwall of the contact still represents the eastern face line of the old open pit indicating that the high grade mineralization was hosted in the hanging wall. The underground development of the exploitation, precisely Văidoaia stope was created by following on strike and dip Văidoaia breccia dyke and its intersection zones with other two smaller scale breccia dyke structures. The adit starting from Văidoaia stope and heading towards west tested a silicification zone corresponding to an E-W contact between vent breccia and Cretaceous basement. This zone was affected by stockwork fissures but apparently it is low grade. This particular situation did not support the opening of a new stope.

CONCLUSIONS

Văidoaia perimeter possesses all the features of a low sulfidation Au deposit. The adularia -sericite alterations are widespread at the mining field scale being accompanied by silicification. The ore bodies are represented by breccia dykes, veins, stockworks and disseminations. Gold placers are also present along Roşia stream. The ore mineralogy is quite simple being dominated volumetrically by pyrite, accompanied by minor quantities of chalcopyrite. Gold is present in veins and breccias and it was deposited late within the available open spaces. The gangue minerals have a limited participation being represented by hydrothermal quartz, adularia, and calcite. The veins and breccia structures contain a black hydrothermal cement, known by the locals as *chinga*. At least two hydrothermal brecciation events occurred in Văidoaia area, the later one being accompanied by gold deposition.

The main control of the ore bodies' genesis was the contact vent breccia-Cretaceous flysch. Along these contact zones, the central part of the perimeter sunk towards the roots of the Roşia Montană diatreme. This sinking was gradually more important towards south or the inner part of the Roşia Montană diatreme. It developed along approximately E-W take off planes within vent breccia as well as along the western and eastern contact vent breccia - Cretaceous flysch. These tectonic lines developed later into mineralized breccia dyke structures which represented the highest grades ore bodies from Văidoaia perimeter. As a consequence, the historical mining activity focused along these breccia dyke structures and especially upon their intersection zone with the N-S striking Văidoaia breccia dyke.

ACKNOWLEDGEMENTS

REFERENCES

Balla, Z. (1987) Tertiary paleomagnetic data for the Carpatho-Pannonian region in the light of Miocene rotation kinematics. Tectonophysics, 139, p. 67– 98.

Balintoni, I., Vlad, S. (1998) Tertiary magmatism in the Apuseni Mountains and related tectonic setting. Studia Univ Babes-Bolyai, Geologie IX, p. 1 – 11.

Balintoni, I., Seghedi, I., Szakacs, A. (1997) Review of the Neogene post-collisional magmatism tectonics interplay in the intracarpathian region. Studia Univ. Babeş-Bolyai, Geologia, XLII/2, p. 33-45.

Borcoş, M. (1968) Observaţii în legătură cu determinarea condiţiilor termodinamice de formare a unor zone mineralizate şi a unor zăcăminte hidrotermale din Munţii Metaliferi (II). St. Cerc. Geol., Geof., Geogr., Ser. Geol., t. 13, nr. 1, p. 93-111.

Borcoş, M., Mantea, G. (1968) Vârsta formaţiunilor şi a activităţii vulcanice neogene din Bazinul Roşia Montană. St. Cerc. Geol., Geof., Geogr., Ser. Geol., t. 13, nr. 2, p. 363-377, Ed. Acad., Bucureşti.

Bordea, S., Ştefan, A., Borcoş, M. (1979) Harta geologică a României, sc. 1:50.000, foaia Abrud. Inst. Geol. Geofiz., Bucureşti.

Ciobanu, C.L., Cook, N.J, Tămaş, C., Leary, S., Manske, S., O'Connor, G., Minuţ, A. (2004) Telluride-gold-base metal associations at Roşia Montană: the role of hessite as gold carrier. In: Nigel J. Cook, Cristiana L. Ciobanu (eds.) - Gold-silver-telluride deposits of the Golden Quadrilateral, South Apuseni Mts., Romania. Guidebook of the International Field Workshop of IGCP project 486, Alba Iulia, Romania, 31st August - 7th September 2004, p. 187-202. (IAGOD Guidebook Series; 12).

Cozubaş, Maria, Ghergari, L., Mârza, I. (1986) Transformarea hidrotermală (faza argilitică) a vulcanitelor de la Roşia Montană (jud. Alba). Muz. Ţării Crişurilor, Crisia, XVI, Oradea, p. 541-551.

Csontos, L., Nagymarosy, A., Horvath, F., Kovaˇc̆, M. (1992) Tertiary evolution in the Intracarpathian area: a model. Tectonophysics, 208, p. 221– 241.

Csontos, L. (1995) Tertiary tectonic evolution of the intra-Carpathian area: a review. Acta Vulcanologica, 7, p. 1 – 13.

Feier, N., Groza, N., Tămaş, C.G. (2004) Breccia and vein structures in Cârnic massif, Roşia Montana ore deposit, Apuseni Mountains, Romania. Rom. Journal Mineral Deposit: "Fourth National Symposium on Economic Geology – Gold in Metaliferi Mountains", 3-5 Sept. 2004, Alba Iulia, Romania; p. 88-90.

Fodor, L., Csontos, L., Bada, G., Györfi, I. & Benkovics, L. (1999) Tertiary tectonic evolution of the Pannonian Basin system and neighbouring orogens: a new synthesis of paleostress data. In Durand, B., Jolivet, L., Horváth, F. & Séranne, M, (eds.): The Mediterranean Basins: Tertiary Extension within the Alpine Orogen. Geological Society of London Special Publication, 156, p. 295–334.

Ghiţulescu, T.P., Socolescu, M. (1940) – Les gisements sédimentaires d'or d'age tertiaire dans les Monts Apuseni. C.R., t. XXIII, (1934-1935), p. 37-46, Bucureşti.

Goossens, J.P. (1991) – Géologie minière, volume II, Exploration Minière, Fascicule B, Université de Liège, Belgique, p. 192-339.

Heinrich, C.A., Neubauer, F. (2002) Cu – Au – Pb – Zn – Ag metallogeny of the Alpine – Balkan – Carpathian – Dinaride geodynamic province. Mineralium Deposita, 37, p. 533-540.

Idriceanu, Tr., Erhan, V., Iorga, N. (1965) Consideraţiuni cristalogenetice şi geotermometrice asupra cristalelor de cuarţ din riolitul de la Roşia Montană. An. Şt. Univ. "Al. I. Cuza", Iaşi, XI, II, p. 1-6.

Leary, S., O'Connor, G., Minuţ, A., Tămaş, G.C., Manske, S. & Howie, K. (2004) The Roşia Montană deposit. In Cook, N. J. & Ciobanu, C. L. (eds.): Gold-silver-telluride deposits of the Golden Quadrilateral, South Apuseni Mts., Romania. Guidebook of the International Field Workshop of IGCP project 486, Alba Iulia, Romania, August-September 2004. IAGOD Guidebook Series, 12, p. 89–98.

Manske, SL., Hedenquist, JW., O'Connor, G., Tămaş, G.C., Cauuet, B., Leary, S., Minuţ, A. (2006) Roşia Montană, Romania: Europe's largest gold deposit. SEG Newsletter, 64, 1, p. 9-15.

Mârza, I., Ghergari, L., Nicolescu, Ş., Avram, R. (1990) Studiul petrografic – mineralogic al zăcământului auro-argentifer de la Roşia Montană (Masivul Cetate), jud. Alba. Raport (nepublicat), Arh. E.M. Roşia Montană, 42 p.

Mârza, I., Ghergari, L. (1992) L'adularisation des volcanites de Roşia Montana (Massif Cetate – Carpates Occidentales). Rev. Roum. Géologie, 36, p. 15-23.

Mârza, I., Ghergari, L., Forray, F., Tămaş, C. (1995) – The glauch-glamm formation associated to the hydrothermal deposits from the Apuseni Mountains: genetic and metallogenetic mechanism. Studia Univ. Babeş-Bolyai, Geologia, XL, 1, p. 185-194, Cluj-Napoca.

Mârza, I., Tămaş, C., Ghergari, L. (1997) Low sulfidation epithermal gold deposits from Roşia Montană, Metaliferi Mountains, Romania. St. Cerc. Geol., t. 42, p. 3-12, Ed. Acad., Bucureşti.

Minuţ, A., Leary, S., Szentesy, C., O'Connor, G. (2004) A new style of mineralization identified at Roşia Montana. Rom. Journal Mineral Deposit: "Fourth National Symposium on Economic Geology – Gold in Metaliferi Mountains", 3-5 Sept. 2004, Alba Iulia, Romania; p. 147-148.

Pécskay, Z., Edelstein, O., Seghedi, I., Szakács, A., Kovacs, M., Crihan, M., Bernad, A. (1995) K-Ar datings of Neogene-Quaternary calc-alkaline volcanic rocks in Romania. Acta Vulcanologica, 7 (2), p. 53-61.

Petrulian, N. (1934) Etude chalcographique du gisement aurifère de Roşia Montană (Transylvanie, Roumanie). Anuarul Inst. Geol. al României, v. XVI (volum festiv), p. 499-539, Bucureşti.

Pitulea, G., Ghiţulescu, I., Chiţimuş, V., Mărunţeanu, C., Mustăţea, E. (1974) Caracterele generale ale formaţiunilor extracrateriale din faza de Rotunda şi procesele de concentrare aluvionară din regiunea Vârtop – Coltău (N Roşia Montană) – Munţii Metaliferi. D.S., v. LXVII (1974-1975), p. 143-164, Bucureşti.

Pop. E., 2008. Placersuri aurifere în perimetrul Roşia Montană: evaluarea conţinuturilor de aur. Lucrare de licenţă, Universitatea Babeş-Bolyai, Cluj-Napoca, 51 p.

Roşu, E., Pécskay, Z., Ştefan, A., Popescu, Gh., Panaiotu, C., Panaoitu, C.E. (1997) The evolution of the Neogene volcanism in the Apuseni Mountains (Romania): constraints from new K-Ar data. Geologica Carpatica, 48, 6, p. 353-359, Bratislava.

Roşu, E., Seghedi, I., Downes, H., Alderton, D.H.M., Szakács, A., Pécskay, Z., Panaiotu, C., Panaiotu, E.C., Nedelcu, L. (2004a) Extension-related Miocene calc-alkaline magmatism in the Apuseni Mountains, Romani: origin of magmas. Schweizerische Mineralogische und Petrographische Mitteilungen, 84, p. 153-172.

Roşu, E., Udubaşa, Gh., Pécskay, Z., Panaiotu, C., Panaiotu, C.E. (2004b) Timing of Miocene – Quaternary magmatism and metallogeny in the South Apuseni Mountains. Romania. Rom. Journal Mineral Deposit: "Fourth National Symposium on Economic Geology – Gold in Metaliferi Mountains", 3-5 Sept. 2004, Alba Iulia, Romania, p. 33-38.

Royden, L.H. (1993) The tectonic expression slab pull at continental convergence boundaries. Tectonics, 12, p. 303–325.

Royden, L.H. (1988) Late Cenozoic tectonics of the Pannonian basin system. In: Royden, L., Horvath, F., (Eds.): The Pannonian Basin: A study in Basin evolution. AAPG Memoir, 45, p. 27– 48.

Săndulescu, M. (1988) Cenozoic tectonic history of the Carpathians. In: Royden, L., Horvath, F. (Eds.): The Pannonian Basin: A study in Basin evolution. AAPG Memoir, 45, p. 17– 25.

Seghedi, I. (2004) Geological evolution of the Apuseni Mountains with emphasis on the Neogene magmatism – a review. In: Cook, N.J. & Ciobanu, C.L. (eds.): Au-Ag-telluride Deposits of the Golden Quadrilateral, Apuseni Mts., Romania. Guidebook of the International Field Workshop of

IGCP project 486, Alba Iulia, Romania, August–September 2004. IAGOD Guidebook Series, 11, p. 5–23.

Seghedi, I., Bojar, A.V., Downes, H., Roşu, E., Tonarini, S., Mason, P. (2007) Generation of normal and adakite-like calc-alkaline magmas in a non-subductional enviroment: An Sr-O-H isotopic study of the Apuseni Mountains neogene magmatic province, Romania. Chemical Geology, 245, p. 70-88.

Tămaş, C.G. (1995) Petrometalogenia masivelor Cârnic şi Cetate şi relaţiile cu formaţiunile sedimentare. Lucrare disertaţie, Univ. Babeş-Bolyai, Cluj-Napoca, 91 p. (nepubl.).

Tămaş, C.G. (2002) Structuri de „breccia pipe" asociate unor zăcăminte hidrotermale din România. Teză de doctorat, Universitatea Babeş-Bolyai, Cluj-Napoca, 336 p.

Tămaş, C.G. (2007) Endogene breccia structures (breccia pipe – breccia dyke) and the petrometallogeny of Roşia Montană ore deposit (Metalliferous Mountains, Romania). Casa Cărţii de Ştiinţă, 230 p. (in Romanian).

Tămaş, C.G. (2010) Endogene breccia structures (breccia pipe – breccia dyke) and the petrometallogeny of Roşia Montană ore deposit (Metalliferous Mountains, Romania) 2th Edition. Editura Mega, 168 p. (in Romanian).

Tămaş, C.G., Bailly, L., Ghergari, L., O'Connor, G., Minuţ, A. (2006) New occurrence of tellurides and argyrodite at Rosia Montana, Apuseni Mountains, Romania and their metallogenetic significance. Can. Min., 44/2, p. 689-705.

Tămaş, C.G., Grobety, B., Bailly, L., Bernhardt, H.-J., Minuţ, A. (2014) Alburnite, $Ag_8GeTe_2S_4$, a new mineral species from the Roşia Montana Au-Ag epithermal deposit, Apuseni Mountains, Romania. American Mineralogist, 99, p. 57-64.

Wallier, S., Rey, R., Kouzmanov, K., Pettke, T., Heinrich, C.A., Leary, S., O'Connor, G., Tămaş, C.G., Vennemann, T., Ullrich, T. (2006) Magmatic fluids in the breccia-hosted epithermal Au-Ag deposit of Roşia Montană, Romania. Econ. Geol., v. 101, p. 923-954.

PRELIMINARY DATA ON SECONDARY COPPER MINERALS FROM THE ŞIGLĂU-URICANI PERIMETER, VÎLCAN MOUNTAINS, ROMANIA

Robert SZABO*, Gheorghe C. POPESCU**
Department of Mineralogy, Faculty of Geology and Geophysics, University of Bucharest, 1, N. Bălcescu Blvd., Bucharest,
*robert.szabo@yahoo.com, **gheorghec.popescu@yahoo.com

Abstract: The Şiglău-Uricani perimeter is located on the northern flank of the Vîlcan Mountains, within the south-western part of South Carpathians. Geologically, mostly corresponds to the Danubian realm and it is made of prehercinic crystalline schists, corresponding to the Lainici-Păiuș series and the Drăgşanu amphibolitic schists. Characteristic to this perimeter is the presence of some alpine-type quartz veins, that were exploited in quarry. The quartz has a concentration of 98.8% in SiO_2. Along with quartz, chalcopyrite and malachite were mentioned. In this perimeter, copper minerals have been observed, some of which are mentioned for the first time (cuprite, a mineral phase with similar chemistry to cuprospinel and dioptase). Laboratory analyzes (optical microscopy, scanning electron microprobe) have shown the existence of an association of secondary copper minerals generated by secondary geological processes that gave a green color specific to the quartz in this perimeter, which we have named *Green Şiglău.*

Keywords: quartz, copper, chalcopyrite, malachite, dioptase, cuprite, Șiglău-Uricani, Vâlcan Mountains.

Introduction – Geological settings

The Şiglău - Uricani Perimeter is located on the north slope of the Vîlcan Mountains, between the Uricani and Câmpu Neag localities. The access road is an industrial road, with a lenght of 11 km from the 66A national road, linking Uricani with Câmpu lui Neag. From the geological point of view, the northern flank of the Vîlcan Mountains belongs to the Danubian realm. There are mesometamorphic type, prehercinic crystalline schists. Petrologically the rock entities are grouped as follows: the Lainici-Păiuș series and the Drăgşanu series. The Drăgşanu amphibolitic series is a petrofacial entity characteristic to this mountain range, being considered a volcanic-sedimentary formation, metamorphosed under the conditions of the amphibolites facies, the staurolite-almandine subfacies, including amphibolitic gneisses, amphibolites, hornblendites, serpentinites, gneissic rocks with mica and occasionally crystalline limestones (Manolescu, 1937; Mutihac and Mutihac G., 2010).

The petrographic types of Şiglău Mt. fit into the Drăgşanu series, the Coarnele Formation (Stănoiu, 1975). The following types of rocks are found: amphibolites, amphibolitic gneisses, leptinites, quartz-feldspar gneisses, biotitic gneisses, migmatites, phyllites, quartzites with inclusions of chlorite in association with quartz and other minerals. The main paragenesis for the study area corresponds to a regional metamorphism characterized by the andesine + hornblende ± almandine mineral association within amphibolites, plus kyanite and staurolite. The age of these formations is considered late Silurian, or even Precambrian (Berza *et al*., 1988).

Characteristic of the perimeter is the quartz deposit, which between 1975 and 1992 was exploited in quarry by S.C. "Quartz - Uricani" S.A. Company. The quartz was exploited in a six step quarry digged on the peak Şiglăul Mic (1420 m) at an altitude of 740 m. The extracted quartz was transported about 23 km to the preparation station in Uricani city, where it was subjected to successive operations of reconditioning, sorting, washing, milling, magnetic separation, and other additional operations. (Visarion and Onescu, 1997).

The quartz vein from the Şiglău - Uricani perimeter

Şiglău Mt. is distinguished by the presence of quartz veins, representing one of the most important quartz veins in Romania, first signalled by Pavelescu early since 1950 (Pavelescu and Pavelescu, 1964). Subsequent research has shown that they are alpine-type veins. The exploration studies conducted with the occasion of the discovery of the main quartz vein in Şiglăul Mic, which outcrops in the east and west side, show that it has an average thickness of 12.6 meters and a length of about 500 meters.

The main orientation of the quartz bodies is ENE-WSW. Along of it, there are two more quartz veins with a thickness between 4 and 37 meters. The main deposit was explored using two galleries only at horizon 1330; the two galleries should have met each other, but the diggings were stopped when they were about 30 meters away. From the tectonic point of view, there are two major fractures in the case of the main

quartz vein, but these fractures do not influence the continuity of the vein in the direction or depth.

There is white metamorphic quartz, with a greasy lustre, a sugar-like look, and a massive structure.

Free quartz crystals were observed in cracks and/or geodes, ranging in size from 4-5 cm to 20 cm. The study of quartz crystals from the geodes showed the presence of 37 crystallographic shapes as follows: hexagonal prisms, 8 positive and 8 negative rhombohedrons, the left and right trigonal bipyramids, as well as 18 left and right trapezohedrons (Strusievicz and Balica, 1995).

Most of the main quartz vein consists of quartz with a content of 98.82% SiO_2. Changes in the chemical composition of the quartz within the main deposit, cause a variation in color, from dark grey to white. This aspect can be seen both in the bedding areas and in the roof where, (especially in the roof), there are amphibolitic schist enclaves, while quartz grains are smaller and breakable. In some places there are feldspar and chlorite inclusions.

In depth, the frequency of mineralization in quartz increases; the most common mineral is pyrite, and rarely marcasite.

From the genetic point of view, the Şiglău quartz is a metamorphic one, formed by segregation under the conditions of the green schists facies, in connection with a retromorphic process that affected the amphibolitic rocks of the Drăgşanu Series. The quartz formation is the result of the activity of hydrothermal solutions. Due to the fact that no thermobaric measurements were made on the fluid inclusions, it was assumed that the temperature and pressure of the quartz formation were 420° C and 2-3 kbars at 14 km depths (Strusievicz and Balica, 1995). We mention that for the alpine-type quartz of the Schela Formation, a region situated in north of Parâng Mt., the temperature measurements indicated 160º-180ºC, and a depth of 3.3 km. (Popescu and Constantinescu, 1982). The difference in temperature from the alpine-type quartz in Drăgşanu Series is given by the fact that the Schela Formation is an ankimetamorphic one.

Our research has been carried out on 19 quartz samples taken from the former quarry and from the access road, both situated on the north-eastern flank of Şiglăul Mic, between 900 and 1300 meters altitude. Thin and polished sections were analyzed using two polarized microscopes: Leitz Wetzlar and Optika B-150 POL; the photos of these sections were taken with a PANPHOT microscope equipped with Nikon Eclipse camera, E-400 lenses. The electron microscope analyzes were performed using a Zeiss Merlin GEMINI II, SEM-EDS (Scanning Electron Microscope – Energy Dispersive Spectrometer, Geological Institute of Romania) instrument with a working regime up to 300 nA, with a 30KV acceleration factor.

Results and discussions

The copper minerals identified by performing the microscope investigations are chalcopyrite, cuprite, cuprospinel(?), malachite and dioptase.

Chalcopyrite, $CuFeS_2$ (Plate I, Figures 1a, 1b; Plate III, Figures 3a, 3b). It is the most common of the copper minerals that have been identified in the Şiglău - Uricani perimeter. It occurs on cracks and in nests, being constantly transformed into secondary minerals. (Table 1).

Table 1 - The chemical composition of chalcopyrite from the Şiglău-Uricani perimeter, determined by SEM-EDS analysis.

Element, Wt%	s21	s22	s23
S	31.18	31.06	30.88
Fe	28.95	29.18	29.33
Cu	39.87	39.76	39.80
Total	100.00	100.00	100.00

Cuprite, Cu_2O (Plate I, Figure 1c; Plate II, Figures 2a, 2b). It is the main secondary copper mineral observed in the samples from the studied perimeter. It was formed by the oxidation of chalcopyrite from the quartz vein and it is constantly accompanied by lepidocrocite.

Table 2 - The chemical composition of cuprite from the Şiglău-Uricani perimeter, determined by SEM-EDS analysis.

Element	Wt%	Oxide	Oxide %
O	20.11		
Cu	79.89	CuO	100.00
Total:	100.00		100.00

Cuprospinel (?), $(Cu^{2+},Mg)Fe_2^{3+}O_4$ (Mandarino and Back, 2004) (Plate I, Figure 1a). In the analyzed samples a mineral phase with a chemical formula similar to cuprospinel was identified. The chemical analysis of the specimen from Şiglău-Uricani perimeter shows a similar composition to the cuprospinel of Baie Verte, Newfoundland, Canada (Nickel, 1973) (Table 3). However, the percentage of iron is lower in the case of the Şiglău sample. Silicon appears in a quantity that cannot be ignored, while the cuprospinel from Baia Verte has no silicon. Oxygen, magnesium and copper indicate closed values to the standard, also aluminum occurs in a higher percentage within the cuprospinel from the Şiglău perimeter.

Table 3 - The chemical composition of the cuprospinel(?) from the Şiglău - Uricani perimeter, Hunedoara County, Romania and the cuprospinel from Baie Verte, Newfoundland, Canada.

The chemical composition of the cuprospinel from the Şiglău-Uricani perimeter, determined by SEM-EDS analysis				The chemical composition of the cuprospinel from the Baie Verte, Newfoundland, Canada (Nickel, 1973)			
Element	Wt%	Oxide	Oxide %	Element	Wt%	Oxide	Oxide %
O	30.50			O	27,96		
Mg	1.94	MgO	3.22	Mg	1,06	MgO	1,76
Al	5.50	Al_2O_3	10.39	Al	1,18	Al_2O_3	2,23
Si	8.83	SiO_2	18.90				
Fe	24.79	FeO	31.89	Fe	47,58	Fe_2O_3	65,7
Cu	28.44	CuO	35.60	Cu	22,21	CuO	27,8
Total:	100.00		100.00	Total:			100.00

Malachite, $Cu_2^{2+}(CO_3)(OH)_2$ (Mandarino and Back, 2004) (Plate I, Figure 1d; Plate III, Figures 3c, 3d). It constantly occurs in relationship with chalcopyrite and some secondary iron minerals, such as lepidocrocite and goethite.

SEM-EDS analysis indicated a chemical composition closed to the standard values for this mineral (Table 4).

Table 4 – The chemical composition of malachite from the Şiglău - Uricani perimeter, determined by SEM-EDS analysis.

Element	Wt%	Oxide	Oxide %
C	12.95	CO_2	47.43
O	45.06		
Cu	41.99	CuO	52.57
Total:	100.00		100.00

Individual malachite crystals are very rare. In the studied samples, both individual crystals and scattered malachite on quartz were observed.

Dioptase, $Cu_6Si_6O_{18} \cdot 6H_2O$ (Mandarino and Back, 2004) (Plate I, Figure 1e, 1f; Plate III, Figure 3e). This mineral was found in the oxidation zones of the primary copper minerals (*i.e.* chalcopyrite). It can be seen with the naked eye in the form of individual crystals on quartz, as well as under the microscope.

The chemical analysis indicated a composition closed to the standard values. Manganese is the new element that occurs in the chemical composition in a significant percentage. Considering that the other elements are according to the standards, it is possible that there is a particular Mn-dioptase. Other minor elements are aluminum, calcium and iron (Table 5).

Table 5 – The chemical composition of dioptase from the Şiglău-Uricani perimeter, determined by SEM-EDS analysis.

Element	Wt%	Oxide	Oxide %
O	31.92		
Al	1.67	Al_2O_3	3.16
Si	14.48	SiO_2	30.97
Ca	2.23	CaO	3.12
Mn	11.91	MnO	15.38
Fe	1.78	FeO	2.28
Cu	36.01	CuO	45.08
Total:	100.00		100.00

Conclusions

The secondary copper minerals identified in the Șiglău-Uricani perimeter are unknown since our research, representing a novelty for the northern flank of the Vîlcan Mountains. Some of these minerals are rare in the Carpathian Mountains, for example dioptase, wich has been mentioned only in Băița-Bihor (Udubașa *et. al.,* 2002); the mineral phase chemically similar to cuprospinel is also a new mention, both for the studied area, and even for Romania. Chalcopyrite and malachite were reported by previous geological research (Visarion and Onescu, 1997).

It can be presumed that these secondary copper minerals could be the cause of the particular green color of quartz from the Șiglău-Uricani perimeter. For the moment, this is the known occurrence of a green quartz in Romania.

The green shade of the quartz, named by us *Green Șiglău* (in Romanian *Verde de Șiglău*), (Plate III, Figure 3f), may be a diffusion in the mass of white quartz of a supergene malachite *who has enormous capacity to color it* (Ramdohr, 1969).

References

Berza T., Seghedi A., Drăgănescu A. (1988) Unitățile danubiene din versantul nordic al Munților Vâlcan (Carpații Meridionali). Dări de Seamă ale Institutului de Geologie și Geofizică, 72-73/51 (1985; 1986); p. 23-41.

Mandarino A.J., Back E.M (2004) Fleischer's Glossary of Mineral Species. The Mineralogical Record Inc., Tucson, 309 p.

Manolescu G. (1937) Étude géologique et pétrographique dans les Munții Vulcan (Carpates Méridionales). An. Inst. Geol. Rom., Vol. XVIII, Imprimeria Națională, București.

Mutihac V., Mutihac G. (1990) Structura geologică a teritoriului României. Editura Tehnică, București, 424 p.

Nickel E.H. (1973) The new mineral cuprospinel (Cu^{2+}, Mg) $Fe_2^{3+}O_4$, and other spinels from an oxidized ore dump at Baie Verte, Newfoundland. Canadian Mineralogist, 11; 1003-1007, Canada.

Pavelescu L., Pavelescu M., (1964) Geologia și petrografia văii Jiului Românesc între Oslea și Petroșeni. An. Inst. Geol. Rom., Volumul XXXIII, București.

Popescu Gh., Constantinescu E (1982) Pyrophyllite from anchimetamorphic schist in the Parâng Mountains, South Carpathians, Romania; Petrogenetic significances. Published in: Crystal Chemistry of Minerals – Proceedings of the 13th General Meeting of IMA, September 19-25, 1982, Varna, p. 675 – 690.

Ramdohr P., (1969) The ore minerals and their intergrowths. Pergamon Press, Oxford, London, Edinburgh, New York, Toronto, Sydney, Paris, Braunschweig.

Strusievicz R.O., Balica C. (1995) Morphology of quartz crystals from Șiglău (Vâlcan mountains, Southern Carpatians, Romania); Studii și cercetări. Muzeul Bistrița Năsăud, Vol. 1, Mineralogie-Petrometalogenie-Paleontologie-Biostratigrafie-Geofizică, Editura Carpatica, Cluj-Napoca, p15-24.

Stănoiu I. (1975) Contribuții la stratigrafia formațiunilor paleozoice din versantul nordic al munților Vîlcan (Carpații Meridionali), cu implicații asupra părții externe a Autohtonului Danubian. Dări de seamă, I.G.R., Volumul LXII/, Tectonică, Geologie regională, p.219-256, București.

Visarion C., Onescu D. (1997) Documentație geologică privind reevaluarea rezervelor de cuarț din zăcământul Șiglău-Uricani, Munții Vâlcan, Județul Hunedoara, România. S.C. Belevion S.R.L., Divizia Geologică, București.

Udubașa Gh., Ďuďa R., Szakáll S., Kvasnytsya V., Koszowska E., Novák M. (2002) Minerals of the Carpathians. Sándor Szakáll (ed.), Granit Prague, 479 p.

Plate I

SEM-SE images: (1a) pyrite (Py), chalcopyrite (Ccp), mineral phase with similar composition to cuprospinel(?); (1b) chalcopyrite, cuprite (Cpr) și lepidocrocite; (1c) cuprite (Cpr) surrounded by quartz (Qtz) with malachite (Mlc); (1d) malachite (Mlc) and quartz (Qtz) grains; (1e) dioptase (Dpt) in quartz; (1f) dioptase (Dpt).
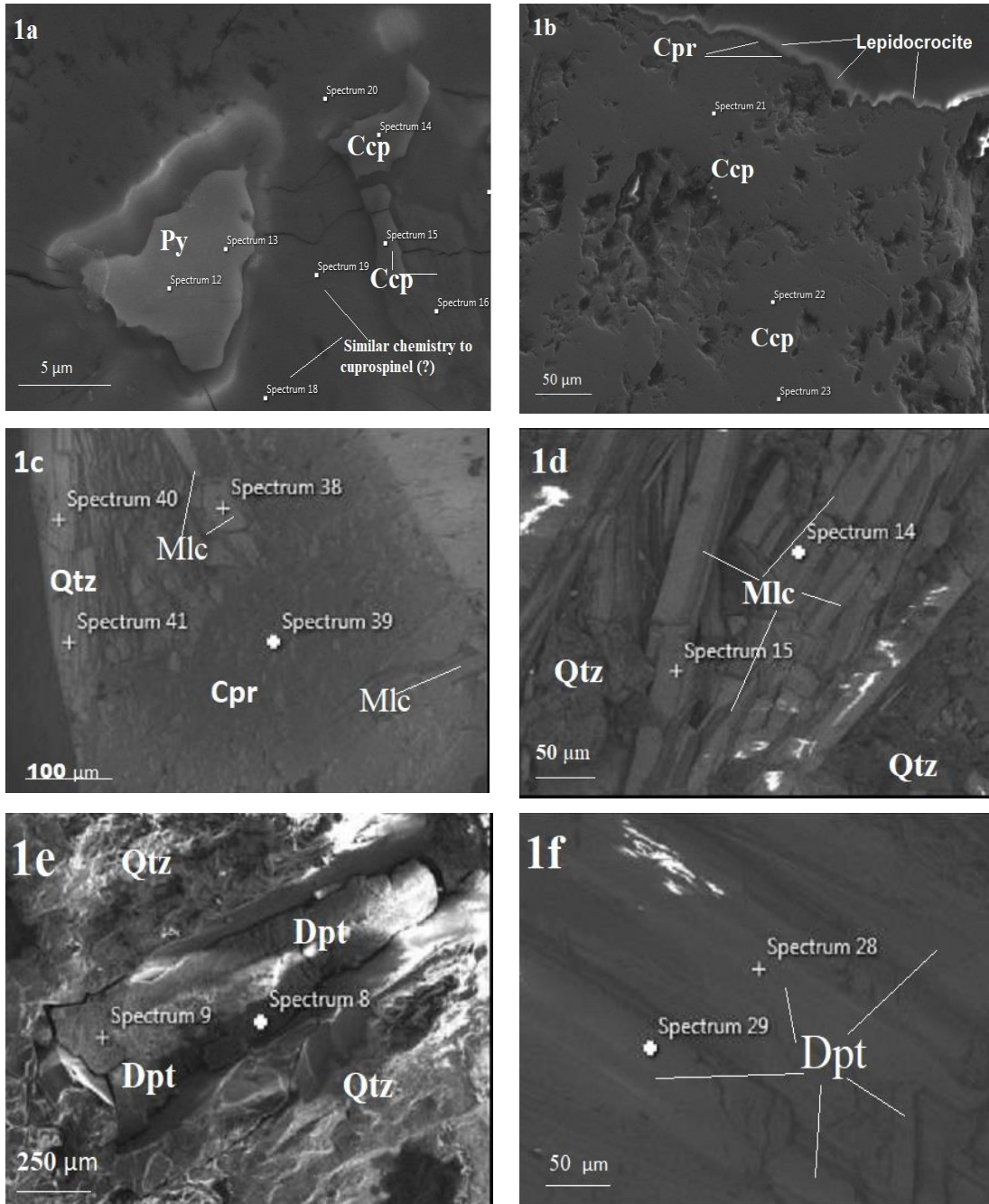
Plate II

Photomicrographs of the copper minerals identified in the Şiglău –Uricani samples: (a, b) plane polarized light – chamosite (Chm), quartz (Qtz), chalcopyrite (Ccp), cuprite (Cpr) and lepidocrocite; chalcopyrite (Ccp) surrounded by cuprite (Cpr) in quartz (Qtz); (c) crossed polarized light – cuprite (Cpr) with chamosite (Chm) in quartz (Qtz); (d) crossed polarized light – quartz with chalcopyrite, cuprite and grains of pyrite, goethite and malachite (Mlc); (e) plane polarized light and (f) crossed polarized light – cuprite (Cpr), chalcopyrite (Ccp) and goethite.
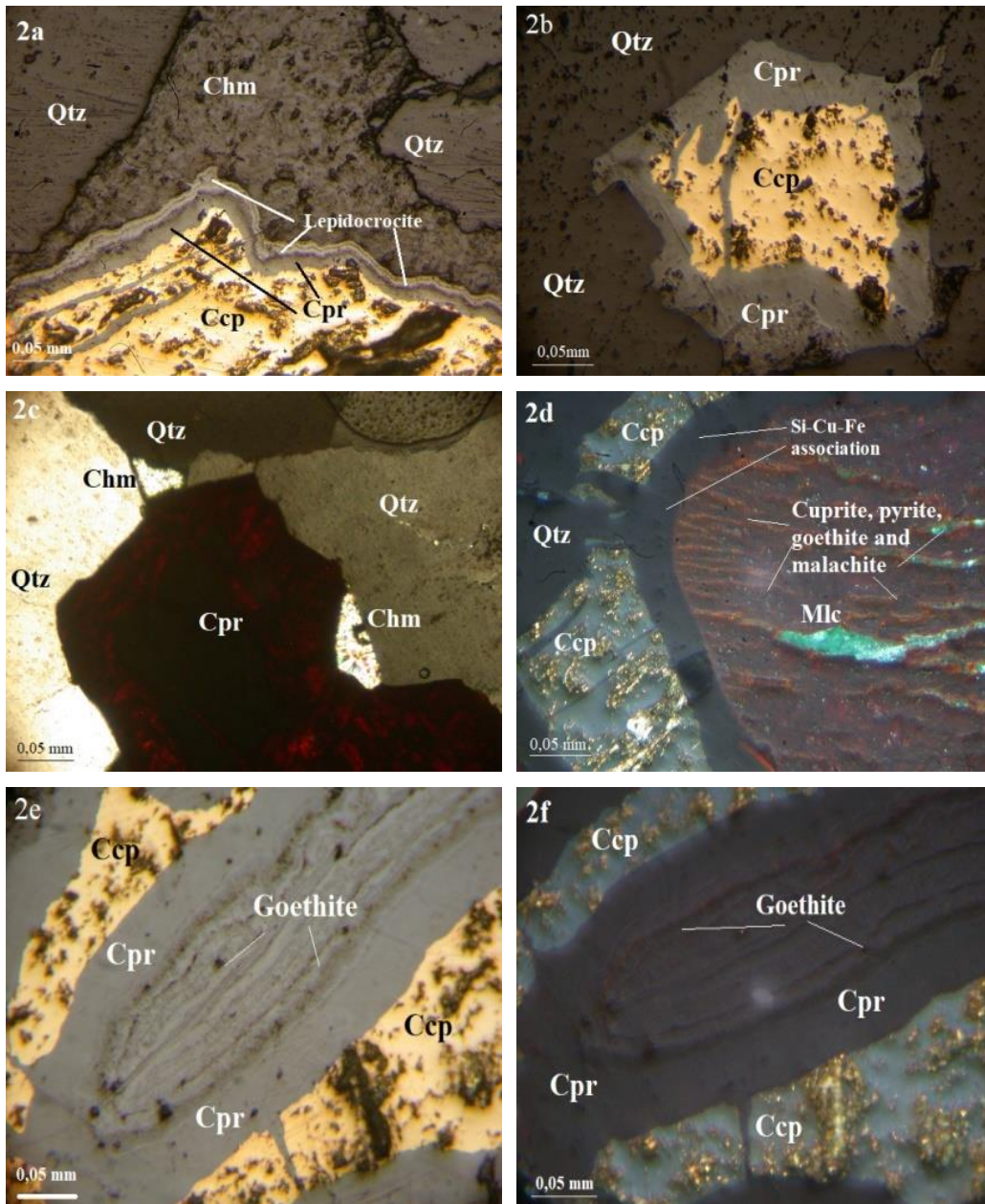
Plate III

Photographs of copper minerals from the Şiglău-Uricani perimeter: (a,b) chalcopyrite in quartz; (c) individual crystals of malachite; (d) malachite scattered on quartz; (e) dioptase; (f) illuminated quartz showing the green shade named as *Green Şiglău*.
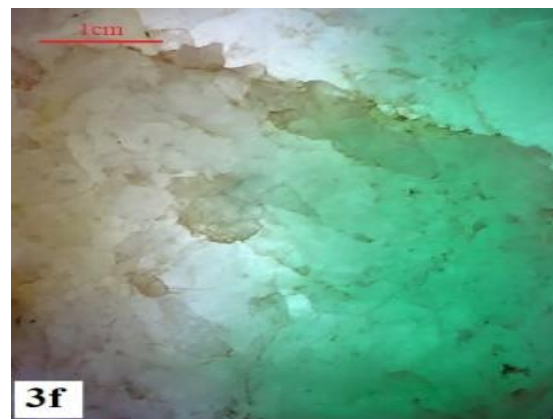
MONAZITE-(Ce) AND ITS ASSOCIATIONS FROM THE DITRAU ALKALINE INTRUSIVE MASSIF, EAST CARPATHIANS, ROMANIA

Paulina HÎRTOPANU[1*], Robert J. FAIRHURST[2], Gyula JAKAB[3], Sorin Silviu UDUBAŞA[1]

[1]Dept.Mineralogy, University of Bucharest, Romania
[2]Technical Laboratory at Lhoist North America, Inc., 3700 Hulen Street, ForthWorth, Texas 7610
[3]IG Mineral Gheorgheni, Romania
paulinahirtopanu@hotmail.com

Abstract: In the DAIC (Ditrau alcaline intrusive complex) the REE-(Y) phosphates constitute an important mineral class along that of common phosphates. The Ditrau REE-(Y) phosphates comprises two major ore minerals, xenotime-(Y) and monazite-(Ce). The REE-(Y) phosphates certainly are the most widespread of all rare-earth elements minerals from Ditrau. The monazite-(Ce) occurs as a constituent and as an accessory mineral in almost all type of rocks and ores in DAIC. There are also several silico-phosphate terms such as cheralite (which forms a series with monazite), and some limited terms between monazite and huttonite ($ThSiO_4$), named huttonitic monazite. The high level of phosphorus of the Ditrau rocks/ores, much higher than that of the crust is due to many other common phosphates from the apatite group minerals, also very widespread in many generations and in all types of ore/rocks. The chemical composition of monazite-(Ce) determined by microprobe has the following chemical variations of its main oxides (%wt): Ce_2O_3=34.0-35.0, La_2O_3=19.0-20.0, Nd_2O_3=10.0-11.0, and F=0.826. Some contents of ThO_2, Y_2O_3, Pr_2O_3, Yb_2O_3, Dy_2O_3, Er_2O_3, Gd_2O_3, Sm_2O_3, ZrO_2 and PbO were also determined. In the two main mineralized areas of Ditrau, Jolotca and Belcina, the monazite-(Ce) has different associations. In the Jolotca mineralization monazite-(Ce) occurs as a constituent mineral, in close association with apatite, magnetite, REE-carbonates and allanite-(Ce) in sulphides veins. It is not associated with the xenotime-(Y), which largely occurs in the Belcina Y, Th, Zr, U mineralization area, outside the Ditrau massif. Here xenotime-(Y) occurs as a constituent mineral, being closely associated with thorite/thorogummite, REE-apatite, Th-apatite, Fe-hydroxides, supergene collomorph Fe-oxides, chlorite, calcite, ankerite and siderite (Hirtopanu et al., 2013). In the Jolotca area, the Nb and REE-elements mineralization are predominant, the monazite-(Ce) being a constituent mineral, while the xenotime-(Y) occurs as accessory one. In the Belcina area the phosphates terms, as the apatites, are widespread, belonging to many generations, specially a late generation of Th-apatite. The biggest Jolotca occurrence from the NV of the massif is of vein type and comprises a complex sulphide mineralization and complex Ti-Nb-Fe-Mn oxides (Hirtopanu et al, 2013). The Nb mineralizations appear to be earlier than the associated sulphides-magnetite-apatite-monazite-REE carbonates, because the first Nb mineralisation is cut by the latter. Also, the two important mineralizations, that of Nb and that of REE, although they are incompatible, being formed at different stages in time, now they occur here together. The textural relationships among the Jolotca REE-ore minerals reveal the evidence of four important stages in their evolution, from oldest to newest, reflected in followings parageneses: (1) old apatite-magnetite-old monazite; (2) monazite-Ce/primary allanite-(Ce); (3) REE-carbonates/secondary allanite-(Ce); (4) the sulphide stage has ended with molybdenite, cinnabar and native mercury.

Key words: monazite-(Ce), old apatite, Th-apatite, cheralite-(Ce), allanite-(Ce), REE-rich epidote, REE-carbonates, sulphides, Nb-rutile, magmatic, metasomatic, carbothermal and hydrothermal processes.

I. Introduction

The monazite group comprises three different mineral species, i.e. monazite-(Ce), (Ce,La,Nd,Th,Y)PO_4, monazite-(La), (La,Ce.Nd)PO_4, monazite-(Nd), (Nd,La,Ce)PO_4, as a function of the dominant REE.

Monazite is a relatively uncommon mineral which was found in some terrestrial, lunar and meteoritic (chondritic) rocks. Monazite-(Ce) can primarily crystallize in magmatic (from a melt), metasomatic, hydrothermal and supergene environments. It occurs as an accessory mineral in granites, granitic and syenitic pegmatites and metamorphic rocks where it appears as isolated minute crystals, which have a great tendency to be included within biotite, garnet and apatite. The big grains/crystals of Ditrau monazite could have a metasomatic replacement/hydrothermal origin without direct contact to igneous rocks being known and termed as replacement bodies.

Until now, the monazite-(Ce) has been determined mainly in Jolotca area while xenotime-(Y) occurs frequently in Belcina area. Although, the crystal structure of monazite-(Ce) shows close relationships to that of xenotime-(Y), the difference in the predominance of some rare earth elements in their formulas is reflected in the two crystal structures. The crystal structure of tetrahedral xenotime-(Y) is isostructural with that of zircon. The Y atoms in xenotime-(Y) form 8-coordinated polyhedra which connect

isolated PO_4^{3-} tetrahedra. The structure of monoclinic monazite-(Ce) consists of PO_4^{3-} tetrahedra linked through Ce^{3+} ions. In the c-direction Ce^{3+} and PO_4^{3-} ions are irregularly surrounded by twelve oxygens belonging to at least seven different phosphates ion groups (Clavier et al., 2011). While the coordination number of the cerium atoms in the crystal structure of monzite-(Ce) is regarded as 8, which is the same as that of yttrium in xenotime-(Y), the mean Ce-O distance in monazite-(Ce), 2.45Å, is slightly larger than the mean Y-O distance in xenotime-(Y), 2.42Å. The arrangement of the PO_4 tetrahedra, which are connected by rare earth atoms in both structures, are distinct due to the differences in volumes and shapes of the rare earth polyhedra (Clavier et al., 2011). Therefore, the size of the REE-polyhedron affects the whole structure.

Monazite-(Ce) and bastnäsite-(Ce) are industrially the most important LREE minerals, mainly Ce, La and Nd, and xenotime-(Y) is a primary source for HREE, including Y, Dy, Er, Yb and Ho.

The electron microprobe data, that are presented below, were collected on a JEOL8200 instrument located at the Camborne School of Mines, University of Exeter, Cornwall, UK. Images and chemical analyses were collected using an accelerating voltage of 15KeV and 30nA beam current. X-ray spectra were collected using EDS and WDS detectors calibrated with natural and synthetic standards. Many backscattered electron (BSE) images were made, thus helping us to establish textural relationships and fine scale intergrowth of monazite-(Ce) with the other REE minerals, illustrated in the text. Many BSE images and EDS of the Ditrau monazite-(Ce) were also made, and are illustrated in this text.

II. General petrography and mineralogy of Ditrau alkaline intrusive complex

The Ditrau alkaline intrusive complex is situated within the crystalline rocks of the inner part of the East Carpathians, Romania. It has a distinct ring structure and a succession of magmatic events ranging from gabbroic and dioritic magma to syenitic and various postmagmatic events all developed between a Triassic extensional stage and a Jurassic rifting stage (Krautner & Bindea, 1995). The succession of magmatic events in Ditrau could be completed with carbonatite intrusion (?) (Streckeisen, 1960; Hirtopanu et al., 2010a) that followed after the alkaline intrusion and used the same pathways of the previous alkaline silicate melt. The main rock groups of Ditrau massif are: peridotites and gabbroids rocks, hornblendites, melanodiorites, diorites, monzonites and monzodiorites, syenites, nepheline syenites, quartz syenites, granites and lamprophyres. The rare element mineralisations are very diverse and are linked to magmatic, metasomatic and hydrothermal processes. The biggest **Jolotca** occurrence (Fig. 1) from the NW of massif is of vein type and generally comprises a complex niobian rutile – magnetite – apatite – monazite – pyrite – LREE-carbonates – sphalerite – galena – allanite – molybdenite etc. ore in calcite, dolomite and siderite gangue. The Jolotca mineralization could be linked to the carbonatites, which are often ferrocarbonatites, iron rich dolomite carbonatites, ankerite carbonatites and calcite carbonatites. These may have the field and textural characteristics of both igneous and hydrothermal rocks. The other important occurrence of vein type is Belcina, situated near the Ditrau massif, in the surrounding metamorphic rocks of Tulghes Group. The **Belcina** occurrence comprises a complex mineralization, different from those previously reported in Jolotca. It is largely constituted of Y-phosphates and Th-silicates, less REE-carbonates (with less of Ce and La), baddeleyite, zircon, Sr-carbonates, Nb, Y and REE-oxides, fluorite, barite, Fe-oxides and hydroxides, and relative less sulphides (pyrite, arsenopyrite, galena, sphalerite, chalcopyrite, tetrahedrite, cinnabar), native Hg, etc. Also, in the Belcina area the phosphate-silicate terms with high Th content are widespread. The Belcina occurrence could be the last later stage, lower temperature carbonatites intrusion (Hirtopanu e al., 2013).

The rare element minerals which have been determined in Jolotca and Belcina veins belong to the following classes (in their predominant order) (Hirtopanu et al., 2010a): *I.* LREE(Y)-carbonates: bastnaesite-(Ce), bastnaesite-(La), parisite-(Ce), parisite-(La), synchysite-(Ce), synchysite-(Nd) kainosite-(Y), thorbastnaesite, REE-Fe-Ca carbonates; *II.* Oxide minerals of Nb, Ta, REE(Y), Ti, Fe: 1. Columbite-Tantalite group: ferrocolumbite, mangancolumbite, yttrocolumbite; 2. Aeschynite group: Aeschynite-(Nd), aeschynite-(Ce), aeschynite-(Y); 3. Euxenites: euxenite-(Y), polycrase-(Y); 4. Niobian rutile; 5. Secondary Th, Ce, U oxides**:** thorianite, cerianite-(Ce), uraninite; *III.* REE-(Y)-phosphates: REE-apatite, REE-carbonate-fluorapatite, monazite-(Ce), brabantite-huttonite and huttonite-monazite series, cheralite, brockite, xenotime-(Y); *IV.* REE-(Y)-Th-Zr Silicate**s**: allanite-(Ce), thorite, thorogummite (Fe-thorogummite, Fe-Zr-thorogummite, Pb-thorogummite), cerite-(Ce), lessingite-(Ce), törnebohmite-(Ce), Th-zircon, chevkinite-(Ce), cerite-(Ce), stillwellite-(Ce) and tritomite-(Ce); *V.* Halides: Fluorite, Yttrofluorite, fluocerite; *VI.* Tellurides: Bi-Te (hedleyite) and unnamed Bi, Pb, Te mineral.
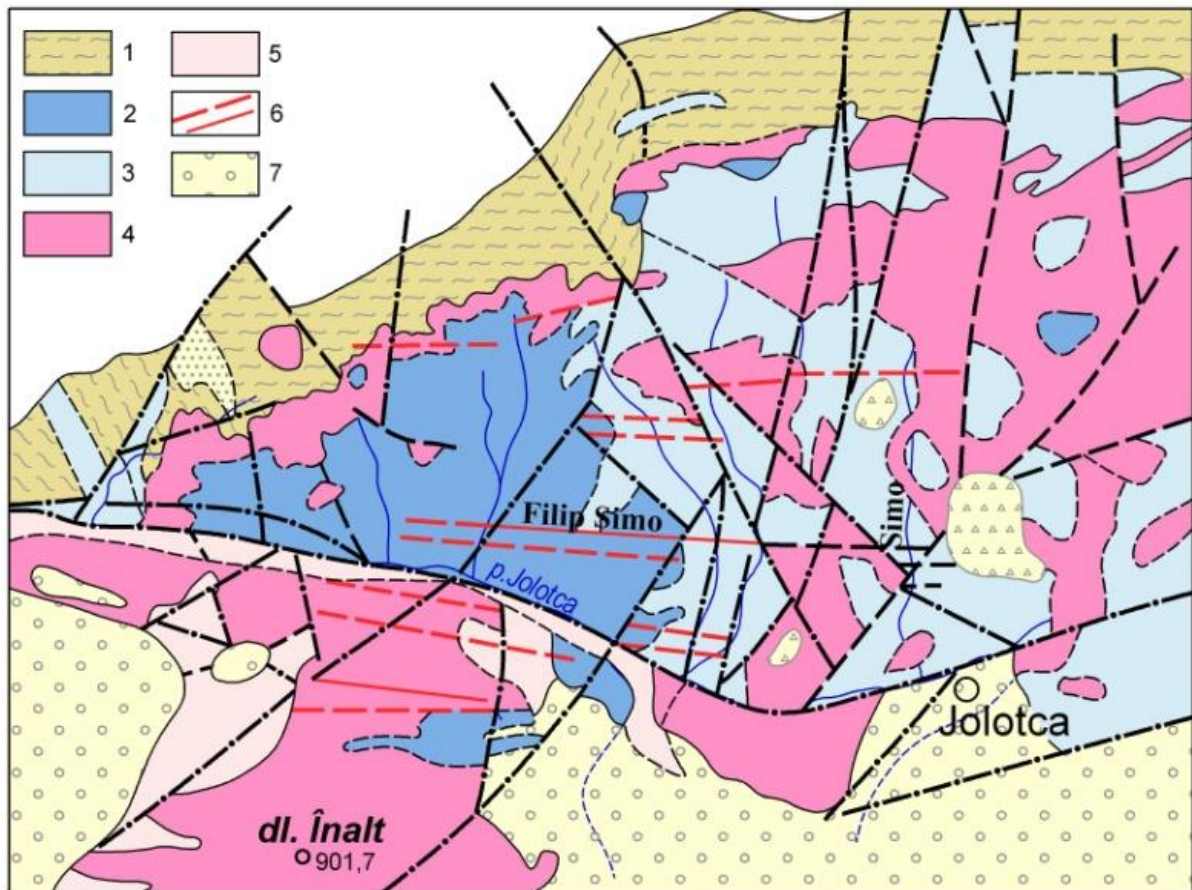
Fig. 1. Jolotca area with mineralized veins field: 1. Metamorphic rocks; 2. Hornblendite; 3. Diorite; 4. Syenite; 5. Monzonite; 6. Veins; 7. Quaternary deposits (Jakab, 2014).

III. Physical description, optical properties, textural relations, chemical composition and mineral associations of monazite-(Ce).

Monazite-(Ce), (Ce,La,Nd,Th)PO$_4$ crystallizes monoclinic. It is the predominant REE-(Y) phosphates mineral at Ditrău, especially in Jolotca area, when it occurs mostly in sulphides veins, as a constituent hydrothermal mineral. In Fig. 2 one can see two samples with monazite-(Ce), allanite-(Ce), REE-carbonates and pyrite from the Filip Simo vein (Fig. 1). The large monazite-(Ce) grains/massive aggregates measure a few cm and have a specific red brick-colour.

The ore texture in Fig. 2A, is tubular showing monazite-(Ce) in the center, followed by monazite-(Ce)+allanite-(Ce), then calcite and synchysite-(Ce) around them and finally the pyrite grown marginally. The macroscopic textural relations from Fig. 2A suggest that the monazite-(Ce) is older than the allanite-(Ce), although they seem to be intergrown. Also, in transmitted light the monazite-(Ce) appears to be older than allanite-(Ce) (Fig. 8B). The mineralized vein shows a telescoping texture (Fig.2A), i.e., the medium to low temperature mineralization, represented by sulphides, is situated outside and the high temperature mineralisation, represented by monazite-(Ce), is situated in the central part of the vein. Among them there are synchysite-(Ce)+calcite. The oldest mineralization of the Filip Simo vein is represented by niobian rutile association, which occurs as relics/exotic nests (Hirtopanu et al., 2015) inside it.

In the scanned polished thin section of sample Dt6 (Fig.3) from Filip Simo vein, the large area with red monazite-(Ce) is substituted by synchysite-(Ce) + calcite and pyrite. The green acicular allanite-(Ce) occurs separately, opposite to the monazite-(Ce), having between them a big area with synchysite-(Ce) enclosed in calcite. In the scanned image of Dt5b polished thin section in Fig. 4, the aggregates of large grains of grey monazite-(Ce), partially allanitized are grown radiary. They are enclosed together with synchysite-(Ce) in calcite. So, the monazite-(Ce) has two distinctive parageneses, with allanite-(Ce), and with REE-carbonates and pyrite, and seems to be, among all of them, the oldest mineral.

29
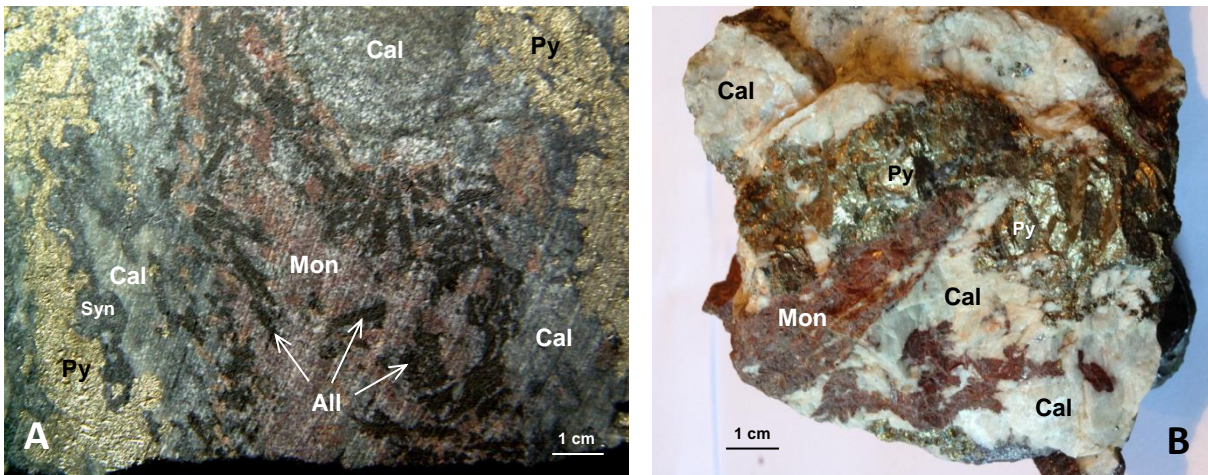
Fig.2. Macroscopical images of primary monazite-(Ce) (Mon, brick red, center) coexisting with primary allanite-(Ce) (All, black prisms), pyrite (Py, yellow), calcite (Cal, grey), synchyste-(Ce) (Syn, dark grey), sample Dt55 (A); Monazite-(Ce) (Mon, red), pyrite (Py, yellow), calcite (cal), sample Dt5c.
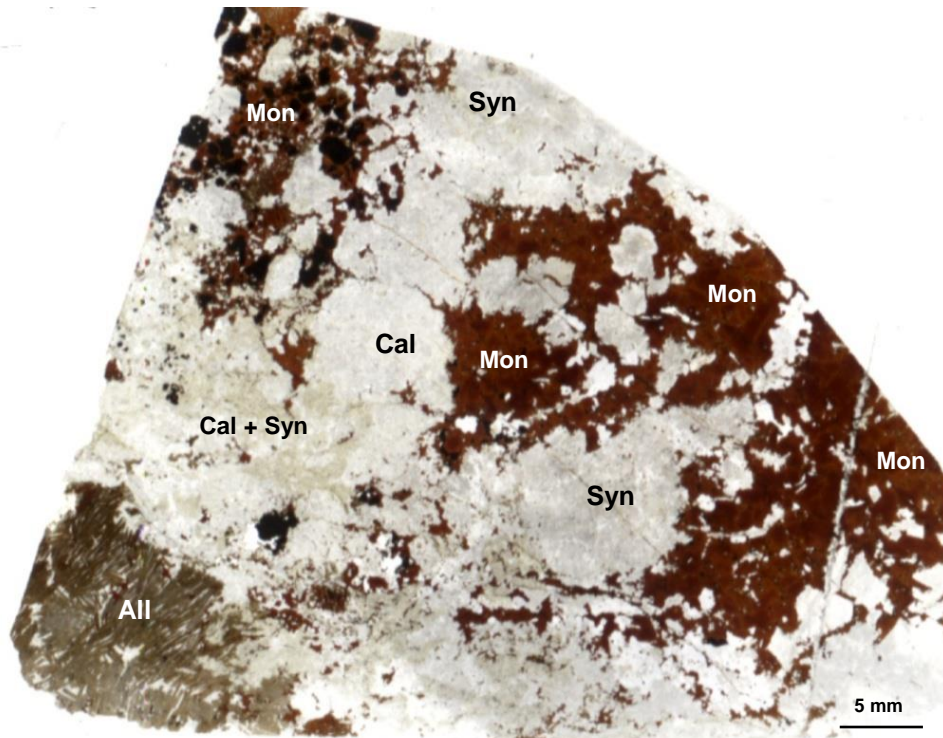
Fig.3. Scanned polished thin section: monazite-(Ce) (Mon, red, right and upper side), allanite-(Ce) (All, acicular crystals, dark brownish-grey, left corner bottom), synchysite-(Ce) (Syn, light grey), calcite (Cal, white, middle), pyrite (black), sample Dt6. See its optical image in Fig. 6A.

Typically, the monazite-(Ce) crystals are prismatic, wedge shaped (Figs. 5A, 5B, 6A and 6B). It is colourless, light yellow or light brown in transmitted light, with weak pleochroism. The refringence and birefringence are high (Figs. 5A, 5B, 6A and 6B), and they increase with the ThO_2 content (more exactly, with Th-silicate component, huttonite) in the monazite structure. The interference colours vary from third order blue to fourth order green or yellow (Figs 5A, 5B, 6A, 6B, 8A and 9A). The monoclinic monazite displays oblique optical extinction. It has a (100) moderate and a (001) weak cleavages. The twinning of monazite-(Ce) is common. The (100) twins could be large (Fig 8A) or thinly (Fig 6A). The monazite-(Ce) has a small optical axial angle, around 15º, being almost uniaxial positive. All grains/crystals are free of inclusions at 30x magnification.
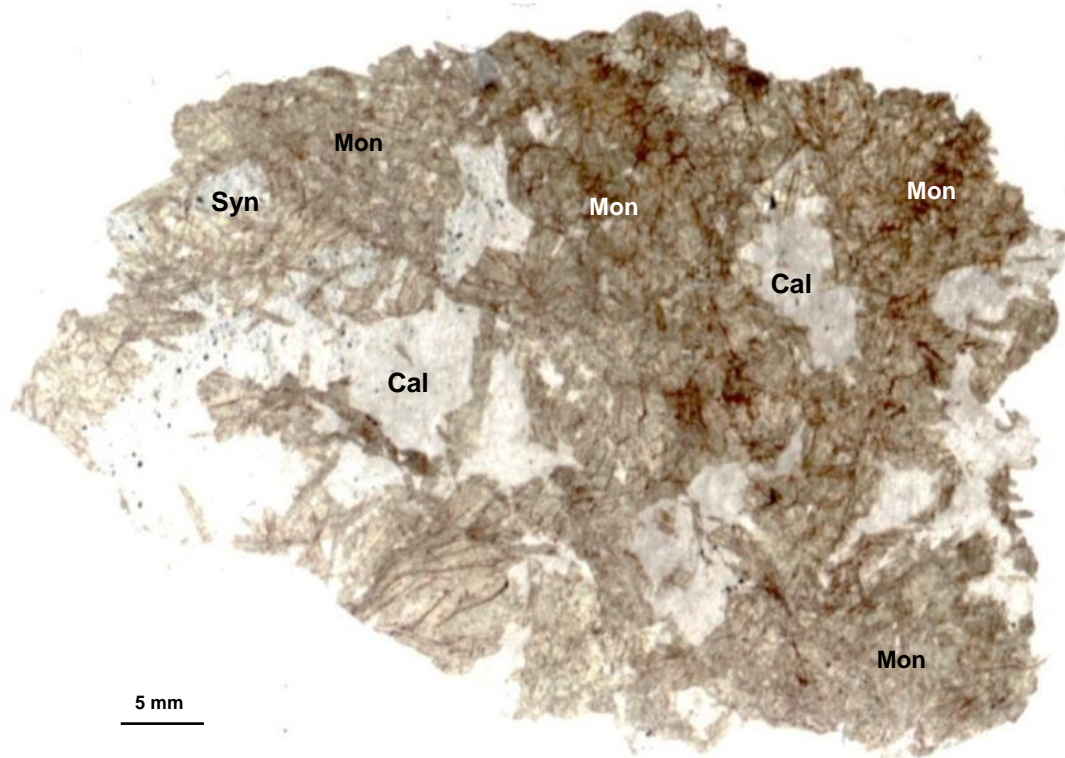
Fig. 4. The scanned image of DT5 polished thin section: monazite-(Ce) (Mon, grey-brownish, partially allanitized), synchysite-(Ce) (Syn, greysh), calcite (Cal, white), Jolotca area. See its optical images in Figs 5A, 5B and 6B.

From the optical images in Figs 7-10 one can understand the relationships of monazite-(Ce) with other minerals with which it occurs together. In Fig 7A and 7B on can see how the monazite-(Ce) is substituted by REE-rich epidote: the monazite-(Ce) remains as small monomineral lens relict in big, large crystals/grains of REE-epidote. The REE-rich epidote is an alumosilicate of Ca, Fe^{2+} and with small REE content. The Fig. 7B shows a magnification detail of this transformation: on the twinned grains of partial allanitized monazite-(Ce) grow fibrous radial aggregates of REE-rich epidote, so the twinned monazite remains as relics in them.
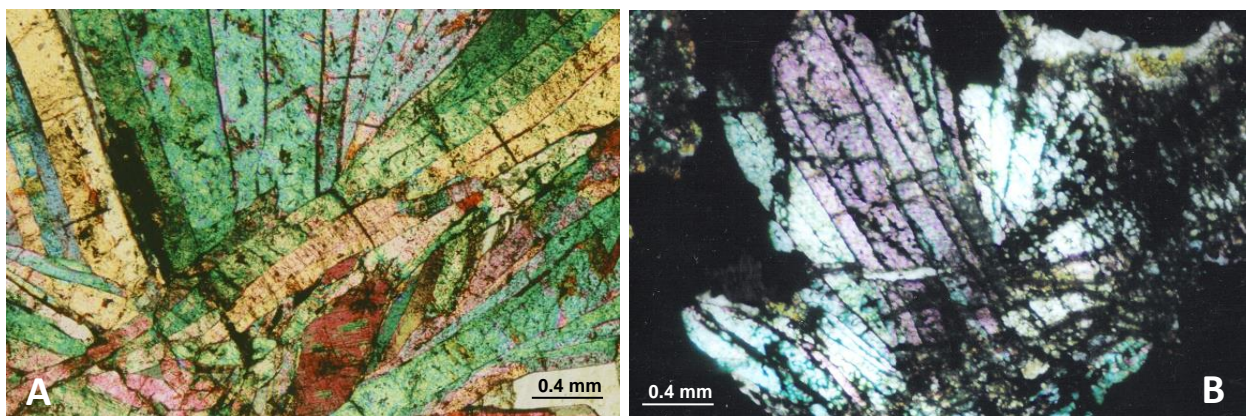
Fig. 5. Optical images of monazite-(Ce) crystals (A and B) from Fig. 4, N+, sample Dt5.
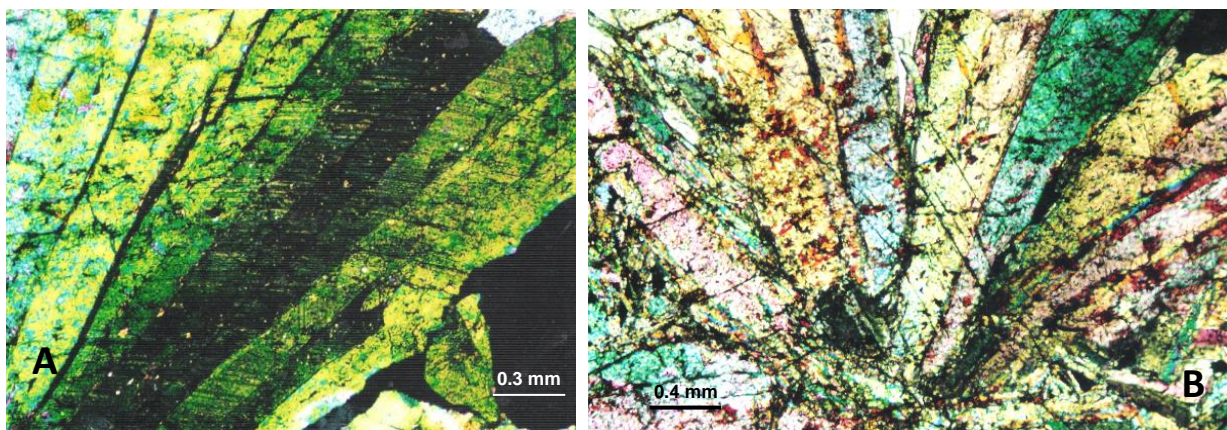
Fig.6. Monazite-(Ce), thinly twinned on (100), N+, sample Dt6 (A); radial growth of monazite-(Ce), N+, sample Dt5 (B).
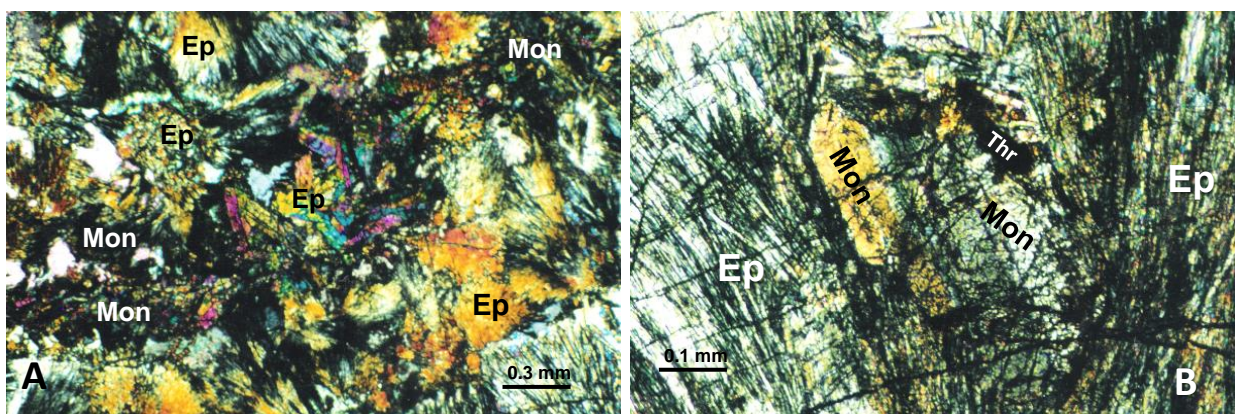
Fig. 7. Monazite-(Ce) (Mon) substituted by REE-rich epidote (Ep) (A); a magnification area from picture A with REE-rich epidote (Ep) grown on twinned monazite-(Ce), N+, sample Dt8 (B).

In Fig. 8B, the monazite-(Ce) grain is corroded by allanite-(Ce), thus the edges of the monazite-(Ce) grain appear indented and looks like a leaf. On the same monazite-(Ce) grains, simultaneous with its allanitization/substitution, parisite-(Ce) grows as grey-white spots on the monazite grains, better seen in N+ (Fig. 8B). The substitutions of monazite-(Ce) by various phyllosilicates one can see in Figs. 9 and 10. In Fig. 10B the monazite-(Ce) is substituted by yellow-black sphalerite.
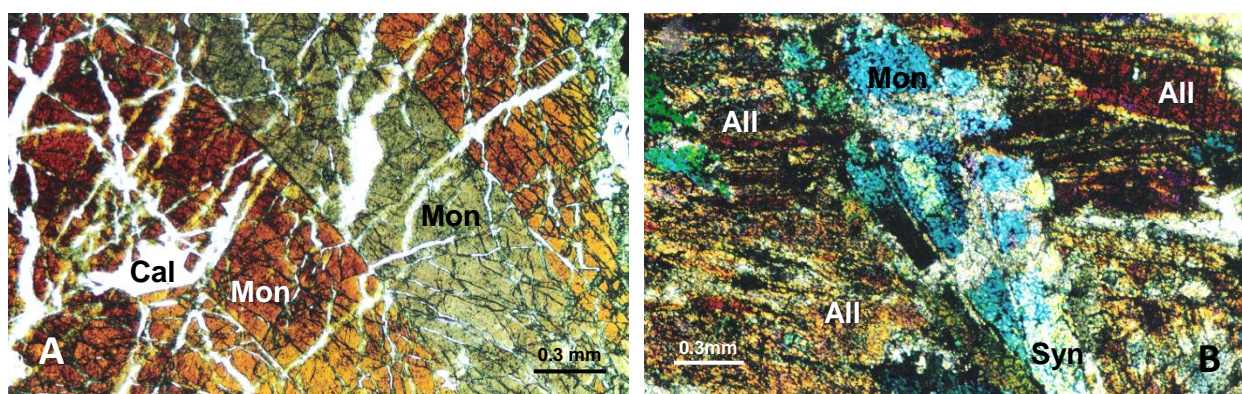
Fig. 8. Largely twinned monazite-(Ce) (Mon) cut by new calcite veinlets (Cal), N+, sample Dt26 (A); Monazite-(Ce) (Mon, middle, like a leaf) relics in allanite-(Ce) and substituted by parisite-(Ce)/synchysite-(Ce) (white spots on monazite), N+, sample Dt8b (B).

32
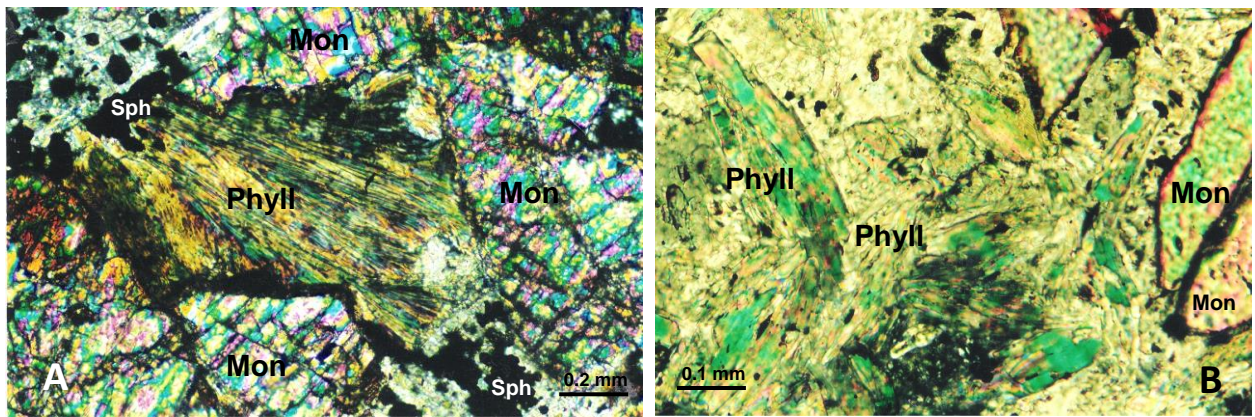
Fig. 9. Monazite-(Ce) (Mon) substituted by phyllosilicates (Phyll), N+, sample Dt24 (A); Monazite-(Ce) (Mon, right side, two prisms) substituted by phyllosilicate/auricalcite (Phyll), N+, sample 5B (B).
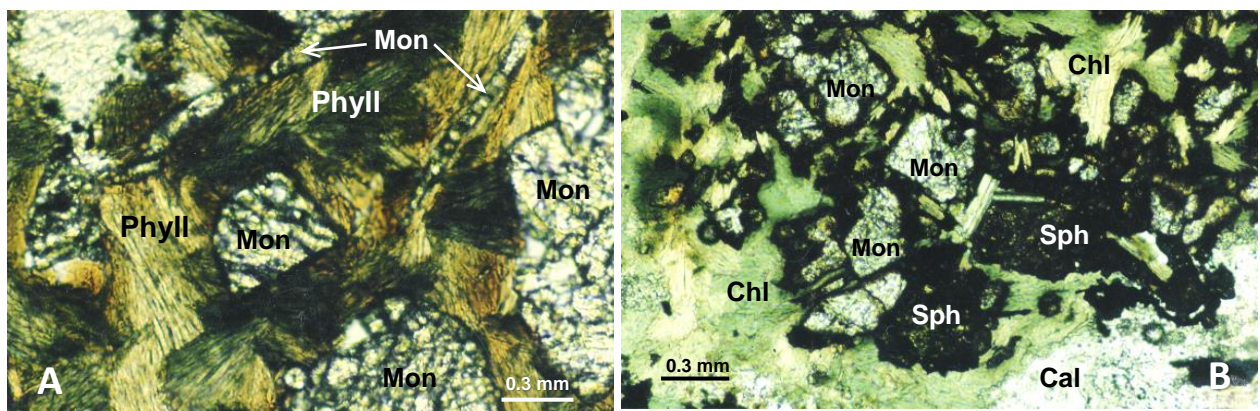
Fig.10. Relics of monazite-(Ce) (Mon) in phlogopite(?) (Phyll, green brown), NII, sample Dt24 (A); Monazite-(Ce) (grey), substituted by sphalerite (Sph, yellow-black), which in its turn is substituted by chlorite (Chl, green), NII, sample D14.

So, from textural relationships observed in transmitted light one can say that the monazite-(Ce) is substituted by allanite-(Ce), REE-rich epidote, new REE-rich phlogopite, LREE-carbonates, sulphides (especially sphalerite, molybdenite) and various phillosilicates, being older than all of these.

The textural relationships of monazite-(Ce) with its mineral associations are displayed also in many BSE images (Figs. 11, 12, 13). The monazite-(Ce) substitutes the old apatite (Fig. 11A, 12A), niobian rutile (Fig. 13B) and in its turn, is substituted by REE-rich epidote (Fig. 12B), allanite-(Ce), Ba-feldspars (Fig. 13A), aegirine and sulphides (Fig. 11B). Frequently, molybdenite grows on the cracks and cleavages of monazite-(Ce) grains (Fig. 14B). So, the monazite-(Ce) is older than allanite-(Ce), parisite-(Ce), REE-rich epidote/dissakissite-(Ce), sulphides, and younger than old apatite, niobian rutile and magnetite.

The BSE image of monazite-(Ce) substituted by the REE-rich epidote (Figs. 12B and 14A), shows its compositional variations of REE-elements reflected in its many grey shades.
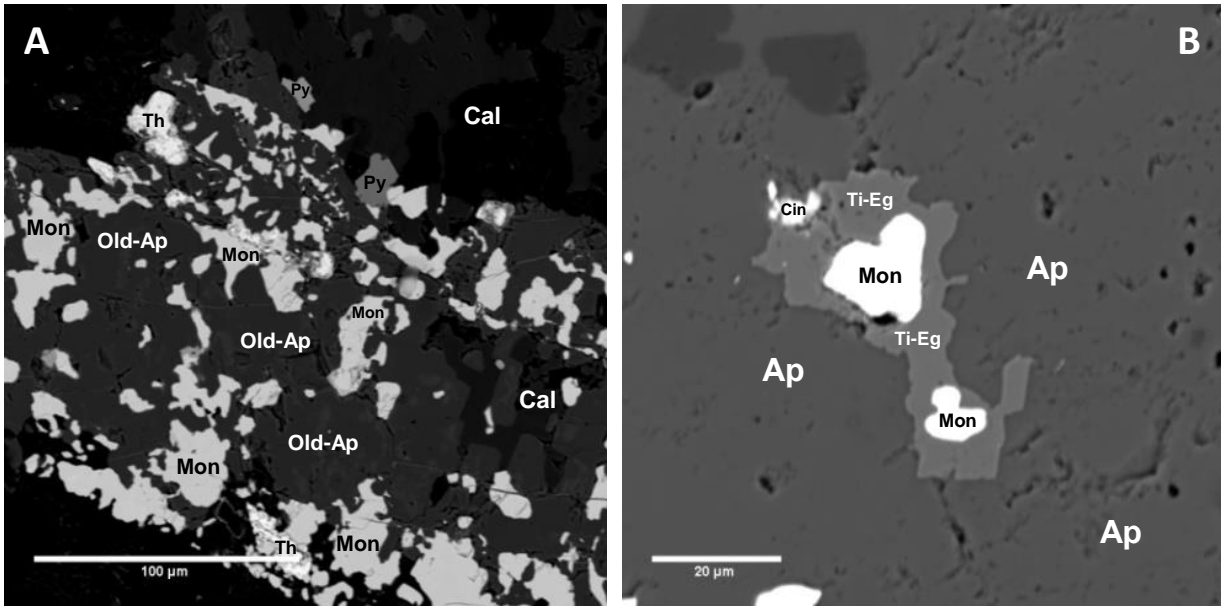
Fig.11. BSE image of the intergrowth/substitution of old apatite (Old-Ap, dark grey) with monazite-(Ce) (Mon, white grey), thorite (Th, white bright), pyrite (Py, grey, top), sample 14J1/4 (A); BSE image of monazite-(Ce) (Mon, two white grains) and cinnabar (Cin, white, small, top) enclosed in Ti-aegirine (Ti-Eg, grey), all in apatite (Ap, dark grey), sample 17J7A/4 (B).
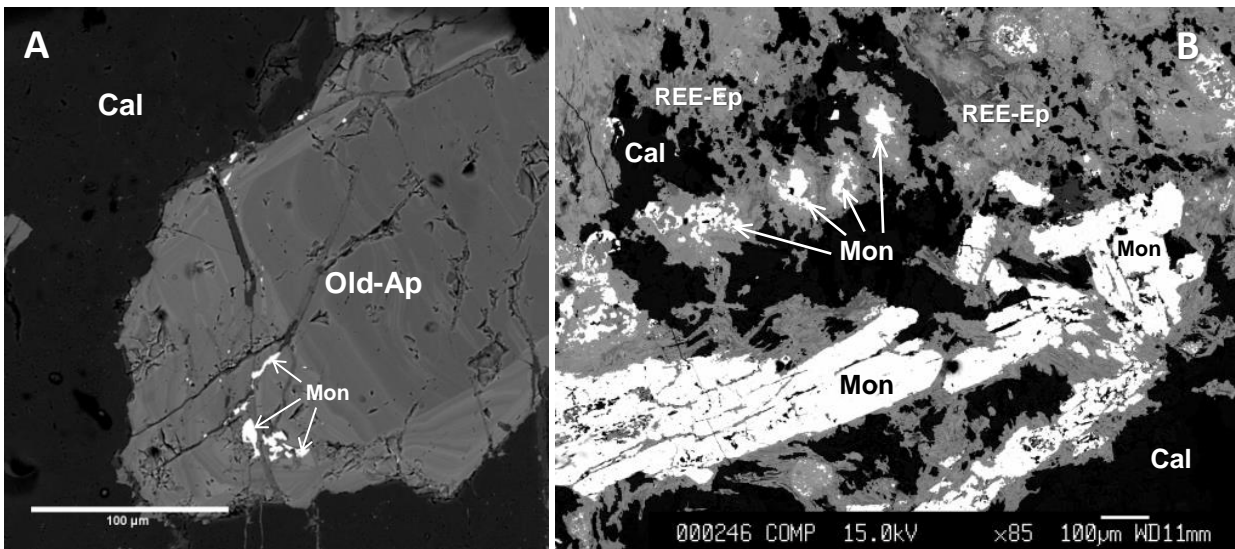
Fig.12. Zoned old apatite (Old-Ap) with Ca variations and with monazite-(Ce) on the cracks, sample 2Bel3 (A); Monazite-Ce (Mon) substituted by REE-rich epidote (REE-Ep, grey, with oscillatory composition), calcite (Cal, black), sample DT2/6 (B).
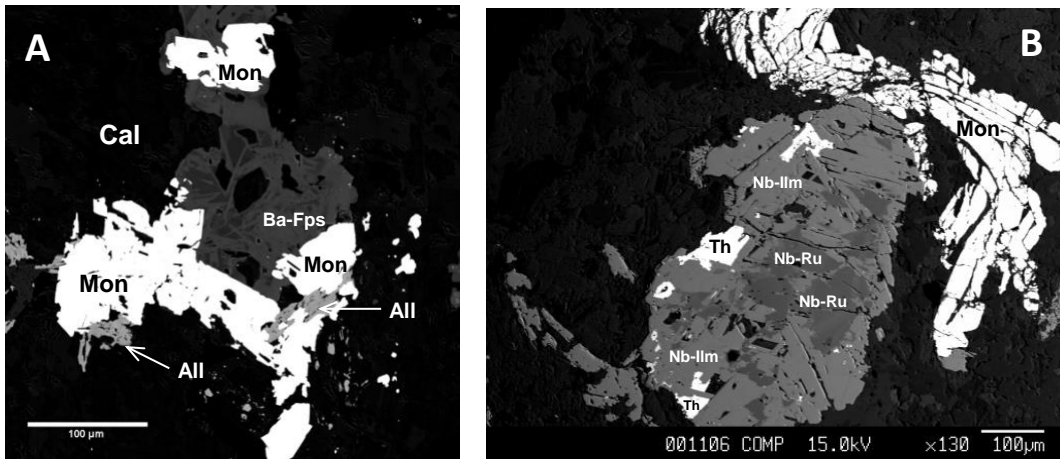
Fig. 13. BSE image of monazite (Mon, white), allanite-(Ce) (All, light grey), Ba-feldspars (Ba-Fps, dark grey with oscillatory composition), calcite (Cal, black), sample 14J1/2 (A); Monazite-(Ce) (Mon, white, top, around niobian ilmenite), niobian ilmenite (Nb-ilm), niobian rutile (Nb-Ru, grey dark, relics in Nb-ilm) and thorite (Th) on the cracks and cleavage, of Nb-ilmenite, sample Dt 37/1.
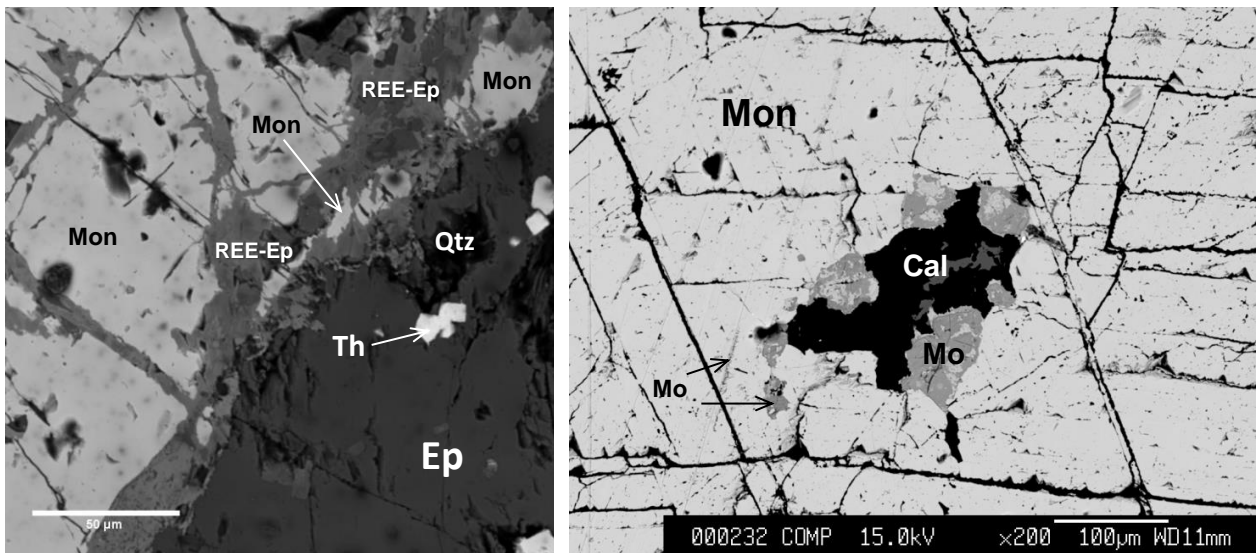
Fig. 14. Monazite-(Ce) (Mon, gray white) substituted by epidote with little Ce and Nd (REE-Ep, oscillatory composition having different grey shades) and with relics of monazite-(Ce), epidote (Ep, dark grey), thorite (Th, light white, small, enclosed in epidote) and quartz (Qtz, black), sample Dt12A/03, point 4 (A); Monazite-(Ce) with molybdenite (Mo) on cleavages and cracks, calcite (Cal, black), sample DT48, point 6 (B).

IV. Chemical Composition of monazite-(Ce)

The first microprobe analyses on Ditrau monazite-(Ce) were made by Prof. V. Bermanec at Zagreb University laboratories (Hirtopanu et al., 2000), and are presented in Table 1. All other monazite-(Ce) analyses were made at CSM, Exeter University, UK (Table 2). So, the chemistry of Ditrău monazite-(Ce) can be seen in Tab. 1 and 2. It has a high content of Ce_2O_3, followed by La_2O_3, Nd_2O_3, ThO_2, Pr_2O_3, Sm_2O_3, Gd_2O_3, Yb_2O_3 and Er_2O_3, in their decreasing order.

Also, there were analysed TiO_2, Al_2O_3, MgO, Fe_2O_3, UO_2, MnO, Dy_2O_3 which have too small/no values of content in Ditrau monazite-(Ce) and were not mentioned in Table 1. The chemical composition of monazite in Table 1 has some similarities with those of monazite from Alinci, Yugoslavia (Bermanec et al., 1988). The presence of silica (0-0.639 wt%) in Ditrau monazite indicates that Th is rather bonded at least partially as $ThSiO_4$, and not incorporated by atomic substitution. The Ditrau monazite-(Ce) may contain Th due to the presence of huttonite compound, $ThSiO_4$. There may exist a continuous substitution series between the two minerals, because the huttonite is isostructural with monazite. The substitution involves a coupled intervalence replacement $Th^{4+}Si^{4+}$ with $Ce^{3+}P^{5+}$ (Deer et al., 1963).

Table 1. Representative microprobe analyses of monazite-(Ce); sample Dt5.

Oxides (wt%)	Sample Dt5			
	1	2	9	10
SiO_2	0.333	0.314	0	0
CaO	0.087	0.135	0.156	0.384
P_2O_5	29.482	29.988	29.503	29.899
ThO_2	2.274	3.627	3.085	3.236
La_2O_3	18.663	16.108	19.036	17.839
Ce_2O_3	34.412	32.348	34.391	34.882
Pr_2O_3	2.604	2.665	2.606	2.710
PbO	0.088	0.264	0.016	0
Yb_2O_3	0.241	0.107	0.122	0.119
Er_2O_3	0.367	0.034	0	0
Gd_2O_3	0.912	1.244	0.671	0.291
Sm_2O_3	1.364	1.973	1.107	0.929
Nd_2O_3	9.814	10.921	9.024	9.536
Total	100.189	99.571	100.313	99.840

Analyst: V. Bermanec (Zagreb Univ.)

Table 2. Microprobe analyses (wt%) of Ditrau monazite-(Ce); samples: Dt19, Dt48, Dt2006/13.

Oxides (wt.%)	Sample Dt19	Sample Dt48								Sample Dt2006/13
	9A	6	7	8	9	16	17	18	21	
SiO_2	0.396	0	0.031	0	0.639	0.065	0.012	0.021	0
CaO	0.084	0.170	0.188	0.138	0.141	0.020	0.148	0.183	0.062
TiO_2	0	0	0	0.007	0.052	0	0	0	0.088
Al_2O_3	0	0	0	0.011	0	0.024	0	0	0
MgO	0	0	0	0	0.164	0	0	0	0
ZrO_2	0.075	0.082	0.067	0.061	0.030	0.073	0.088	0.06	0.099
P_2O_5	27.689	29.559	30.556	30.674	30.386	28.764	29.004	29.07	30.11
UO_2	0	0	0	0	0.028	0.025	0.057	0.048	0.009
ThO_2	0.093	1.253	1.47	1.018	1.504	1.208	1.411	1.061	0.175
La_2O_3	16.886	18.486	18.44	18.687	18.769	16.92	17.458	17.254	18.721
Ce_2O_3	28.039	32.016	31.853	33.191	32.602	30.008	29.950	29.070	31.581
Pr_2O_3	nd	nd	nd	nd	nd	nd	nd	nd	nd
Y_2O_3	0.221	0.006	0	0	0	0	0	0	0
Yb_2O_3	0.043	0	0	0.604	0	0.017	0	0	0
Er_2O_3	nd	nd	nd	nd	nd	nd	nd	nd	nd
Dy_2O_3	0.063	0	0	0	0	0	0	0	0
Gd_2O_3	2.420	2.231	2.312	2.368	2.312	1.977	1.945	1.964	2.273
Sm_2O_3	nd	nd	nd	nd	nd	nd	nd	nd	nd
Nd_2O_3	9.057	8.585	8.969	8.629	8.454	8.763	8.171	8.552	10.164
F	0.826	0.755	0.939	0.933	0.978	0.988	0.982	0.938	0.755
TiO_2	0	0	0	0	0	0	0	0	0
Nb_2O_5	0	0.003	0.029	0	0.017	0	0.003	0	0.01
FeO	0	0.136	0	0.070	0.052	0	0.023	0.040	0.137
Mn	0	0	0	0	0	0	0	0	0
PbO	nd	nd	nd	nd	nd	nd	nd	nd	nd
Total	100.234	93.338	94.414	95.759	96.071	89.028	89.262	89.978	94.201

Analyst: J. Andersen (Exeter Univ.)

A comparison of REE levels in monazite from other localities shows that the Ditrau monazite-(Ce) has a regular enrichment in LREEs with small content variations. Their values have the following variations (wt%): Ce_2O_3 = 28.03-33.19, La_2O_3 = 16.92-18.76, Nd_2O = 8.4-10.16 (Tab. 2), Pr_2O_3 = 2.60-2.71, Sm_2O_3 = 0.92-1.97 (Tab. 1); Eu_2O_3 has been not determined/detected. The majority of determined oxides belong to the light REE/Cerium or lanthanides group. Yttrium and other heavier REEs have a low oxides content: Y_2O_3 = 0-0.22, Yb_2O_3 = 0-0.60, Dy_2O_3 = 0-0.06, Er_2O_3 = 0-0.36 (Tab. 1) and Gd_2O_3 = 0.29-2.42 (Tab. 2).

The general formula of monazite-(Ce) is ABO_4. The A site usually contains large cations like $LREE^{3+}$, Y, Ca^{2+}, U^{4+}, Th^{4+}, Pb^{2+}, whereas the B-site is occupied by small cations as P^{5+} and Si^{4+} tetrahedrally coordinated (Harrison et al., 2002). In monazite-(Ce) the REEs are often largely replaced by actinides and one or two possible replacements are: $2REE^{3+} \rightarrow Ca^{2+} + (U,Th)^{4+}$, $REE^{3+} + P^{5+} \rightarrow Si^{4+} + (U,Th)^{4+}$. The Pr and particularly Nd are preferentially substituted by Ca (Cesbron, 1989). According to their size, actinides should preferentially replace the heavy REE, but no correlation between them was found. The substitution of REE trivalent elements by tetravalent actinides, with the formation of vacancies is reported to occur in natural monazite. The proposed mechanism corresponds to: $REE^{3+} \leftrightarrow 3(Th,U)^{4+} + vacancy$. The formation of vacancies seems to limit the U and Th content to a few weight percent in natural monazite. This limit was determined to be equal to 17.68 wt% ThO_2 and 15.64 wt% UO_2 (Clavier et al., 2011). The incorporation mechanism of tetravalent elements in the structure of monazite-(Ce) is described by the means of coupled substitution. This substitution leads to the formation of cheralite family. In apatite the most common substitution is: $Ca^{2+} + P^{5+} \leftrightarrow REE^{3+} + Si^{4+}$.

The Ditrau monazite-(Ce) is usually unaffected by metamictization, because its low Th and U contents. Also, strong ionic bondings in the structure of this mineral are very likely responsible for this resistance to metamictization.

The monazite-(Ce) is associated with LREE carbonates, especially synchysite-(Ce), bastnäsite-(Ce), parisite-(Ce), synchysite-(Nd) and other REE-carbonates, pyrochlore, allanite-(Ce), many sulphides, phlogopite and various phyllosilicates. Also, in the Jolotca vein mineralization monazite-(Ce) as a constituent mineral of the ore is associated with relics of exotic niobian rutile in carbonatites calcite gangue.

V. Some solid solutions of Ditrau monazite-(Ce)

Minerals of the monoclinic monazite are classified in the ternary system **monazite** (LREE PO_4) - **huttonite**($ThSiO_4$) - **brabantite** $CaTh(PO_4)_2$. Minerals which are intermediate in composition between end members monazite and huttonite are termed huttonitic monazite. Minerals which are intermediate in composition between end members monazite and brabantite are termed cheralite (LREE,Ca,Th,U)(P,Si)O_4 (Forster and Harlov, 1999).

The mixed crystals of huttonite and monazite as solid solutions occur frequently in Belcina area, where the tetragonal thorium minerals, thorite and thorogummite (Hirtopanu et al., 2013) are widespread, and less present in Jolotca area. The published compositional data provide evidence for complete miscibility in the monazite-brabantite solid solutions series and for limited miscibility for monazite-huttonite.

Brabantite-huttonite solid solutions occur as elongated small isolate crystals or in fine granular aggregates, associated with thorite, thorogummite, zircon, hematite, lepidocrocite and various common carbonates in Belcina area. It is partially metamictic. Its EDS spectrum can be seen in Fig. 15, from sample Bel7ce.
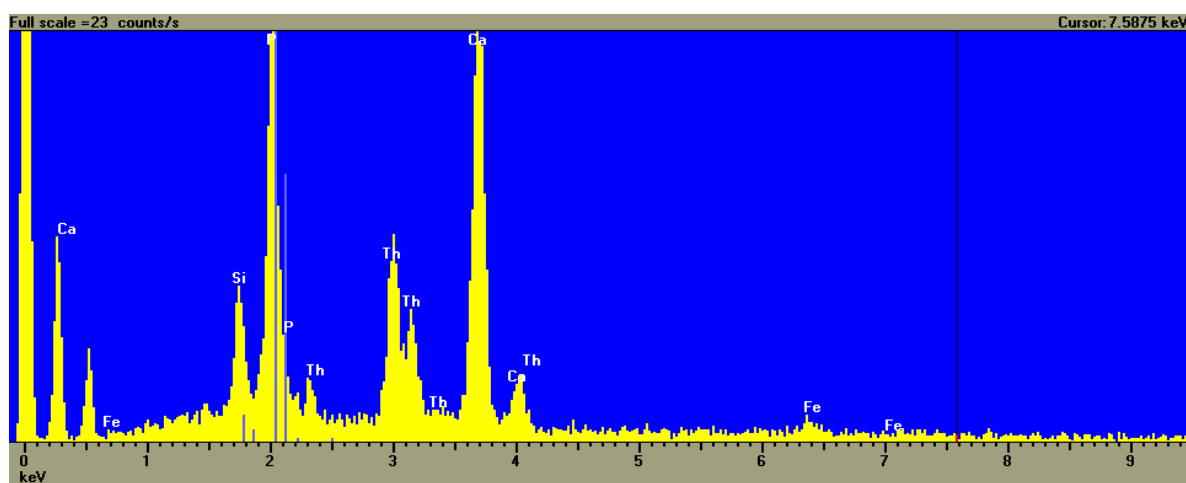
Fig. 15. EDS spectrum of brabantite/huttonite, sample Bel7ce.

The EDS spectrum from Fig. 15 looks like a mixed solid solution between brabantite and huttonite because of the presence of Si, Th and Ca and deficiency of LREE in its composition. Some small Ce and Fe contents can be seen on this EDS spectrum.

Cheralite, (LREE,Ca,Th,U)(P,Si)O₄ is an intermediary member with composition between monazite and brabantite with the formula $(Th,Ca,Ce)(P,Si)O_4$. Th-rich brabantite, monazite-(Ce) (Fig. 16) and the brabantite-huttonite term appear to represent late stage mineralizing process rather than early formed magmatic/metasomatic old monazite-(Ce). The cheralite-(Ce) is isostructural with monazite-(Ce). There is a systematic decrease of elementary cell dimensions with increase of substitutions of Ca and Ce ions by Th and U. The cheralite-(Ce) was determined with X-ray analyses and with the microprobe. Because of the Th and U contents, the grains of cheralite-(Ce) are metamictic, amorphous, and have isotropic zones. The unmetamictised areas of the cheralite-(Ce) grains have a high refringence and birefringence alike with that of monazite-(Ce).

Britholite-(Ce) (Ce,Ca)₅(SiO₄,PO₄)₃(OH,F), as independent mineral, occurs as dark brown hexagonal crystals. It is one of the oldest mineral which was crystallized in the magmatic stage, being associated with the nepheline in the alkaline rocks. In the Jolotca vein mineralization, the britholite-(Ce) seems to be altered into bastnäsite-(Ce).

Brockite (Ca,Th,Ce)(PO₄)·H₂O is a hydrothermal product, occurring in veins, together with other late minerals, as thorite, new zircon, fluorite, xenotime-(Y), new monazite, bastnäsite and apatite, and with hematite (especially in Belcina area).
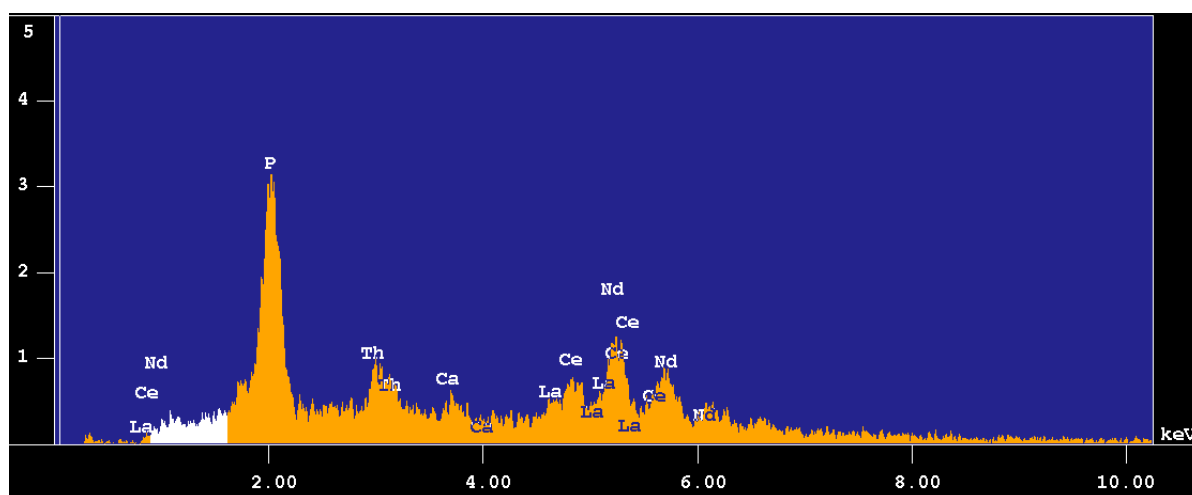
Fig. 16. EDS spectrum of monazite-(Ce) with some brabantite term, sample 7Bel10A.

VI. Genetical remarks

It is known that the peralkaline rocks are commonly characterized by extreme enrichment in alkali metals (Na, K) and high field strength elements (HFSE), such as zirconium, titanium, yttrium, niobium and REE. The formation of HFSE mineralization in alkaline rocks is poorly understood. It is generally agreed that the initial enrichment of HFSE results from magmatic processes. In some instances, magmatic processes are entirely responsible for the mineralization. In other examples, hydrothermal processes have played the dominant role upgrading initial magmatic concentrations. The fluids can be derived from carbonatites which significantly postdate the first intrusion. The carbonatites are igneous rocks that contain more than 50% carbonate minerals. They are originated in CO_2 rich and SiO_2 poor magmas from the upper mantle. Intrusive carbonatites are commonly surrounded by metasomatically altered rocks, enriched in Na and/or K. These desilicified zones, known as fenites, develop as result of reaction with Na, K rich fluids produced from carbonatites intrusion. The REE-(Y) deposits associated with peralkaline rocks are typically relatively low grade, although they are commonly enriched in Yttrium and HREE.

The Jolotca mineralization is polygenetic, being formed in many stages:

A. Magmatic process with exotic niobian rutile, originated from upper mantle, with later exsolutions/unmixed of aechynite-(Ce), aechynite-(Nd), aeshynite-(Y), euxenite-(Y), polycrase-Y, fergusonite-(Y), yttrocolumbite, ferrocolumbite/manganocolumbite/columbite, in niobian rutile/ilmenite intergrowth, from an old common solid solution (Hirtopanu, 2015).

B. Magmatic -metasomatic stage with old magnetite, old apatite, old zircon, old monazite-(Ce), which follows as later mineralizing process the previously one.

C. Hydrothermal/carbothermal stage with mostly large crystals of monazite-(Ce), that cut the old magnetite-apatite association being later than the last one, belonging to a new genetical process; REE-

carbonates: bastnäsite-(Ce), bastnäsite-(La), parisite-(Ce), synchysite-(Ce), old allanite-(Ce) and a new generation of apatite. This stage upgrades the two previously processes.

D. To the hydrothermal (of lower T) processes belong various sulphides, new Ce-apatite, new Th-apatite, xenotime-(Y), thorite/thorogummite, hydrothermal zircon/cyrtolite, hematite/goethite, many and various REE-rich alumosilicates of Ca, Fe^{2+}, plyllosilicates, many and various common carbonates (of Ca, Mg, Fe, Sr and Ba), and large chlorite varieties.

E. Secondary REE-carbonates, grown on monazite-(Ce) and secondary allanite-(Ce), grown on monazite-(Ce).

VII. Conclusions

The microscopic investigations and by means of microprobe of many samples showed that the Ditrau vein mineralization is polyphasic.

The mineralized veins of Jolotca area are situated predominantly in the hornblendite and diorite areas. No genetical affiliation has been observed between the mineralized veins and the host rocks. The mineralogical composition of the veins is extremely variable, but the main components are sulphides, REE-carbonates, monazite-(Ce), allanite-(Ce) and Nb-Ta-Ti-Fe minerals. The sulphides occurring in Jolotca veins are various, about 40 species were recently determined (Hirtopanu et al., in press). In the association magnetite-sulphides, the first one is older. The pyrite, monazite-(Ce) and REE-carbonates are sometimes associated with older exotic ilmenite - Nb-rutile (as nodules) which represent around 3% of all mineralized vein in the Filip Simo vein, and around 6-7% in the Toth Vesze vein (Hirtopanu et al, 2015).

The Ditrau monazite-(Ce) has been formed under a variety of conditions. The old monazite-(Ce) has crystallized in magmatic phase, and it has now irregular shapes. Also, it has many various inclusions. The hydrothermal monazite-(Ce) is predominant in Ditrau, and its spectacular appearance was described in this paper. It has no inclusions. It constitutes an important economic resource. The youngest secondary monazite-(Ce) has been formed by alteration of allanite-(Ce) and REE-carbonates in supergene environments.

Rare earth mineral deposits produced by primary crystallization from a carbonatite magma are rare, hydrothermal REE mineralizations being much more common. The Ditrau monazite-(Ce) occurs in Jolotca hydrothermal/carbothermal veins accompanied by bastnäsite-(Ce), bastnäsite-(La), parisite-(Ce), synchysite-(Ce), allanite-(Ce), apatite, magnetite, many sulphides (predominantly pyrite) and fluorite. Among these all rare earth minerals, the monazite-(Ce) aggregates seem to be the oldest, because they are cut by sulphides and are substituted by allanite-(Ce) and REE-carbonates. Low temperature hydrothermal solutions may cause the breakdown of monazite-(Ce), thus releasing REE to form secondary rare earth minerals. Secondary allanite-(Ce), many secondary REE-carbonates, REE-rich epidote, REE-rich phillosilicates and chlorites could be formed in this way through replacing monazite-(Ce). The mineralization may have formed by one or by a combination of two agents: (1) hydrothermal solutions originating from the nearby granitic to sienitic rocks and (2) by carbonatitic magma.

The vast majority of rare earth minerals resources are associated with three minerals: monazite-(Ce), bastnäsite-(Ce) and xenotime-(Y). Bastnäsite-(Ce) and monazite-(Ce) are the primary source of LREE, mainly Ce, La and Nd, and xenotime-(Y) is a primary source for HREE, including Y, Dy, Er, Yb and Ho. The Ditrau mineralized area comprises both type of mineralizations with separate localization: Jolotca, enriched in LREE minerals, and Belcina, enriched in HREE.

Refrerences

Bermanec V., Tibljas D., Gessner M., Kniewald G. (1988) Monazite in Hydrothermal Veins from Alinci, Yugoslavia. Mineralogy and Petrology, v.38, p.139-150.

Cesbron F.P. (1989) Mineralogy of the Rare Earth Elements. Lanthanides, Tantalum and Niobium. Ed.: P. Moller, P. Cerny, F. Saupe. Springer-Verlag, Berlin, New York, London, Paris, Tokyo, 380p.

Clavier N., Podar R., Dacheaux N. (2011) Crystal chemistry of the monazite structure. Journal of European Ceramic Society, v.31, p. 941-976.

Deer W.A., Howie R.A., Zussman J. (1963) Rock forming minerals. V. 5, Longmans, Londra.

Foster H.J., D.E. Harlov (1999) Monazite-(Ce)-huttonite solid solutions in granulite facies metabasites from the Ivrea-Verbano Zone, Italy. Mineralogical Magazine, Vol. 63, (4), p. 587-594.

Hîrtopanu Paulina, Bermanec V., Udubaşa G., Melgarejo J.C. (2000) Monazite and allanite from the Ditrău alkaline massif EastCarpathians, Romania. The 4th Symposium of the GSR, Baia Mare, An. Inst. Geol., v.72, Special Issue, p. 41, Bucureşti.

Hirtopanu Paulina (2006a) One hundred minerals for one hundred years (dedicated to the Centennial of the Geological Institute of Romania). Ed. Cartea Universitara, 94p, Bucuresti.

Hirtopanu Paulina (2006b) One hundred minerals for one hundred years (dedicated to the Centennial of the Geological Institute of Romania). 3rd Conference on Mineral Sciences in the Carpathians, Miskolc Hungary, Acta Min. Petr. Univ. Szeged Hungary, Abstr. Series 5, pp. 86.

Hirtopanu Paulina, Andersen J.C., Fairhurst R.J. (2010a) Nb, Ta, REE(Y), Ti, Zr, Th, U and Te rare element minerals within the Ditrau alkaline intrusive complex, Eastern Carpathians, Romania. Mineralogy of Szekelyland, Eastern Transylvania, Romania. Ed. by Sandor Szakall and Ferenc Kristaly, Tg Mures, pp. 89-128.

Hirtopanu Paulina, Andersen J.C., Fairhurst R.J. (2010b) Nb, Ta, REE(Y), Ti, Zr, Th, U and Te rare element minerals within the Ditrău alkaline intrusive complex, East Carpathians, Romania. 20th General Meeting of the International Mineralogical Association (IMA), 21-27 August 2010, Budapest, Hungary, CD Abstracts, p.570.

Hirtopanu Paulina, Jakab G., Andersen J.C., Fairhurst R.J. (2013) Thorite, thorogummite and xenotime-(Y) occurrence in Ditrau alkaline intrusive massif, East Carpathians, Romania. Proc. Rom. Acad. Series B, 15(2), p.111-132.

Hirtopanu Paulina, Jakab G., Fairhurst R.J. (2015) Niobian rutile and its associations at Jolotca Ditrau alkaline intrusive massif, East Carpathians, Romania. Proc. Rom. Acad., Series B, 2015, 17(1), p. 39-55.

Jakab, Gy. (1998) Geologia masivului alcalin de la Ditrău. Miercurea Ciuc. Ed. Pallas-Akademia. 297p.

Jakab, Gy. (2014) Geneza masivului alcalin Ditrau si zestrea sa minerală. Unpubl. manuscript.

Krautner H., Bindea G. (1995) The Ditrau alkaline intrusive complex and its geological environment. Rom.J. Min, 77, Suppl. 3, pp 44, Bucuresti.

Miyawaki, R., Nakai, I. (1993) Crystal structures of rare-earth minerals. Rare Earths, No 21, p.1-18.

Streckeisen A. (1960) On the structure and origin of the Nephelinsyenite Complex of Ditro (Transylvania, Roumania). Rep. 21st IGC, V.13, p. 228-238.

THE MAGMATIC-HYDROTHERMAL HISTORY OF THE β-QUARTZ POLYMORPHS FROM ROȘIA MONTANĂ DACITE INFERRED BY SOLID-, MELT-, AND FLUID INCLUSION ASSEMBLAGES

Ioan PINTEA[1*], Elena Luisa IATAN[2]
[1]Geological Institute of Romania, Cluj-Napoca branch, Romania
[2]Institute of Geodynamics of Romanian Academy, Bucharest, Romania
* *ipinteaflincs@yahoo.com*

Abstract: The quartz phenocrysts from Roșia Montană show distinct oscillatory zonation which together with epithermal quartz crystals, recorded the entire geological history of the Au-Ag ore deposit. Silicate melt inclusion homogenized at high temperatures up to 1370ºC for a basic composition and between 786º-939ºC for the acidic rhyolite/dacite melt. Complex silicate/silicate±sulfide, silicate/salt melts inclusions were homogenized between 1050º and 1200ºC. Secondary brine and fluid inclusions were formed in magmatic quartz in "situ" after α/β transition. A vapor-rich inclusion trapped for example at 535ºC and 0.5kb having salinity of 0.7 wt% NaCl eq. must be coexistent with brine of 45 wt % NaCl eq. which is in accord with measured Th and salinities. Aqueous fluid inclusions with salinity between 0.18-3.23 wt% NaCl eq., homogenized between 180º-290ºC in both epithermal and magmatic quartz phenocrysts. The study suggests that two vectors determined the scavenge and precipitation of ore elements: (1) a hydrosilicate alkali-rich melt at high P-T and (2) a gaseous mixture of H_2O-CO_2-CH_4-H_2S at neutral-pH in low-temperature and low-salinity aqueous-rich fluids. Zircon and apatite are the main solid microphenocrysts embedded in the magmatic quartz phenocrysts and they could be used as timing and stratigraphic tools for the magma chamber crystallization history.

Keywords: fluid and melt inclusions, solid inclusions, quartz phenocrysts, internal zonation, microthermometry, cathodoluminesce, epithermal Au-Ag deposit, Roșia Montană, Metaliferi Mountains, Romania

1. Introduction

The main goal of this work is to decipher the magmatic-to-hydrothermal history of the Roșia Montană Au-Ag ore deposit from the solid-, melt-, and fluid inclusions trapped in β-quartz phenocrysts and additionally the fluid inclusions from epithermal quartz crystals. The study is based upon petrography, microthermometry, optic-microscopy cathodoluminescence (OM-CL) and chemical analyses (EPMA). A specific internal microtexture is revealed by the presence of two main zones which defined two different processes in the β-quartz phenocrysts: a dissolution or resorption layer caused by hot magmatic influxes in the crystallizing magma chamber, and secondly the formation of a large growth zone after magma homogenization. These were successively repeated as shown by an oscillatory zonation. Each zone contains specific silicate melt inclusions characterized by different composition and temperature. High values of homogenization temperature were recorded in the resorption layers up to 1370ºC specific for a deep and hot basic magmatic influx and much lower temperature between 786º-939ºC characterizing the growth condition from a more acidic (rhyolite-dacite) magma composition. Complex mixture of silicate/silicate±sulfide and silicate/salt melts, were trapped heterogeneously and formation temperatures from 1050º to 1200ºC, were recorded. This is the first attempt to describe such complex melt inclusions in the magmatic quartz phenocrysts from Roșia Montană. The second important topic of this paper is related to the secondary processes which generate "in situ" several types of fluid inclusions after repeated α/β transition supported by the magmatic quartz phenocrysts. They are represented by specific "sweat" halos formed around the primary silicate melt inclusions, clusters and trails decorating the recicatrized microfissure planes. These were overprinted by late epithermal processes which change the initial content of the primary silicate melt inclusions by strong alteration effects. As the main result of these transformations was the generation of "in situ" various secondary brine-, and fluid inclusions described only in the magmatic quartz phenocrysts. All the previous studies dedicated to fluid inclusions at Roșia Montană revealed that secondary fluid inclusions from magmatic phenocrysts and primary (pseudosecondary) inclusions from the epithermal quartz crystals have the same P-T-X characteristics, but halite daughter mineral was never found in the late epithermal minerals. Additionally, is stated in this paper that all inclusions types described in the Roșia Montană environment could be used to emphasized the behavior of the main ore elements (Au, Ag and others) starting from the magmatic stage at high P-T conditions and finishing at very low temperature and low salinity of the meteoric fluid phases (including magmatic component in some rejuvenation pulses). Two kinds of gold vectors are proposed in this study, one represented by a high temperature hydrosilicate alkali-rich melt and the second vector formed by

gaseous mixtures of H_2O-CH_4-CO_2-H_2S in a neutral-pH aqueous liquid rich-phase, at low temperatures. It is suggested that there is a gap between the early magmatic stage and the late epithermal events. Finally, to support these statements further investigations by modern analytical techniques as SEM-CL, BSE-EPMA, LA-ICP-MS and TEM/SAED is proposed to be done in further works.

2. Geological setting

During the last 2000 years the "Golden Quadrilateral", to which Roșia Montană Au-Ag epithermal ore deposit belongs, was one of the Europe's main goldfields (e.g. Udubașa et al., 2001, Kouzmanov et al., 2005; Fig.1). Mining and metallogenetic fruitful research was started in the modern time (Ştefan et al., 1974; Ghiţulescu & Socolescu, 1941; Petrulian, 1934) and continued until nowadays, showing numerous and important discoveries which still sustain the fame of this metallogenetic district (Manske et al., 2006; Harris et al., 2012).

The most recent finding is related to a specific caldera volcanic activity ("trap door") when the upper part of the shallow magma chamber expands and flows-up in the S-W part as a vent (Popescu et al., 2008). The caldera collapse forced the growth of a dacite/rhyolite dome(s) which rose and exploded in contact with the crater lake above it. This was a catastrophic tectonic-structural event enhancing the unique Au-Ag mineralizations deposited mainly in the phreato-magmatic diatreme breccia (O'Connor et al., 2004).
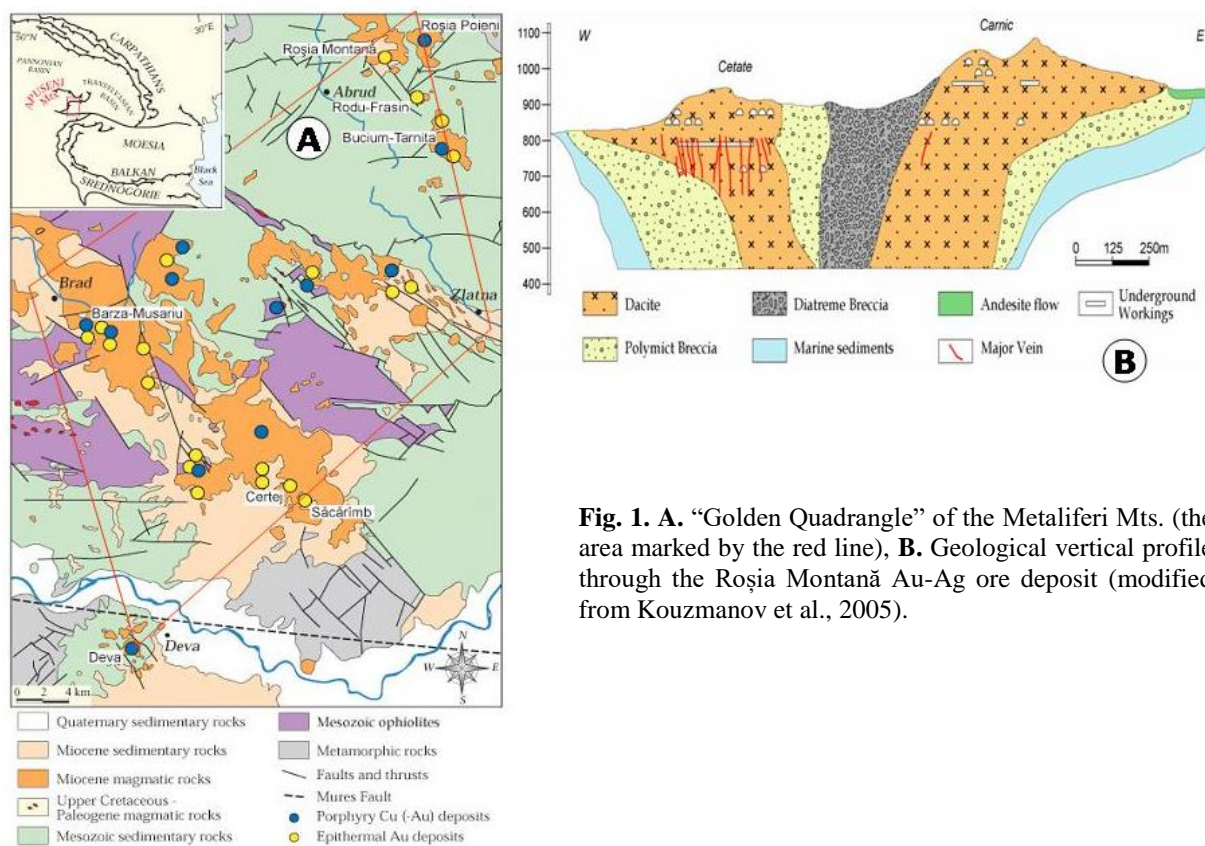
Fig. 1. A. "Golden Quadrangle" of the Metaliferi Mts. (the area marked by the red line), **B.** Geological vertical profile through the Roșia Montană Au-Ag ore deposit (modified from Kouzmanov et al., 2005).

It was emphasized recently that the different types of mineralization from the Metaliferi Mountains were related to the degree of the Miocene extension and partial mantle melting above the astenospheric upwelling front (Udubașa et al., 2001; Harris et al., 2012). Additionally, a geophysical anomaly delineating an area of 112 km^2, suggesting the presence of a quartz-diorite batholite in the Bucium - Roșia Poieni - Roșia Montană zone, formed in Langhian (13.5 to 14.87 Ma) as the main result of this lithosphere expansion process (Andrei, 2012). The magmatic quartz phenocrysts together with epithermal quartz crystals recorded this long magmatic-to-hydrothermal history in their internal microtexture features and their assemblages of solid-, silicate melt-, and fluid inclusions typology. These processes started in the plutonic environment (quartz diorite - microdiorite) continued in the upper, more differentiate (andesite - dacite - rhyolite) shallow level (ca. 10 km) and finished very close to the surface in the phreato-magmatic diatreme, during the late epithermal stage.

3. Magmatic quartz phenocrysts (polymorphs).

First description published about the presence of the magmatic bipyramidal quartz phenocrysts (polymorphs) from the Roșia Montană shallow dacite bodies was made long ago by Idriceanu et al. (1965) at "A.I Cuza" University of Iași. Microthermometry and petrography of melt inclusions in the same quartz crystal type was presented by M. Borcoș in his PhD thesis (Borcoș, 1970), and in further published paper (Borcoș, 1973). The author measured in a "Leitz-1350" high temperature stage some uncommon homogenization temperature up to 1600ºC (!), recorded in silicate melt inclusions, probably affected by post-entrapment modification or thermic decrepitation during the microthermometric cycles. The microthermometry and petrography of silicate melt and fluid inclusions from both magmatic phenocrysts and epithermal quartz crystal were initially studied by the first author of this paper during 1992-1999. Data on "fluid and melt inclusion study" from both epithermal and magmatic quartz phenocrysts from Roșia Montană were presented by I. Pintea in an unpublished IGR report (2000) and a published abstract (Pintea, 1999). More information and data on fluid inclusions from fragments of β-quartz phenocrysts and epithermal quartz crystals were presented by Tămaș and Bailly (1998), Wallier et. al. (2006) and, more recently in the PhD thesis by L. Iatan (2009) at Bucharest University, and in several extend abstracts (Iatan, 2008 a, b; Pintea and Iatan, 2013).

The β-quartz exoscopy is defined by external well preserved bipyramidal shape (Fig. 2) of the phenocrysts, sometimes rounded with embayment, or broken fragments in the dacite/andesite matrix. Perhaps the uncommon large size, up to 3 cm, suggested inheritance from a contemporary deep-seated magma chamber or they were recycled from an old volcano-sedimentary sequence (?).
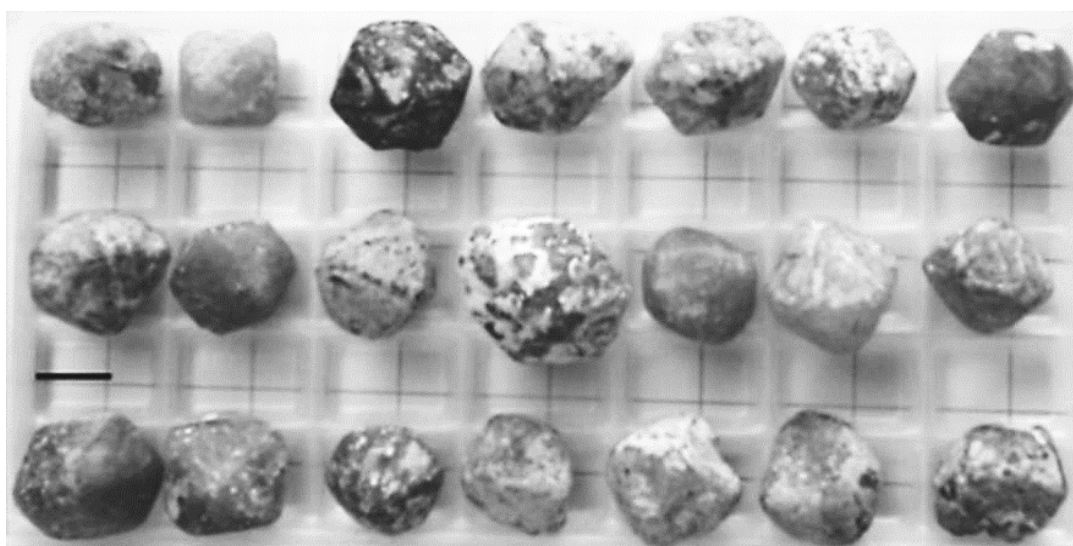
Fig. 2. β-Quartz phenocrysts from Roșia Montană dacite. Scale bar 10 mm.

They are not phenoclasts in the sense defined in the literature (Best & Christiansen, 1997) as explosive volcanic products because of melt inclusion decrepitation, although some fragmentation - type is present, mainly in the advanced breccia zones, but always overprinted by the epithermal alteration processes. They are certain plutonic quartz phenocrysts moved upward during explosive breccia formation, and contain almost complete crystallization history started deep in the magma chamber, probably sinking repeatedly. This could be another feasible way to explain the large size of these phenocrysts (up to 3 cm). The endoscopy of the magmatic quartz from Roșia Montană is defined by several successive stages recorded by the internal microtexture as two main growth zones (IA and IB in Fig. 3a) showing oscillatory feature by the repetition of up to ten alternating zones. The resorption layer is about 20 to50 µm wide and the large growth zone has variable width from 50 to 350 µm. They contain specific silicate melt inclusion assemblages suggesting successive growth/resorption stages probably because of intrusion of a hot and volatile-rich mafic magma or by contamination with crustal solid rocks (Udubașa et al., 2001; Wark et al., 2007; Peppard et al., 2001; Bachmann et al., 2003).
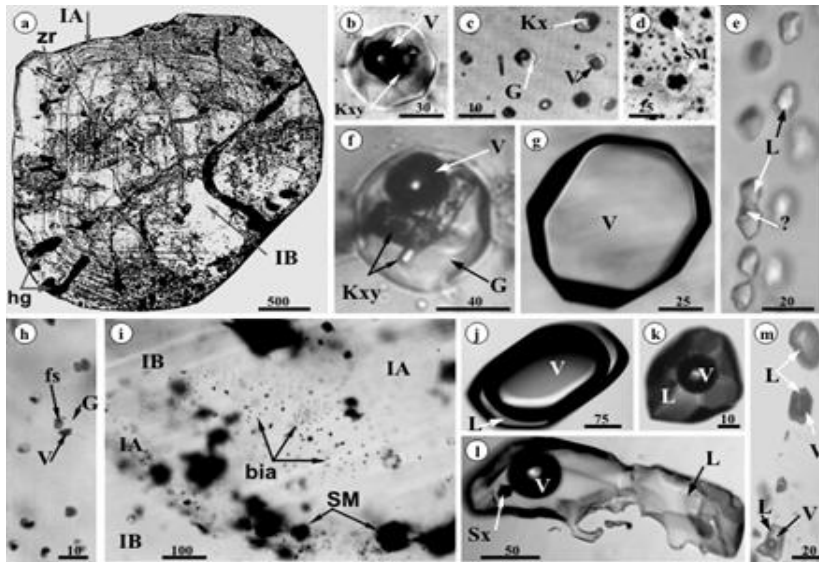
Fig. 3. Silicate melt and fluid inclusions in quartz phenocrysts from Roșia Montană. **a.**-Transversal double polished thin section on typical β-quartz crystal from Roșia Montană dacite showing oscillatory zoned feature of a thin resorption layer- IA and a wide growing zone- IB. Specifically they contain various silicate melt-, fluid inclusions and sometimes embedded solid inclusions as zircon-zr, and hourglass inclusions - hg; **b.** and **f.**- Silicate melt inclusions containing glass (G), vapor (V) and daughter solid phases (Kxy); **d.**- Completely altered silicate melt inclusions with characteristic decrepitation halos formed by secondary fluid inclusions; **e.**- Monophase liquid (L) rich inclusion +/- vapor (V) in epithermal quartz; G. Vapor (V) rich inclusion looking empty at room temperature conditions, but during microthermometry a special kind of phase transition were recorded (see Fig. 3).**h.** - Brine (fs) trapped in silicate glass inclusions (G-glass, V-vapor); **i. -** Brine inclusions assemblage (bia) formed "in situ" in a large zone (IB) of β-quartz from decrepitated silicate melt inclusions (SM) in a subsequent decompression stage; **j. k.**- Biphasic vapor – rich and liquid –rich inclusions in epithermal quartz phenocrysts (L-liquid, V-vapor);**l**- Three phase fluid inclusion in epithermal quartz trapped frequently a liquid (L), vapor (V) and accidentally a solid grain phase of carbonate, silicate or sulfate, but never a real daughter saline (halite) mineral; **m.**- Biphasic fluid inclusions with variable phase ratios between vapor (V) and liquid (phase) in a secondary trail in magmatic quartz formed "in situ" around decrepitated silicate melt inclusions. Scale bar in μm.

The presence of mixed silicate melt inclusions mainly in the resorption layers is suggestive for immiscibility between melts with different composition or "in situ" fractionation process of a mafic melt by decompression (Fig. 4).

More information could be gained by using cathodoluminescence (CL) which was proven to be an efficient technique for the visualization of intra-granular growth textures and alteration structures in quartz. These structures which become visible using CL are principally based on the distribution of trace elements and defects in the crystal lattice. Changes in the quantity and quality of defects in a mineral revealed by CL and complementary microanalytical methods reflect physico-chemical changes of melts and fluids (nature, concentration and oxidation state of trace elements, temperature and pH of solutions etc.) during crystal growth, deformation, alteration or post-crystallisation. CL is well suitable to distinguish between different mineral generations of quartz in igneous rocks (Müller, 2000; Takahashi et al., 2007).

For this study were used 150-200 μm thick double polished sections of quartz crystals. The samples were analyzed with a cold cathode CL equipment model CL 8200 MK3 (CITL) mounted on a Nikon E 400 microscope. The CL stage consists of a vacuum chamber containing the X-Y stage control and the electron gun. A control unit allows for precise control of the vacuum conditions and kV beam intensity. Polished samples are introduced in the vacuum chamber. Analytical conditions are between 0.05 to 0.1 torr, 15 to 20 kV and about 200 mA.

The magmatic quartz crystals are dark luminescent and the late formed cracks appears to be partially re-filed with carbonate. The melt inclusions trapped in the quartz phenocryts are light luminescent and shows a concentric pattern (Iatan, 2008, 2009; Fig. 5).
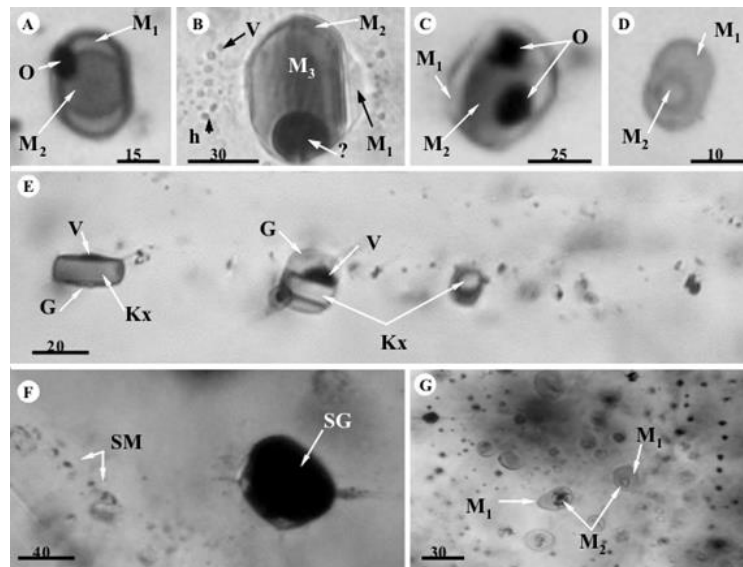
Fig. 4. Possible mafic magma influx trapped as complex silicate melt inclusions in β-quartz phenocrysts from Roșia Montană. **A.** Biphase silicate glass inclusion contain two different glass phases (M_1 and M_2) and an opaque (see Fig. 12 for microthermometry); **B.** Complex multiphase silicate glass inclusion with three differentiated glass at room temperature (M_1, M_2 and M_3 plus a vapor phase or a spherical opaque-?). This inclusion has been decrepitated after trapping, probably during decompression, showing a characteristic halo formed by separate silicate glass-, and vapor- rich inclusions. It seem that was trapped first as homogeneous mafic melt which then fractionated "in situ" after decrepitation; **C, D**- The opaque (O) is frequently contained by M_2 phase which is surrounded by fractionated M_1 melt phase; **E.** Complex crystallized silicate melt inclusions in a trail superimposed on a resorption layer decorated with inhomogeneous silicate glass inclusions showed in Fig. 11, for microthermometry, G-glass, V-vapor, Kx – silicate undetermined (daughter -?) microcrystals; **F.** globular sulfide (?) included in silicate melt inclusion in a large growth zone close to the resorption layer decorated with silicate melt inclusions (SM); **G.** Immiscible silicate melts M_1 and M_2 (salt -rich ?) in a pseudosecondary plane. Scale bar in µm.
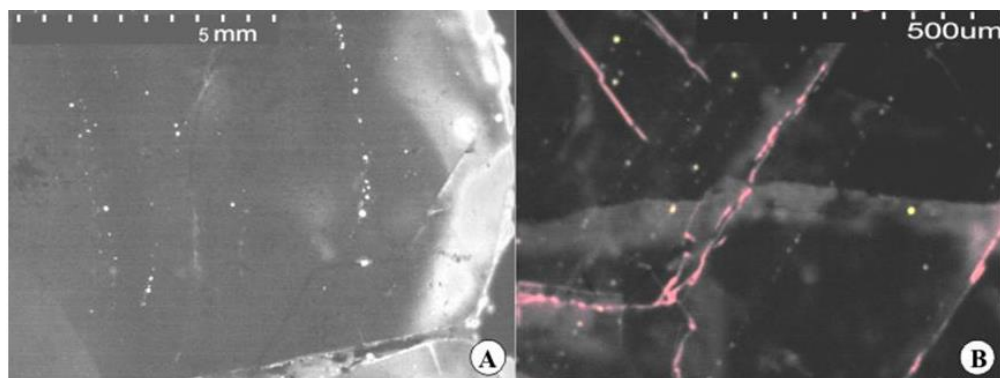
Fig. 5. A. CL image of magmatic quartz shows dark luminescence in the middle and white luminescent rim. High luminescent dots delineated altered silicate melt inclusions, mainly in the resorption layers; **B.** High magnification of the β-quartz internal structure showing yellow luminescent dots of altered silicate melt inclusions, calcite (pinkish-red) and late epithermal quartz (light grey) precipitated into microfissures (modified from Iatan, 2008).

The cathodoluminescence (CL) petrography revealed two-three different types of hydrothermal prismatic quartz. The first generation of quartz shows dark and light luminescent internal zonation. The second generation is dark luminescent with no internal zonation. The CL response might be related with composition changes of the quartz-forming fluids (temperature or pH changes and variability in the trace elements content) during mineral formation. For example, the third (3) quartz crystal from Fig. 6 shows dissolution pattern which could be related to a late rejuvenation stage recorded by the high-temperature homogenization in the vapor-rich inclusions from epithermal quartz crystals (Iatan, 2008; Fig. 6).
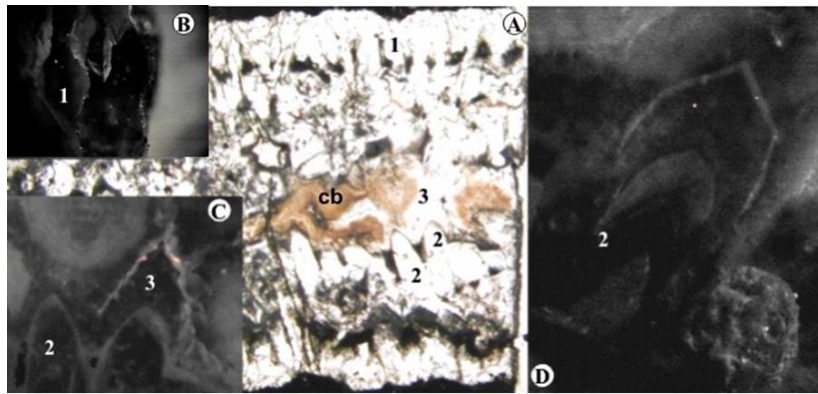
Fig. 6. Different generations of hydrothermal quartz revealed by the CL petrography. **A.** the quartz vein polished sample; **B.** Detail of the the first generation of quartz; **C.** The second and the third quartz generation; **D.** a close-up view of the second generation of quartz, showing the internal luminescent zonation; (1, 2, 3)- quartz generations, cb-carbonate. Note the irregular surface of the third quartz generation (3) which could be related to a rejuvenation high temperature vapor-rich stage, see text for explanation (modified from Iatan, 2008).

Each zone contains silicate glass inclusions always decrepitated along the c – axis (strong recognition criteria suggested long time ago by Clocchiatti, 1975), specifically in the resorption zones where uncommon silicate glass remnants show ultra-high homogenization temperature (around 1400ºC), or more often they failed to homogenize during heating procedure in the stage (e.g. Fig. 7 c and Fig. 13 C).
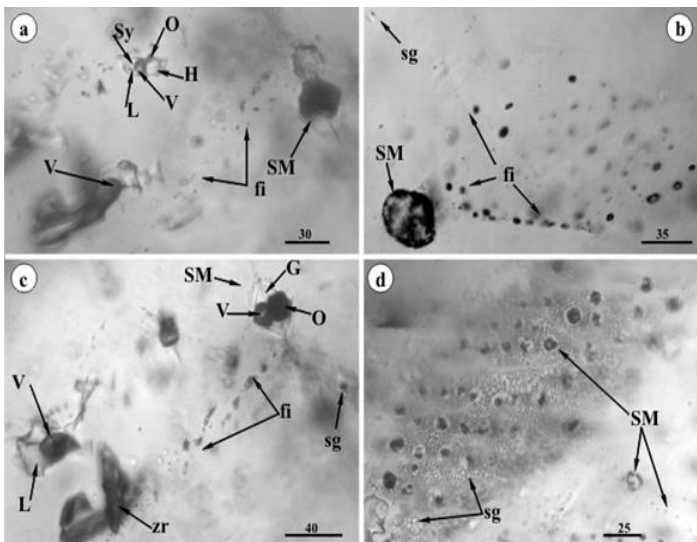
Fig. 7. Secondary hydrosilicate melt and fluid inclusions including brine were formed "in situ" from primary (pseudosecondary) silicate melt inclusions decrepitation during repeated α/β transition temperature. **a.** Multiphase brine inclusions containing halite (H), sylvite (Sy), liquid phase and vapor formed around a decrepitated and altered silicate melt inclusion (SM); **b.** pseudosecondary trail with vapor–rich fluid inclusions formed by radial microfissure around a decrepitated silicated melt inclusion; **c.** a zircon microcryst (zr), and silicate melt inclusion decrepitated and released fluid in a radial microfissure system; **d.** "In-mass" decrepitation of pseudosecondary silicate melt inclusion assemblage produced a continuous cloudy zone of silicate glass globules traill into the surface of microfissure plane. Scale bar in µm.
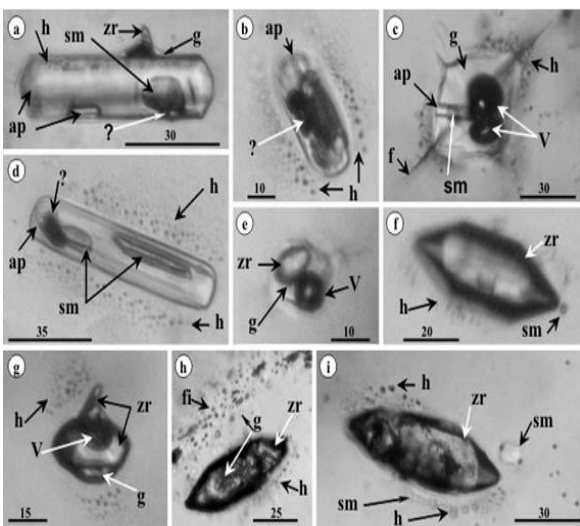
Fig. 8. Hydrosilicate fluid released by successive decrepitation-alteration cycles, inside the β-quartz phenocrysts from Roşia Montană. **a.** Apatite microcryst surrounded by a film of glass (g), agglutinated zircon and another apatite attached needle. A large silicate melt inclusions is also visible (sm,?); **b.** and **d.** Decrepitated and altered apatite surrounded by halo formed by silicate glass globules and vapor rich inclusions (the black dots). Undetermined solid inclusions were formed insid e the remained apatite, sm- silicate melt inclusion-?. Frequently apatite (**c**) and zircon (**e.** and **g.**) were trapped accidentally and formed multiphase silicate melt inclusions and then decrepitated and altered together, producing silicate melt globules and aqueous fluid in the surrounding "sweat" halos and microfissures (f), g- glass, zr-zircon, ap-apatite, V-vapor, h-halo; **f. h. i.** The entrapped zircon microcrysts were decrepitated and partially dissolved releasing silicate rich phases and generate "in situ" trails of fluid inclusions in microcracks. Scale bar in µm.

Frequent microsolids of apatite and zircon are embedded as isolated or agglutinated assemblages, and always show remelted and decrepitation features, surrounded by "sweat" halos (Audetat & Günther, 1999) of fluid and silicate melt inclusions. (Fig. 8).

Hydrothermal events are represented by fluid inclusion assemblages as brines-, vapor-, and aqueous-rich pseudosecondary and secondary fluid inclusions. Many of them, seems to be generated "in situ" after repeated α/β transition of the magmatic quartz, achieving new shape and microstructure as neonate inclusions seemingly like in those "induced changes by the deviatory stress experiments" (Tarantola et al., 2010). Perhaps majority of brine inclusions were formed in this way, because they are not present in the epithermal quartz related to the main mineralization events of the Au-Ag ore deposit, despite that these are also characterized by multiple internal zonations (Fig. 9A).

Nevertheless, there are some microthermometric sequences in cluster of very tiny melt inclusions (see below) trapped in a large growth zone which revealed two immiscible liquid separated at high temperature between 1150°C and 1200°C (Pintea, 1999), suggesting fused salt phase separation, early in the magma chamber.
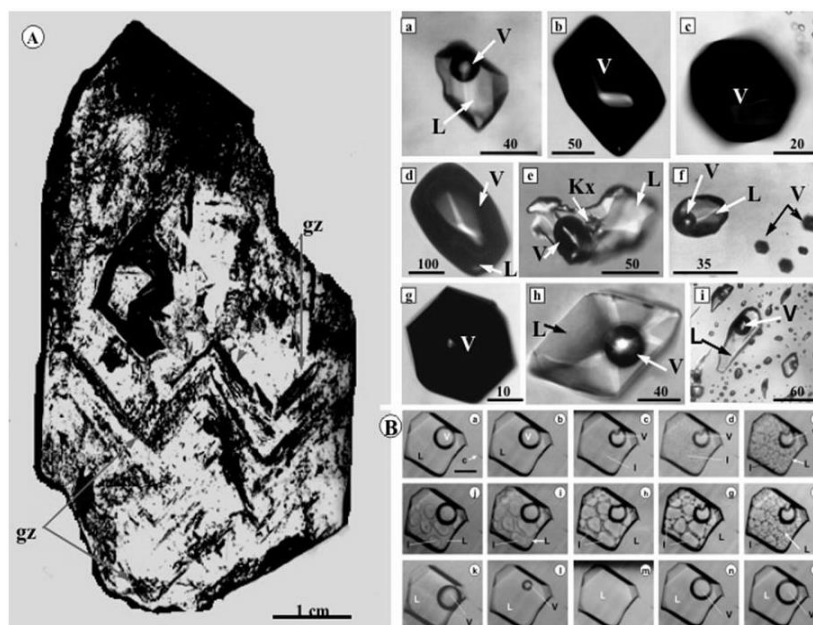
Fig. 9. Typical aqueous fluids trapped in epithermal quartz from Roşia Montană. **A.** Double terminated prismatic quartz crystal with parallel double zonation (gz). **a, h.**- Primary biphasic fluid inclusion with vapor (V) and liquid (L); **b, c, d, g**- Isolated vapor-rich inclusions containing a vapor phase (V) and a film of liquid (L); Presumably boiling event recorded by pairs of aqueous- rich (L+V) and vapor- rich (V), trapped in a restricted zone; **j.-** Pseudosecondary biphasic (L+V) assemblage in epithermal quartz. **B**. Sequences show the complete microthermometric cycle, typical for aqueous-rich inclusions in the epithermal quartz from Roşia Montană, first recorded by Pintea with an original microthermometric stage, working between -196 to +750°C (Pintea et al., 1992): **a.** and **o.** +25°C, **d.** - 40°C (Tf), **e.** -20.8°C (Te), **k.** -0.2°C (Tmi), **m.**+221.5°C (Th), salinity = 0.35 wt% NaCl eq. **b. c. f. g. h. i. j. l. n.** intermediate temperatures; the fine capillary (*c* in **a.**) had no visible influence on microthermometry; Notations: L- liquid, I-ice, V- vapor; Scale bar in B = 20µm.

4. Fluid (FIA) and melt (MIA) inclusion assemblages

The most instructive practicals in fluid and melt inclusions petrography is the recognition of fluid inclusion assemblage (FIA) or melt inclusion assemblage (MIA) in such a way that multiple individual inclusions can be related to a P-T-X-t snapshot inside a fluid/melt evolution descent line. Diamond (2003) "coined" the term "fluid inclusion assemblage" for such a group of inclusions, then abbreviated obviously "FIA" (Goldstein & Reynolds, 1994). By analogy Touret (in Diamond, 2003) used the term "group of synchronous inclusions" (GSI) for fluid phases trapped in the same time in metamorphic minerals delineating a paleo-P-T equilibrium assemblage. By using similar petrographic technique, it is shown more recently that melt inclusions trapped in the same P-T-X-t conditions should be defined by the term of "melt inclusion assemblage" abbreviated as "MIA" (Bodnar & Student, 2006). Sometimes defining such an assemblage is very difficult and instead alternative approaches technique were proposed for silicate melt inclusion selection (Johnson et al., 1994), as following: the average-, the high -, and one-by-

one approach, the ultimate method being generally the best choice when a normal assemblage, mentioned above, cannot be defined. Based upon number of phases present at room temperature conditions under the petrographic microscope and occurrence mode in the host, the β-quartz phenocrysts from Roșia Montană dacite contain the following assemblage typology:

4.1. Silicate melt inclusions

A. Glass + vapor; glass + vapor + crystals, glass + aqueous saline fluid, devitrified inclusions, thermic-decrepitated by reheating episodes and hydrothermally altered by reaction with external fluids, after host crystallization ceased (Fig. 3 a, b, c, d, f, h); Their size ranged between 20 - 80 µm up to 100µm, often more for hourglass inclusions (Fig. 3 a) or others irregular microcavities. It should be noted that they are often surrounded by "sweat" halos formed by small silicate globules (e.g. Fig. 7 d) resulted by reheating of the initial silicate content of inclusions by the magmatic influx in the magma chamber.

B. Silicate glass + vapor ± solid, less than 1µm to 10 µm (an alkalic hydrosilicate-rich phase (possible the first gold dispersed vector - see Discussion), having obviously negative crystal shape but other forms could be seen as tubular, elliptic, rounded or irregular ones.

C. Mixed melt inclusions: immiscible silicate glass phases ± vapor ± opaque (Fig. 4 A, B, C, D, E, G). Generally, they have bipyramidal shape but often the rounded form is characteristic and sizes between 10 - 100µm. Sometimes contain more than 2-3 glass phases at room temperature delineated by visible menisci amongst them. When not affected by thermal decrepitation, they are suggestive for melt immiscibility but frequently show decrepitated halos around them because decompression and probably the 2-3 melts inside were separated by "in situ" fractionation process of a single trapped melt phase. Originally, they could be immiscible mafic blebs or a piece of solid rock remelted in the magma chamber (country rock contamination), but generally contain a metallic separate phase (globular or crystallized euhedral form).

4. 2. Fluid inclusions

A. Pseudosecondary and secondary brine (liquid + halite ± another salt ± carbonates ± sulfate ± opaques trapped in "sweat" halos or dispersed around silicate melt inclusions and embedded microphenocrysts (Fig. 3 c, d, h, i). Necking-down and decrepitation - reequilibration feature seems to be the most post-entrapment modification processes. Perhaps these were the "in situ" formation processes by trapping the fluids released from the destructive reaction of the primary silicate melt inclusions with external fluid phases (magmatic and/or meteoric). Often, they decorate the large growth zoned between the resorption layers (Fig. 3i), forming distinctive cluster assemblages.

B. Secondary and pseudosecondary liquid-, and vapor- rich inclusions (Fig. 7 a, b, c) trapped in microfissures planes or decrepitation halos around primary silicate melt inclusions. Repeated α/β transitions in the magmatic quartz induced many post-entrapment modifications so it is very difficult to find a normal fluid inclusion assemblage defined above, and "one-by-one" approach being more adequate technique to study this kind of fluid inclusion (see Discussions below). Nevertheless, in terms of microthermometry their P-T-X values are close to the similar fluid inclusions trapped in the host epithermal quartz (Pintea et al., 1992; Pintea, 1999; Tămaș & Bailly, 1998; Wallier et al., 2006; Iatan 2008a), which are pictured in the photomicrographs from Fig. 3 (e, g, j, k, m) and Fig. 9A (a to i), and Fig. 9B (a to o).

C. Secondary aqueous fluid + solid residual silica (?). They form indeed a late secondary assemblage in β-quartz phenocrysts defining a group of fluid inclusion containing in the central part a vapor bubble surrounded by agglutinated grains or circular layers of secondary silica (?) in dominated liquid aqueous phase (Fig. 15 B). They are related also to the alteration process of primary silicate melt inclusion, homogenizing in liquid phase between 203° – 221°C with salinity of 0.18 to 1.7 wt% NaCl eq., and the solid phase never melted (Pintea, 1999).

4.3. Solid microinclusions

A. Isolated or agglutinated microphenocrysts. Zircon and apatite are the frequent solid inclusions and carry information on different magma batches where ß-quartz phenocrysts crystallized. They were trapped accidentally also in the silicate melt inclusions ("step daughter mineral"), but frequently occur as isolated or agglutinated clusters (Fig. 7 and Fig. 8). Partially decrepitated and dissolved they are surrounded by characteristic decrepitation halos formed by fluid inclusion assemblages. These features suggested a geological time-gap between the quartz phenocrysts formation inside the magma chamber and the episodic mineralization events in the shallow breccias structures and vein network. Generally,

zircon microphenocryst inclusions are useful in refining the mineral growing time and stratigraphy deep in the magma chamber, and to trace the geochemistry of the earlier magma batches (Pettke et al., 2005).

B. Globular sulfide. Rarely isolated, more often trapped as rounded globules in silicate melt inclusions, this kind of inclusions could be a metallic immiscible melt (Fe-O-S) related to the mafic magma influx in the crystallizing magma chamber (e.g. Laroque et al., 2000). An extraordinary sample was found after crushing a bunch of quartz phenocrysts, as unique metallic shiny globules shown in Fig. 10.
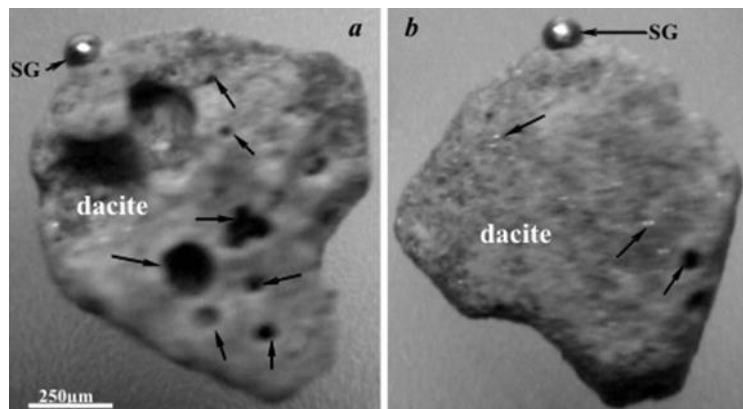
Fig. 10. Globular sulfide (re-melted?) imbedded in dacite–like matrix trapped or attached to β-quartz phenocrysts from Roșia Montană. There are many empty vacuoles originally containing the same globules (SG) on the side: **a.** On the opposite side; **b.** there are still present tiny sulfide globules incorporated in the spongy rock inclusion (black arrows). Presumably this piece of solid rock was a molten bleb or a remelted mafic rock inside the magma chamber during quartz crystallization (I. Pintea, pers. coll.).

This piece of "rock" seem to be a remelted feature of an unknown source material (a former immiscible mafic bleb or solid country rock) dispersed as liquid globules (perfect rounded shape) in the silicate matrix, sometimes trapped accidentally in silicate melt inclusions (Fig. 4 F). If they contain Au, Ag and other metallic elements we can presume that this kind of globules spreaded inside the magma chamber together with the hydrosilicate alkali - rich melt, as the vector mentioned above, would be the primary source of the mineralization and they were then recycled by the low salinity and low temperature epithermal fluids in the late convective system, formed around the shallow dacite intrusions. Unfortunately, there are no analytical data on this sample at this moment.

5. Microthermometry

To do microthermometry in β-quartz phenocrysts (polymorphs) from Roșia Montană was a difficult task from the first study initiated by Borcoș long time ago (1973). As mentioned above, even at 1600ºC some of the bipyramidal shaped silicate melt inclusions still contain glass and contraction vapor bubble, and never homogenize. That is because the majority of silicate melt inclusions were decrepitated (mainly along their long axis, which regularly remain parallel to the c-axis of the host quartz (Clocchiatti, 1975).

Methods. In this study, two kinds of microthermometric stages were used to record silicate melt homogenization behavior, firstly at IMP ETH Zurich (1993 - 1994), a Linkam TS1500 was used and then the study was continued in a "homemade" microthermometric device which works up to 1100ºC. Both stages were calibrated with Potassium dichromate (398ºC), Halite (800ºC), Silver (961ºC) and Gold (1064ºC). Heating rate ranged generally between 10º to 100ºC, but close to phase change a low rate between 2ºC to 5ºC was used, or lower as suggested obviously by the published protocols on the heating procedure (Bodnar & Student, 2006; Roedder, 1994; Davidson, 2004). Accuracy and measurements precision ranged between ±(10-20ºC). Fluid inclusions were analyzed with heating/cooling USGS-, and two Linkam THMSG600 stages, with accuracy and precision between ±0.1ºC to ±1-2ºC from −196º up to +600ºC, respectively.

5.1. Silicate melt inclusions

A huge number of silicate melt inclusions were trapped in β-quartz from Roșia Montană, but just a few were suitable for high temperature microthermometry. Firstly, because majority of them were thermal decrepitated, probably during repeated α/β transition episodes. The most damaged area is the resorption layers were several "heterogeneous" assemblages could be defined and there is most feasible to use the "on-by-one" approach to study them.

The most common types of silicate melt inclusions, in these resorption layers, are represented by multiphase silicate glass inclusion composed by several vapor bubbles, opaque and transparent solid grains and show the highest recorded homogenization temperature (Fig. 11).
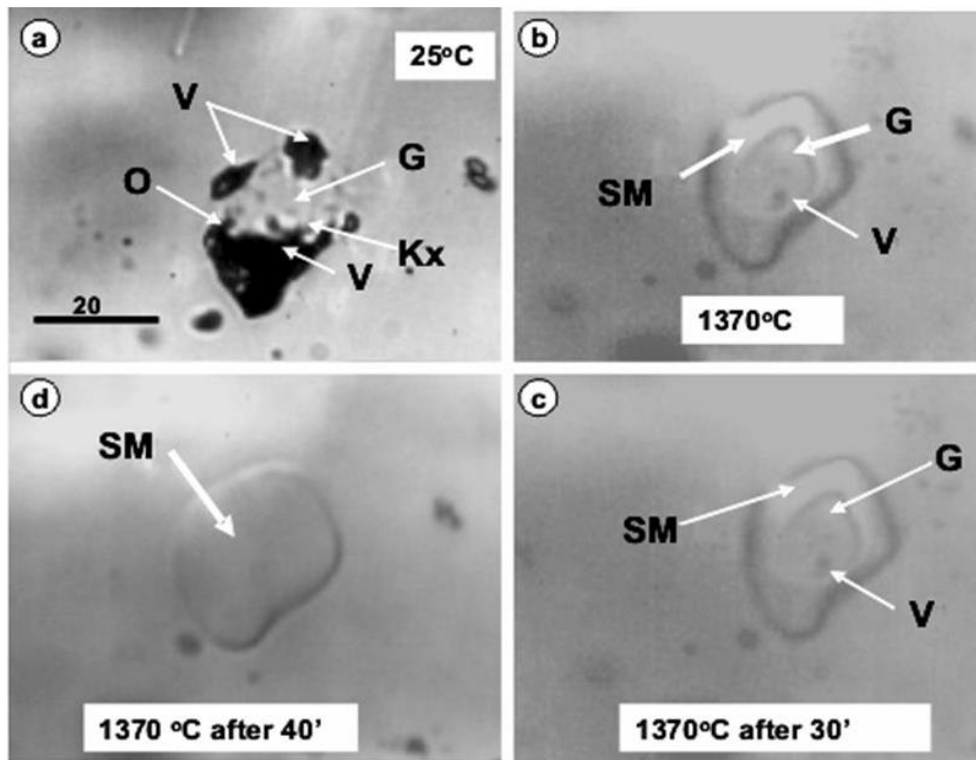
Fig. 11. Silicate glass inclusion type trapped mostly in the resorption layers (IA in Fig. 3a). The inclusion contains at room temperature in **a.** silicate glass (G), a vapor phase as multiple bubbles (V) and solid silicate phases (kx) and opaque (O). During heating procedure in the stage up to 1300°C, the phase disappeared one by one and now contains only silicate melt (SM), a vapor bubble (V) and remaining glass in **b.** and **c.** which melted completely at 1370°C showed in **d.** This behavior is uncommon and trapping temperature cannot be estimated, but this seems to be the initial temperature of a new melt charge trapped in the resorption layer (IA in Fig. 3a). The new overheating magma influx induced overgrowth of the β-quartz phenocryst, after homogenization of the mafic and felsic melt during decompression the following wide internal zone developed (IB, in Fig. 3a). Scale bar in µm.

This kind of silicate melt inclusion seem to be a heterogeneous and decompressed melt representing the new hot magma influx which is in disequilibrium with the anterior quartz growth zone (IA in Fig. 3a) generating the resorption layers themselves (IB in Fig. 3a). There are not chemical analyses on this inclusion type, but if the recorded temperature is the real trapping temperature (or close to) then a basic composition would be taken in account for its content. These basic influxes seem to be more accurately represented by the complex silicate melt inclusions (e.g. Fig. 4) which contain several glass phases separated by menisci inside the inclusions and generally contain an opaque metallic phase. One of these inclusions which contained at room temperature three glass phases and an opaque grain (Fig. 12 B- a, b, c) homogenized by showing critical behavior (?) by fading disappearance of the internal melt globule (M_3) at Th=1050°C.

It is presumed, for the moment, that a homogeneous basic silicate melt was trapped and separated after trapping in two principal silicate melt M_2 and M_3, surrounded by a third "fractionated" silicate melt film (M_1) wetting the cavity wall. Many of this complex inclusion type (e.g. Fig. 4B) show decrepitation feature by a secondary halo formed by vapor-rich (?) inclusions, suggesting a fractionation "in situ" process because pressure drop after reequilibration process. Alternatively, the sudden homogenization temperature recorded in Fig 12B- b could be indicative for a mixing (or unmixing ?) process between the felsic crystal mush and a new hot basic input (Bachmann et al., 2003; Audetat & Pettke, 2006), or simply by heterogeneous trapping of two conjugate silicate melts (Lester et al., 2013).

A most important feature of the silicate melt inclusions from the magmatic quartz from Roşia Montană is the presence of silicate melt assemblage formed by very tiny cavities from less than 1µm and up to 10µm. Those are inframinerals sized and their homogenization temperature cannot be record because the included phases, obviously glass, vapor bubble and other solid daughter phase, are too small to be observed under normal petrographic microscope. Generally, they are spread uniformly inside the large growth zones (zone IB in Fig. 3 a and Fig. 15).
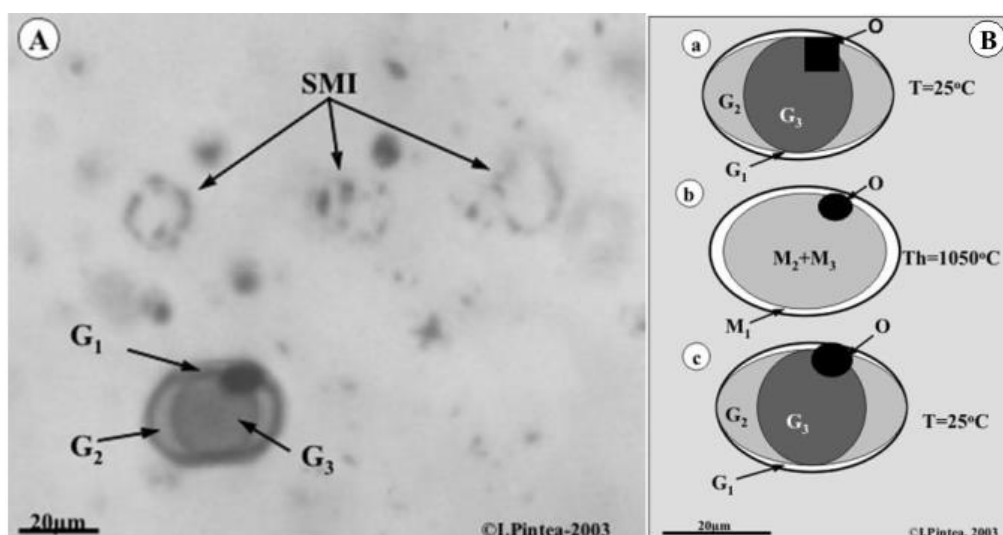
Fig. 12. The complex silicate melt mixture in **A.** showing 2-3 glass phases at room temperature and during heating procedure in the stage, under the optical microscope the G_2 and G_3 clearly homogenized by fading disappearance of G_3, as M_2+M_3 in **B:** in **a**. silicate rich phase containing the partially melted rounded opaque too, showed in **b.** at indicated Th temperature and quenched at room temperature in **c**. They homogenized by fading vanish of M_3 in M_2 and the process was reproducible, suggesting a critical behavior (?). Probably the complex melt mixture was unmixed "in situ" during decompression or was trapped as immiscible silicate melt phases.

We presume that they could have a special signification in the magmatic evolution of the magma chamber (see Discussions). Anyhow the large inclusion (around 10μm) from the same type could be measured at high magnification and one example is pictured in Fig. 13 A.

As it is suggested in many basic papers dedicated to the silicate melt inclusion microthermometry the smaller inclusion gives more accurate homogenization temperature (e.g. Roedder, 1979). In our case this kind of silicate melt inclusions formed by silicate glass, vapor and $\pm$ solid(s) show homogenization temperature between 786-939ºC (n=10), which could be a value close to the formation temperature for inclusions with rhyolite-dacite composition (Pintea, 1999; Naumov et al., 2010, 2011, 2013; Blundy et al., 2006, Table 1), although the same types of silicate melt inclusions show even higher homogenization temperatures between 1100ºC and 1200ºC (Pintea, 1999).

Table 1. Chemical EMPA analyses of the silicate melt inclusions from β-quartz phenocrysts from Roșia Montană. Authors: 1-Pintea, 1999 and unpubl.; 2- Naumov et al., 2010; 2011; 2013.

Composition	1	2	3	4	5	6	7	8
SiO_2	71.56	72.30	54.99	72.15	53.00	56.92	76.84	76.22
$TiO2$	-	-	-	-	0.00	0.01	0.19	0.11
Al_2O_3	16.61	15.63	28.64	16.15	30.47	25.42	6.16	14.32
FeO	0.61	0.87	0.19	0.48	0.14	0.12	4.25	0.66
MnO	0.18	0.13	0.12	0.07	0.00	0.00	0.01	0.17
MgO	0.10	0.03	0.04	0.02	0.01	0.01	0.72	0.31
CaO	2.26	2.49	11.51	2.32	12.72	10.42	3.74	2.32
Na_2O	1.40	1.69	4.82	1.74	4.34	4.47	2.37	3.83
K_2O	2.36	2.03	0.20	2.70	0.10	0.27	4.70	2.20
P_2O_5	-	-	-	-	-	-	0.10	0.13
Cl	0.06	0.05	0.00	0.06	-	-	0.00	0.06
S	-	-	-	-	-	-	0.02	0.00
Total	95.11	95.21	100.51	95.66	100.78	97.64	99.10	100.33
Authors	1	1	1	1	2	2	2	2
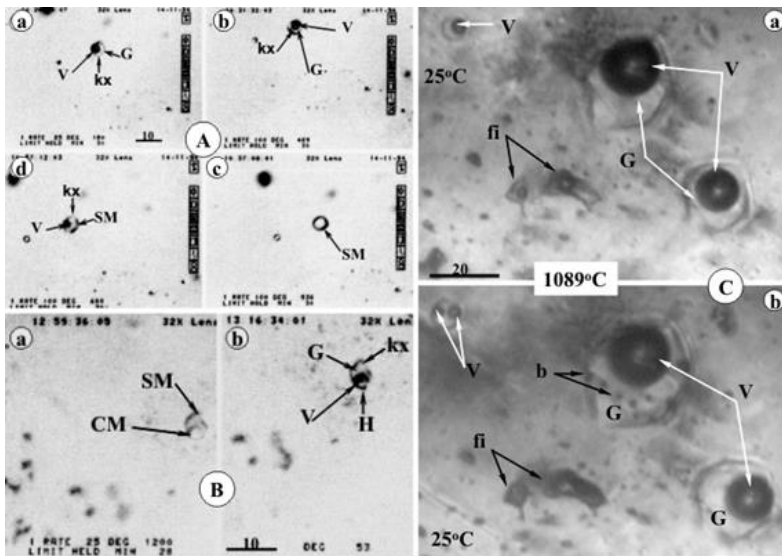
Fig. 13. Silicate melt inclusions microthermometry: **A.** The smallest silicate melt inclusion selected for homogenization measurements shown at room temperature in **a.** the coexistence of a vapor bubble (V) and a tiny solid phase (Kx) in the glass matrix (G). During heating in the stage the solid phase melted first above 650°C and the inclusion homogenized by vapor bubble disappearance at 786°C. On further heating above 900°C the silicate melt is in the homogeneous liquid state and do not show any decrepitation feature. Back to the room temperature the cavity contains again the same phase association showed in **c.** around 600°C, and is still formed by silicate melt (SM) vapor (V) and the growing solid daughter microcryst (kx). On further cooling the silicate melt turned back to glass as it was at the beginning in **a**. In **B.** two immiscible phases becomes visible around 1100°C formed by silicate melt (SM) and chloride rich phase released by halite melting and followed by vapor disappearance around 1175°C (Table 2); back to room temperature four phases are present: halite (H), another solid phase (kx), glass (G) and vapor (V) in the same ratios as they were initially, before heating procedure in the stage. **C.** Generally, the bigger silicate melt from β-quartz phenocrysts from Roșia Montană (i.e. 50 to 100µm or more) cannot be homogenized under one atmosphere pressure in the stage under microscope, perhaps the quenching method in cold seal high pressure vessel would be more appropriate for this purpose. In the pictures from **C.** the silicate melt inclusions had shown only few melting signs up to 1089°C, recorded temperature in the stage. Back to the room temperature another bubble nucleated in the inclusion up left in the picture and small bubbles nucleated in the two bigger inclusions in the right side. The fluid inclusion (fi) biphasic in **a.** were completely decrepitated at high temperatures being almost empty in **b.** The vapor (V) phase from the two silicate melt in the right side do not show any volume change at mentioned high temperature. Anyhow they are not a vacuum because after heating/cooling cycle in the vapor phase (V) a solid grain was re-precipitated. Scale bar in µm.

Table 2. Selected microthermometric data, characterizing the main silicate melt inclusion assemblages (MIAs) from Roșia Montană β-quartz phenocrysts. *- contain very small halite daughter salt, **- contain 2-3 black-brown yellowish glass phases, showed in Fig. 4, ***by quenching method from indicated literature.

Inclusion type	*Tm, °C*	*Th, °C*	*Source*
G+V (30)		≥ 1084-1089	*this study*
G+V±Kx±O (10)	665 (silicate) 833 (opaque)	786-939	*Pintea, 1999*
***Multiphase (10)**	413-438	1150-1200	*Pintea, 1999 and unpublished data*
****Complex (2)**		1050	*this study*
*****Recrystallized**		1000-1040	*Naumov et al., 2013*

In the same large growth zones of the magmatic quartz could be observed isolated or clustered tiny complex melt inclusions which shown the presence of salt (halite-?) daughter microcrysts, vapor (± another solid daughter silicate phase -?) and silicate glass. By heating-up the salt melted around 300-500°C and vapor bubble disappeared in the floating globule (salt) around 1150-1200°C (n=10), where silicate and salt melts were coexistent (Fig. 13B).

Salinity was estimated between 38-60 wt% NaCl at 300 MPa and 1175°C (Table 2), based upon SoWat calculation (Driesner & Heinrich, 2007). As it was already mentioned the large silicate melt inclusion cannot be easy homogenized at one atmosphere pressure, direct, under the microscope in the high temperature stage. In Fig. 13 C (a, b) a group of such inclusions were heated up to 1089°C and the

contraction vapor bubbles remain unchanged during the microthermometric cycle. Perhaps heating/quenching in cold seal high pressure vessel (Bodnar & Student, 2006) would be the technique of choice to homogenize these kinds of silicate melt inclusions.

5.2. Fluid inclusions
Until now the studies dedicated to microthermometry of fluid inclusions from Roșia Montană stated that they are related to late epithermal evolution at less than 300ºC, rarely more especially recorded of Th L+V(V) by vapor homogenization in vapor-rich inclusions trapped both primary in epithermal quartz and secondary in the magmatic phenocrysts (Pintea, 1999; Tămaș & Bailly, 1998; Wallier et al., 2006; Iatan, 2009).

Table 3. **A.** Microthermometry of liquid-rich FIAs from epithermal and β-quartz phenocrysts (polymorphs); **B.** Homogenization temperatures recorded by different authors in vapor-rich fluid inclusions from Roșia Montană.

A

Te, ºC	Tmi, ºC	Th, ºC
-20.5 to -21.0 (36)	-0.1 to -0.3 (57)	180-190 (8)
-21.0 to -21.5 (20)	-0.3 to -0.5 (65)	190-200 (10)
-21.5 to -22.0 (79)	-0.5 to -0.7(38)	200-210 (5)
-22.0 to -22.5 (50)	-0.7 to -0.9 (10)	210-220 (12)
-22.5 to -23.0 (19)	-0.9 to -1.1 (38)	220-230 (33)
-23.0 to -23.5 (23)	-1.1 to -1.3 (29)	230-240 (52)
-23.5 to -24.0 (25)	-1.3 to -1.5 (15)	240-250 (57)
		250-260 (52)
		260-270 (10)
		270-280 (6)
Epithermal quartz		280-290 (7)
-20 to -21.8 (28)	-0.1 to -0.3 (18)	190-200 (1)
-21.8 to -22.8 (43)	-0.3 to -0.5 (14)	200-210 (16)
-22.8 to -23.8 (20)	-0.5 to -0.7 (16)	210-220 (15)
-23.8 to -24.8 (25)	-0.7 to -0.9 (25)	220-230 (4)
	-0.9 to -1.1 (8)	230-240 (16)
	-1.1 to -1.2 (10)	240-250 (23)
	-1.1 to -1.5 (2)	250-260 (16)
	-1.7 to -1.9 (7)	260-270 (5)
β-quartz		270-280 (4)

B

Sample	Th LV-V,ºC	Tm solid (H2O-CO2-CH4-H2S)	Salinity wt % NaCl eq.	Source
β-quartz	458-500			*Iatan, 2008*
	530-555			
	-		0.2-0.7	*Wallier et al, 2006*
Epithermal quartz	362-364 (n=10)	-100 to -90 (5)	0.71	*Pintea, 1999 and unpublished*
		-90 to -80 (6)		
		-80 to -70 (8)		
		-70 to -60 (2)		*Fig. 14A*
		-60 to -50 (1)		
	259-277			*Iatan, 2008*
	401-443			*Iatan, 2008*

In addition, a saline rich fluid was identified as secondary (pseudosecondary) trails in the magmatic quartz where the presence of the halite cube daughter phase offered possibility to estimate a high salinity ranged between 30 – 55 wt% NaCl eq. (Pintea, 1999; Wallier et al., 2006). Nevertheless, halite cubes were never found in epithermal quartz, so in this study we suggest that the presence of high salinity brine is just a secondary feature that characterizes only the β-quartz phenocrysts. Moreover, excepting some isolated clusters in the large growth zones (IB) which seem to be related to an exsolving process inside the magma chamber at high temperature (immiscible salt globules), the majority of the three-phase or multiphase fluid inclusions which contain liquid + halite + vapor ± other solid(s) were formed also "in

situ" by post-entrapment processes in the recicatrized planes of the microfissures or "sweat" halos (e.g. Fig. 7). This means that the late epithermal event from Roșia Montană could be decoupled by the magmatic activity reflected mostly by the various silicate melt inclusions described above which generally show some ephemeral hydrothermal phenomena. The magmatic quartz phenocrysts were flushed upwards and partially fragmented together with the dacite host rocks in the shallow breccia zone where a convective epithermal system precipitated quartz, carbonates, sulfates and metallic sulfides in veins and/or dispersed in a network of small veinlets, reminding a porphyry-like stockwork (Berbeleac et al., 1995). The low salinity fluid inclusions from epithermal quartz (primary and pseudosecondary) have low salinity (Pintea et al., 1992; Pintea, 1999, Fig. 9B) ranged between 0.18-2.57 wt% NaCl eq and Th= 180°-290°C (n=252), almost the same values were recorded for pseudosecondary and secondary fluid inclusions from magmatic quartz phenocrysts (Pintea, 1999): 0.18-3.23 wt % NaCl eq and Th=190°-280°C (n=128), all presented in Table 3. Similar values were also reported in different published works (e.g. Tămaș & Bailly, 1998; Wallier et al., 2006; Iatan, 2009). The vapor-rich inclusions were difficult to be homogenized (see Discussions), although tubular inclusions in magmatic quartz were homogenized in two distinct intervals between 458°-500°C and 530°-555°C (Iatan, 2008b). In the epithermal quartz such vapor-rich inclusions showed very low salinity between 0.2 and 0.7 wt % NaCl eq. (Wallier et al., 2006). Our data show homogenization temperature between 362°-374°C (n=10) for inclusions with salinity 0.71 wt % NaCl eq. and others two homogenization intervals between 259°C - 277°C and 401°- 443°C (Iatan, 2008b).
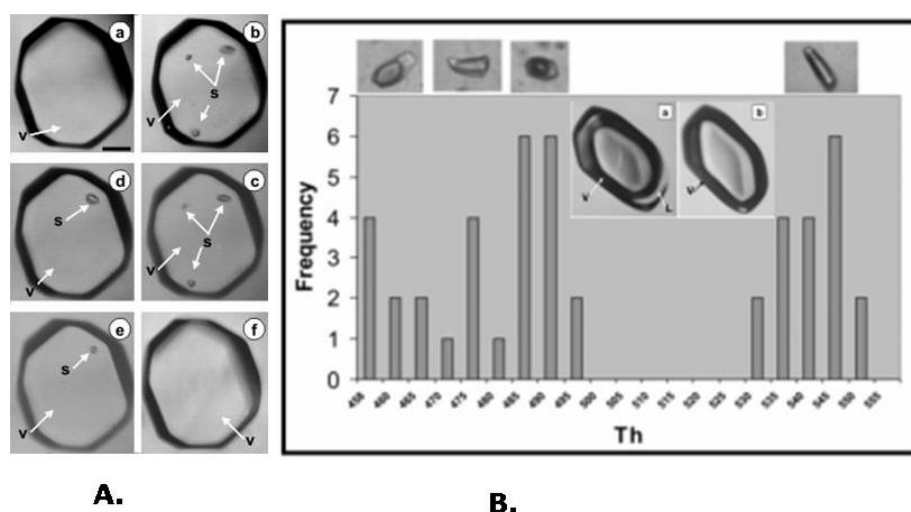
Fig. 14. A. Microthermometric cycle in a vapor-rich inclusion trapped in epithermal quartz. At temperature room condition in **a.** the microcavity looks like empty but when was cooled down to -170°C, in **b.** three grains of solid were sublimated (s). The first solid grain melted in **c.** between-112° and -94°C (H_2S), **d.** the second grain melted around -84°C (CH_4) and in **e.** the last grain melted sharply at -56.6°C (CO_2), in **f.** back to room temperature the fluid inclusion contains a presumably pure and invisible gas mixture of CO_2-CH_4-H_2S, no liquid phase was detected by microthermometry in this fluid inclusion type. Scale bar: 30 µm. **B.** Histogram of vapor homogenization in vapor-rich inclusions from β-quartz in selected fluid inclusions depicted in the upper part of the picture, they were selected based upon their tubular shape. For comparison a vapor-rich inclusion with more regular shape from epithermal quartz is shown at room temperature in **a.** and close to homogenization temperature around 370°C in **b.** showing a small unhomogenized white corner down left (modified from Iatan, 2008). Scale bar in A= 30µm.

They could be related to the intermediate temperature, and moderate to high salinity, high temperature and also intermediate density aqueous inclusions reported in literature (Wallier et al., 2006), but no halite daughter phase was ever mentioned in the epithermal quartz crystals at Roșia Montană. Perhaps a rejuvenation stage by magmatic fluid influx in the late epithermal system as it could be envisaged by CL images from Fig. 6C, where irregular growth surfaces of the epithermal quartz suggest dissolution feature followed by successive overgrowths (hot acidic fluid pulses). The microthermometric behavior of vapor-rich inclusion from epithermal quartz is presented in Fig. 14 A and homogenization histogram for vapor rich inclusions in magmatic phenocrysts and a homogenization sequence in the epithermal quartz were recorded in Fig. 14 B.

6. Discussions

6.1. Trapping temperature and "in situ" post - entrapment modifications of the fluid and melt inclusions

The β-quartz phenocrysts (polymorphs) from Roșia Montană dacite are characterized by an oscillatory zoned microtexture defined by two distinct zones, a resorption layer (IA) and a large growth zone (IB) (Fig. 3). Both had trapped silicate melt inclusions which recorded the formation temperature: a high temperature for heterogeneous melt inclusion from 1150° and up to 1370°C for the resorption zone and 786° and 939°C for the more homogeneous trapped melt in the large growth zone. Anyhow some pseudosecondary clusters trapped in these large zones indicated high temperature for heterogeneous melt coexistence between 1150-1200°C. A fractionation (?) process was recorded by critical homogenization at 1050°C. Which temperature is the real formation temperature in the magma chamber? If we take in account the EPMA analyses of the silicate melt inclusions from Roșia Montană by different authors written in Table 1 and compared them with data published on similar compositions from melt inclusions in plagioclase formed at St. Helens (Western USA) and Shiveluch (Kamchatka) volcanoes prior to eruptions, we can presume that the trapping P-T conditions of the silicate melt inclusions from Roșia Montană, with almost similar chemical composition, could be approximated well between 750-995°C and 15-313 MPa (Blundy et al., 2006). These would be taken as crystallization conditions after homogenization between basic and rhyolite/dacite melts in the upper magma chamber before rising up close to the shallow level. So, we can presume that the decompression process started approximately from 10 km depth and raised up to several tens of meters below the crater lake where a catastrophic explosive event generated the phreato - magmatic breccia types.

The microtexture evidences show that the primary magmatic oscillatory zoning of the β-quartz phenocrysts was overprinted by thermal and hydrothermal alteration features which creates internal microstructures after quartz crystallization like those reported recently in the deviatoric stress experimental work (Tarantola et al., 2010).

6.2. Homogenizing vapor-rich inclusion and fluid phase separation

It was documented experimentally that measurements in vapor-rich inclusions yields erroneously low temperatures by tacking in account that some liquid is remaining at the apparent homogenization temperature (Bodnar et al., 1985; Sterner, 1992). The authors mentioned that in their experiments in synthetic fluid inclusion a difference of ≈500°C and ≈25°C were recorded, lower that the true ThL+V(V) in the H_2O-NaCl and CO_2-H_2O systems, respectively. It is recommended that only vapor- rich inclusions which show a narrow reentrant (tubular shape) "into which the last bit of fluid phase has been concentrated by capillarity" (Roedder, 1994) are suitable for vapor homogenization. Such inclusions were selected in our epithermal and magmatic phenocrysts from Roșia Montană (Fig. 14 B). Comparatively it is shown in the same picture (a, b) a rectangular vapor- rich fluid inclusion which still have an unhomogenized corner (white corner) at "apparent" homogenization temperature snap shot. The majority of vapor-rich inclusions from β-quartz phenocrysts from Roșia Montană were trapped in trails (recicatrized microfissures) or in decrepitation halos of the primary silicate melt inclusions. They are not primary inclusions, so they were trapped below the α/β transition of the host around 573°C. The homogenization temperatures recorded in such populations of vapor-rich inclusion are always lower than this transition temperature. Nearby were documented frequently high salinity and high temperature brine inclusions which perhaps were trapped together as boiling assemblages or were equilibrated by necking-down in the same microfissure plane. For example, a vapor-rich inclusion homogenized at 550°C (Iatan, 2008b) having salinity between 0.2 and 0.7 wt% NaCl eq (Wallier et al., 2006) must be coexistent with brine salinity of 45 to 55 wt% NaCl eq. (Driesner & Heinrich, 2007). Such values are commonly obtained by microthermometry in this study, as it was mentioned above. Because these assemblages are not found in the epithermal quartz crystal it is more adequate to suggest that they are not representative for an important hydrothermal stage, instead they are secondary features generated during magmatic quartz recrystallization after repeated α/β transition. These are even more enhanced by incursion of the external diluted fluids evolved during the main epithermal stage between 280-190°C and large fluid pressure variations (from 3 kb to several ten of bars) during different breccias formation. Additionally, this strong decompression can be emphasized by the presence of globular silica and vapor-rich inclusion surrounding the decrepitation halos of the apatite and zircon microphenocrysts (Fig. 8).

6.3. Metal spreading and precipitation vectors

Probably a hot volatile rich phase was exsolved after each mafic influx and altered the already formed silicate melt inclusion in the quartz phenocrysts growth zones. In the meantime, heterogeneous silicate/silicate ± sulfide and silicate/salt melts were trapped as pseudosecondary heterogeneous inclusions. This is the time when a silicate spry seems to be trapped as clusters, trails or halos formed by very small silicate melt inclusions, frequent < 1µ (inframineral sized melt inclusion - Fig. 15).
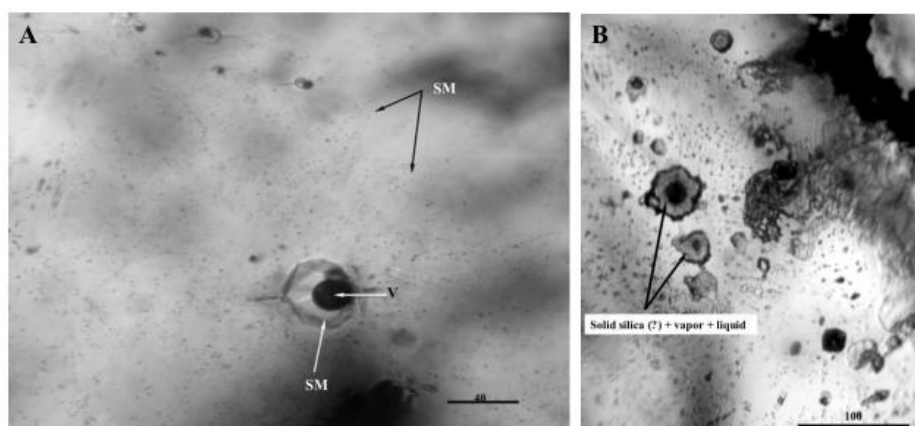
Fig. 15. A. Minute silicate melt inclusions (<1µm to 1-5µm, i.e. inframineral sized) sprayed around primary silicate melt inclusions in a large growth zone (IB) in the β-quartz phenocrysts from Roșia Montană. SM- silicate melts inclusion, V-vapor. Scale bar in µm. (see text for more explanation). **B**. Secondary fluid inclusions in β-quartz phenocrysts containing granular silica, vapor bubble and aqueous liquid phase as a thin rim. The hexagonal shape of the inclusions indicates that the microcrack recicatrized at low temperature. Scale bar in µm.

If this melt fraction contained chloride and sulfide phases (with gold, silver and other ore elements) it is presumably that they also were sprayed inside the magma chamber as ephemeral immiscible droplets. This could be the first step when gold and others metallic element would be separated from the silicate melt and dispersed in the crystallizing dacite melt, in the upper magma chamber and raising conduit at high temperature and pressure.

It was demonstrated by experimental works that gold solubility is enhanced in magmatic volatile phases (e.g at T= 1000°C and P= 150 MPa) if the silicate melt exsolved simultaneously H_2S and alkali chloride (Zajacz et al., 2010). The coexistence temperature of silicate and chloride rich phases recorded in β-quartz phenocrysts from Roșia Montană close to the experimental P-T conditions reported above and the presence of globular sulfide remelted phases (e.g. Fig. 10) and H_2S in the vapor-rich type inclusions determined qualitatively by microthermometry and tentatively by Raman microprobe (Pintea and Benning, unpubl.), allow us to emphasize that gold evolution starts indeed in the magmatic stage vectored first by the hydrosilicate alkali-rich melt. This could be a pertinent explanation for the constant gold content in a huge quantity of dacite and country rocks in the Roșia Montană environment: 214.91 million metric tons (Mt) of ore at 1.46 g/t Au and 6.9 g/t Ag (10.1 Moz Au and 47.6 Moz of Ag) making Roșia Montană, one of the largest gold deposit in Europe (Wallier et al., 2006). Moreover it is known that melting temperature of gold decreases as the particle size decreases (Reich et al., 2006) and the nanogold particles (AuNPs) melted obviously at less than 500°C in the presence of an arsenian pyrite [Fe(S,As)₂]. The color of nanogold is reddish and we question about the presence of nanogold released in the waste water above the tailings deposited in Cetate Hill at Roșia Montană environment as it is suggested by a picture (Fig. 16) published in a project of RMGC (Roșia Montană Gold and Silver Project – Roșia Montană Gold Corporation). This can be proven by using ultrasophisticate analytical methods as it was done elsewhere by Constantinescu et al. (2006) by TEM/SAED technique. On the other hand, it is obvious that invisible (colloidal) gold could be adsorbed on the growing surfaces of pyrite, arsenopyrite and marcasite (Widler & Seward, 2002) complexed in hydrothermal solution as hydrosulfide (Benning & Seward, 1996) and then could be released by alteration of sulfides in the waste water and tailings. So we emphasize that the second vector of transport and precipitation of gold in Roșia Montană epithermal Au-Ag ore deposit is the gas mixture of H_2O-CH_4-H_2S and/or H_2O-CO_2-H_2S as it was documented by microthermometry and Raman spectroscopy in vapor-rich inclusions from the epithermal prismatic quartz crystals (Pintea, 1999). Additionally, the organic matter present in the various polymictic breccia zones of the ore deposit had been a pH controller triggering precipitation of free gold in veins and open voids of breccia bodies.

Fig. 16. A. Tailing waste water in the Cetate Hill from Roșia Montană. The reddish color of the waste water could be questioned if it is generated by the presence of reddish nanogold particle as it is the color of the colloidal gold in the bottle figured in **B.** (web source).

6.4. Future work

This fluid and melt inclusion study related to the internal microtexture feature of the β-quartz phenocrysts (polymorphs) and additionally those of epithermal quartz crystals related to the Au-Ag mineralization pulses, suggested further key-research on the magmatic-to-hydrothermal activity of the Roșia Montană ore deposit. These would be supported by the next work implying more sophisticated analytical methods including the SEM-CL analyses for defining more accurately the relationships between CL microtexture, trace element concentration of different quartz zones and metal precipitation mechanism (Müller, 2000; Takahashi et al., 2007). We propose to use Electron probe microanalyses (EPMA) to measure concentration of Al, K, Ti, Fe, Mn, and the "Titani-Q" geothermometer will be applied to calculate growing quartz temperature in comparison with silicate melt inclusion microthermometry and perhaps $\delta^{18}O$ geothermometry in quartz, and zircon microinclusions, by secondary-ion mass spectrometry (SIMS). Timing and crystallization stratigraphy based upon zircon U-Pb analyses by LA-ICP-MS technique is also necessary to be implemented. Another important topic would be related to the presence of invisible gold in sulfide minerals, waste water and tailings by using TEM/SAED and others possible facilities on imaging nanoparticles in geologic materials. A main question related to the time relationships between magmatic and tectono-structural steps in generating the epithermal fluid system still remains in debate.

7. Conclusions

The main conclusions and further suggestions related to the magmatic-to-hydrothermal processes which generate the famous Roșia Montană Au-Ag ore deposit, resulted from this study, are the followings:

- The β- quartz phenocrysts (polymorphs) from Roșia Montană recorded almost entire magmatic-to-hydrothermal history of the Au-Ag deposit;
- Their internal oscillatory microtexture was formed by two main zones, a thin layer (20 to 50µm) and a large growth zone (50 - to 350 µm). These contain silicate melt inclusions which homogenized up to 1370ºC in the resorption layer and between 786º-939ºC and up to 1200ºC in the growth zone. Silicate/silicate ± sulfide and silicate/salt immiscible melt inclusions show homogenization or coexistence temperature between 1050-1200ºC. Salinity in heterogeneous silicate/salt inclusions was estimated between 38-60 wt% NaCl eq.at 1175ºC and 300 MPa. A critical (?) homogenization behavior was recorded in complex silicate/silicate±sulfide melt inclusions around 1050ºC;
- The main characteristics of the silicate melt inclusions in the magmatic quartz phenocrysts from Roșia Montană are that they generally failed from homogenization because of natural decrepitation and hydrothermal alteration. Anyhow the chemical composition of typical silicate glass inclusions from Roșia Montană quartz phenocrysts allowed a pertinent approximation on the trapping P-T conditions, of our homogenized silicate melt inclusion between 786º-939ºC,

57

based upon published data (Blundy et al., 2006) on similar inclusions trapped in plagioclase, prior to eruption, which were calculated between 750°-995°C and 15-313 MPa, respectively;

- Secondary brine and fluid inclusions were trapped in β-quartz phenocrysts as "sweat" halos, and neonate assemblages around the primary silicate melt inclusions suggesting an intermediate temperature-high salinity ephemeral stage. Two vapor-rich assemblages were homogenized in the vapor phase between 458°-500°C and 530°-555°C, probably the counterparts of high salinity secondary inclusions trapped below the α/β transition temperature as secondary trail or generated by necking-down in the same ephemeral high - temperature hydrothermal process;

- Late epithermal fluids with low-salinity (0.18-3.23 wt% NaCl eq., n=393) and low-temperature (180°-290°C, n=380), measuring almost the same value in the secondary fluid inclusions in the magmatic quartz phenocrysts and in the primary (pseudosecondary) fluid inclusions in the epithermal quartz crystals where never halite daughter microcrystals were found. Homogenization temperature (ThL-V(V) in vapor-rich inclusions was measured between 362-374°C and salinity of 0.71 wt% NaCl eq. was determined, and other two assemblages between 259-277°C and 401-443°C were recorded. The last values may be the counterpart of the moderate to high salinity, high temperature and intermediate density aqueous-rich inclusions already reported (Wallier et al., 2006), perhaps in a late rejuvenation boiling episode;

- Two precipitation vectors were emphasized to be the main gold, silver and other ore elements carriers in the magmatic-to-hydrothermal processes, first a hydrosilicate alkali-rich melt and second a gaseous mixture of $H_2O-CO_2-CH_4-H_2S$ in a neutral pH low-salinity, low-temperature aqueous-rich fluid; it is suggested that gold and other ore elements were sprayed as nanoparticles by these two vectors in the dacite matrix and invisible gold was adsorbed on the sulfides mineral surfaces or ripened as free-gold in veins and voids in the various brecciate bodies. Further works is need to be done including analytical methods such as: SEM-CL, BSE-EPMA, LA-ICP-MS, SIMS, and TEM/SAED etc.

- **Additional note**: We just find crucial references (Saunders and Burke, 2007; Saunders, 2012; Helmy et al., 2013; Prokofiev et al., 2017) which constitute strong argument about the presumption inserted in our paper that gold could be dispersed firstly as nanoparticles by hydrosilicate alkali-rich fluid and also adsorbed as "invisible gold" on the sulfide surfaces in the late epithermal stages.

References:
Andrei J. (2012) Geological-metallogenetic considerations based specially on geophysical data for Bucium-Roșia Montană-Roșia Poieni area. Rom. J. of Min. Dep., Abstracts, 85, 2, p.90-92.
Audetat A., Günther D. (1999) Mobility and H_2O loss from fluid inclusions in natural quartz crystals. Contrib Mineral Petrol, 137, p.1-14.
Audetat A., Pettke T. (2006) Evolution of a porphyry-Cu mineralized magma system at Santa Rita, New Mexico (USA). Journ. of Petrology, 47, 10, p.2021-2046.
Bachmann O., Bergantz G.W. (2003) Rejuvenation of the Fish Canyon magma body: A window into the evolution of large-volume silicic magma systems. Geology, 31, 9, p.789-792.
Benning L.G., Seward T.M. (1996) Hydrosulfide complexing of Au(I) in hydrothermal solutions from 150°-400°C and 150-1500 bar. Geochim. Cosmochim. Acta, 60, p.1849-1871.
Best M.G., Christiansen E.H. (1997) Origin of broken phenocrysts in ash-flow tuffs. GSA Bulletin,109, p.63-73.
Berbeleac I., Popa T., Ioan M., Iliescu D., Costea C. (1995) Main characteristics of neogene-volcanic-subvolcanic structures and hosted ore deposits in Metaliferi Mountains. Geologica Macedonica, 9/1, p.51-60.
Blundy J., Cashman K., Humphries M. (2006) Magma heating by decompression – driven crystallization beneath andesite volcanoes. Nature, 443, p.76-80.

Bodnar R.J., Burnham C.W., Sterner S.M. (1985) Synthetic fluid inclusions in natural quartz. III. Determination of phase equilibrium properties in the system H_2O-NaCl to 1000ºC and 1500 bars.Geochim Cosmochim Acta, 49, p.1861-1873.

Bodnar R.J., Student J.J. (2006) Melt Inclusions in plutonic rocks: petrography and microthermometry. Min. Assoc. Can. Short Course 36, Montreal, Quebec, p.1-25.

Borcoş M. (1970) Geological microthermometric research with special view to some metallogenetic and petrographic processes from Romania. PhD thesis abstract, Bucharest University (in Romanian).

Borcoş M. (1973) Some observations on magmatic relicts signification in minerals from volcanic rocks. An. Bucharest Univ., p.23-30 (in Romanian).

Clocchiatti R. (1975) Les inclusions vitreuses des cristaux des quartz. Etude optique, thermo-optique et chimique. Applications geologiques. Mem. Soc. Fr. 122p.

Constantinescu S., Udubaşa G., Popescu-Pogrion N., Hirtopanu P., Udubaşa S.S. (2006) Nano-minerals identification by different physical techniques. Rom. J. of Min. Dep. and Rom. J. of Min., 82, p.175-178.

Davidson P. (2004) A new methodology for the study of the magmatic-hydrothermal transition in felsic magmas: applications to barren and mineralized system. PhD thesis, Univ of Tasmania, 289p.

Diamond L.W., (2003) Systematics of H_2O inclusions. In: Fluid Inclusions: Analysis and Interpretation (I. Samson, A. Anderson, D. Marshall, Eds) Min. Assoc. of Canada Short Course Ser., vol. 32, 3, p.55-79.

Driesner, T., Heinrich, C. A. (2007) The system H_2O-NaCl. Part I: Correlation formulae for phase relations in temperature-pressure-composition space from 0 to 1000 degrees C, 0 to 5000 bar, and 0 to 1 XNaCl: Geochim. Cosmochim. Acta, v. 71, p.4880-4901.

Harris C.R., Pettke T., Heinrich C.A., Rosu E., Woodland S., Fry B. (2012) Tethyan mantle metasomatism creates subduction geochemical signatures in non-arc Cu-Au-Te mineralizing magmas, Apuseni Mountains (Romania). Earth and Planet. Sci. Lett. 366, p.122-136.

Helmy H.M., Balhaus C., Fonseca R.O., Wirth R., Nagel T., Tredoux M. (2013) Noble metal nanoclusters and nanoparticles precede mineral formation in magmatic sulfides melts. Nat. Commun. 2013 Sep 6; 4: 2405. Published online 2013 Sep 6. DOI: 10.1038/ncomms3405

Ghiţulescu T.P., Socolescu M. (1941) Etude géologique et minière des Monts Metalifères. Ann. Inst. Geol. Rom, XXI, p.181-283.

Goldstein, R.H., Reynolds, T.J. (1994) Systematics of fluid inclusions in diagenetic minerals. SEPM (Society for Sedimentary Geology).

Iatan E.L. (2008a) Cathodoluminescence petrography and fluid inclusions study of some quartz samples from Roşia Montană epithermal Au-Ag deposit, Metaliferi Mountains, Romania, Geophysical Research Abstracts,Vol. 10, EGU2008-A-07094.

Iatan E.L. (2008b) New data concerning fluid inclusions and cathodoluminescence petrography of some quartz samples from Roşia Montană epithertmal deposit, Metaliferi Mountains, Romania, Rom. J. of Min. Dep. and Rom. J. of Min., 83, p.66-69.

Iatan E.L. (2009) The relationship between magmatism and metallogenesis in the Roşia Montană and Roşia Poieni ore deposits environment. PhD thesis, abstract, Bucharest University (in Romanian).

Idriceanu T.R., Erhan V., Iorga N. (1965) The sudy of the quartz crystals from the Roşia Montană rhyolite (Apuseni Mountains). An. Univ. "Al I. Cuza", Iasi, Ser. II, Section II, XI (in Romanian).

Johnson M.C., Anderson A.T. Jr., Rutherford M.J. (1994) Pre-eruptive volatile content of magmas. In "Volatile in magmas" (Carroll M.R. and Holloway J.R., eds), Rev. in Mineralogy, 30, 8, p.281-330, Min. Soc. America.

Kouzmanov, K., Ivăşcanu, P., and O'Connor, G., (2005) Porphyry Cu-Au and epithermal deposits in the southern Apuseni Mountains, Romania. Box 1–1: Ore Geology Reviews, v. 27, p.46–47.

Laroque A.C.L., Stimac J.A., Keith J.D., Huminicki M.A.E. (2000) Evidence for open-system behavior in immiscible Fe-S-O liquids in silicate magmas: implications for contributions of metals and sulfur to ore - forming fluids. Canadian Mineral., 38, p.1233-1249.

Lester G.W., Clark A.H., Kyser T.K., Naslund H.R., (2013) Experiments on liquid immiscibility in silicate melts with H_2O, P, S, F and Cl: implications for natural magmas. Contrib. Mineral. Petrol., 166, p.329-349.

Manske S.L., Hedenquist J.W., O'Connor G., Tămaş C., Cauuet B., Leary S., Minut A. (2006) Roşia Montană, Romania: Europe's largest gold deposit. SEG Newsletter 64, p.9-15.

Müller A. (2000) Cathodoluminescence and characterisation of defect structures in quartz with applications to the study of granitic rocks. PhD thesis, Mathematics and Natural Science Faculties Georg-August-University Göttingen, Dresden, 229 p.

Naumov V.B., Prokofiev V.YU., Kovalenker V.A., Tolstykh M.L., Damian G., Damian F. (2010) Peculiar melt inclusions in quartz phenocrysts of Roşia Montană dacite breccia hosted epithermal Au-Ag deposit, Romania. ACROFI III and TBG XIV, Abstracts, p.148-149, Novosibirsk, Russia.

Naumov V.B., Prokofiev V.Yu., Kovalenker V.A., Tolstykh M.L., Damian G., Damian F. (2011) Unusual acid melts at unique epithermal Roşia Montană (Romania) gold deposit. ECROFI-XXI, Abstracts, p.148-149, Montanuniv. Leoben, Austria.

Naumov V.B., Prokofiev V.Yu., Kovalenker V.A., Tolstykh M.L., Damian G., Damian F. (2013) Unusual acid melts in the area of the unique Roşia Montană gold deposit, Apuseni Mountains, Romania: evidence from inclusions in quartz. Geochemistry International, 51, 11, p.876-888.

O'Connor G.N., Nash C.R.Dr., Szentesy C. (2004) The structural setting of Roşia Montană gold deposit, Alba, Romania. Rom. Jour. of Min. Dep. 81, p.51-57.

Peppard T.B., Steele I. M., Davis A.M., Wallace P.J., Anderson A.T. (2001) Zoned quartz phenocrysts from the rhyolitic Bishop Tuff. Amer. Mineral., 2001, 80, p.1034-1052.

Petrulian N. (1934) Etude chalcographique du gisement aurifere de Roşia Montană (Transylvanie, Roumanie). Ann. Inst. Geol., XVI, p.499-519.Bucharest.

Pettke T., Audetat A., Schaltegger U., Heinrich C.A. (2005) Magmatic-to- hydrothermal crystallization in the W-Sn mineralized Mole Granite (NSW, Australia) Part II: Evolving zircon and thorite trace element chemistry. Chem. Geol., 220, p.191-213.

Pintea I. (1999) New microthermometric data on fluid inclusions from Roşia Montană quartz crystals. In "Mineralogy in the System of Earth Sciences". Abstr.vol supplement An: XLVIII/, p.74 – 75.

Pintea I., Cherebetiu T., Iurian D., Hirit A., Manoila I. (1992) Termoinc-01, a microthermometric stage for fluid inclusion studies. Rom. Jour. Mineral., Suppl. Abstracts, 75, p.34.

Pintea I., Iatan E.L. (2013) The magmatic-hydrothermal history of the β-quartz phenocrysts from Roşia Montană dacite inferred by solid-, melt-, and fluid inclusion assemblages. ECROFI XXII, Antalya-Turkey, 4-9 June, p.114.

Popescu G.C., Ilinca G., Neacşu A. (2008) Mineralogy of Vivianite from Roşia Poieni; Metalogenetic significance. Rom. Jour. of Min. Dep. and Rom. Jour. of Mineral. Abstracts, 83, p.119-122.

Prokofiev Yu.V., Kamenetsky V.S., Selektor S.L., Rodemann T., Kovalenker V.A., Vatsadze S.Z. (2017) First evidence for natural occurrence of colloidal silica in chalcedony-hosted vacuoles and implications for ore-forming processes. Geology, 45, 1, p.71-74.

Reich M., Utsunomiya S., Kesler S.E., Wang L., Ewing R.C., Becker U. (2006) Thermal behavior of metal nanoparticles in geologic materials. Geology, 34, p.1037-1040.

Roedder E. (1979) Origin and significance of magmatic inclusions. Bulletin de Mineralogie, 102, 5-6, p.487-510

Roedder E. (1994) Fluid Inclusions. Min Soc America 644p, Washington.

Saunders J.A., Burke M. (2007) Formation and aggregation of gold (electrum) nanoparticles in epithermal gold. Minerals, 7, 163; DOI:103390/min7090163.

Saunders J.A. (2012) Textural Evidence of Episodic Introduction of Metallic Nanoparticles into Bonanza Epithermal Ores. Minerals, 2, p.228-243; DOI:10.3390/min2030228.

Ştefan R., Cosma S., Cristescu T. (1974) Petrographic, structural and metallogenetic characterization of the Roşia Poieni-Roşia Montană structure. D.S. IGG (1972-1973), LX, p.89-105 (in Romanian).

Sterner S.M. (1992) Homogenization of fluid inclusions to the vapor phase:the apparent homogenization phenomenon. Econ. Geol., 87, p.1616-1623.

Tamaş, C.G. Bailly L. (1998) Fluid inclusion study for Roşia Montană ore deposit. Rom. J. Min. Deposits, 78, suppl. 1, p.97-98.

Tarantola A., Diamond L.W., Stünitz H. (2010) Modification of fluid inclusions in quartz by deviatoric stress I: experimentally induced changes in inclusion shapes and microstructures. Contrib Mineral Petrol, 160, p.825-843.

Takahashi R., Müller A., Matsueda H., Okrugin V. M., Ono S., Kerkhof den A. von, Kronz A., Andreeva E. D. (2007) Cathodoluminescence and Trace Elements in Quartz: Clues to Metal Precipitation Mechanisms at the Asachinskoe Gold Deposit in Kamchatka. In: Okada, H., Mawatari, S.F., Suzuki, N. and Gautam, P. (eds.), Origin and Evolution of Natural Diversity, Proceedings of International Symposium "The Origin and Evolution of Natural Diversity",1-5 October 2007, Sapporo, p.175–184.

Udubașa G., Roșu E., Seghedi I., Ivășcanu P.M. (2001) The "Golden Qadrangle" in the Metaliferi Mts., Romania: what does this really mean? Jour. Min. Dep.79, suppl. 2, Spec. Issue, the Second ABCD-GEODE Workshop,Vata, 2001, p.23-32. Bucharest.

Wallier, S., Rey, R., Kouzmanov, K., Pettke, T., Heinrich, C.A., Leary, S., O'-Connor, G., Tămaş, C. G., Vennemann, T., and Ullrich, T. Magmatic fluids in the breccia-hosted epithermal Au-Ag deposit of Roșia Montană, Romania. Econ. Geol., 2006, 101, p.923-954.

Wark D.A., Hildreth W., Spear F.S., Chemiak D.J. (2007) Watson E.B. Pre-eruption recharge of the Bishop Magma system. Geology, 35, 3, p.235-238.

Widler A.M., Seward T.M. (2002) The adsorption of gold(I) hydrosulfide complexes by iron sulfides surfaces. Geochim. Cosmochim. Acta, 66, 3, p.383-402.

Zajacz Z., Seo J.H., Candela P.A., Piccoli M.P., Heinrich C.A. (2010) Guillong M. Alkaly metals control the release of gold from volatile-rich magmas. Earth and Planet. Sci. Lett., 2010, 297, p.50-56.

* *
*

Roșia Montană Gold and Silver Project. RMGC. (2012) "A project for Romania" http://www.gabrielresources.com/documents/GBU_Corp_Pres_March 2012_Letter.pdf